2-1-2016

Microbial Biofilm Development and Electron Transfer in Electrochemical Systems

Jose Cornejo

Jose Alberto Cornejo
Candidate

Chemical and Biological Engineering
Department

This dissertation is approved, and it is acceptable in quality and form for publication:

Approved by the Dissertation Committee:

Plamen Atanassov, Chairperson

Andrew Shreve

Andrew Schuler

Linnea Ista

Sofia Babanova

MICORBIAL BIOFILM FORMATION AND ELECTRON TRANSFER IN BIOELECTROCHEMICAL SYSTEMS

by

JOSE ALBERTO CORNEJO

B.S. Chemical Engineering, University of New Mexico, 2009

M.S. Chemical Engineering, University of New Mexico, 2013

DISSERTATION

Submitted in Partial Fulfillment of the
Requirements for the Degree of

Doctor of Philosophy
Engineering

The University of New Mexico
Albuquerque, New Mexico

December, 2015

DEDICATION

I dedicate this work to my wife, Vicki.

ACKNOWLEDGEMENTS

I would like to thank my family for their unconditional love and support throughout this process. Vicki, my wife, my parents, Jose Walther and Martha Cornejo, my sisters Cristina and Lucia, and my father and mother in law, Lou and Susana have all provided love, support, and much appreciated words of encouragement when needed.

I would like to thank my advisor, Plamen Atanassov, for giving me the opportunity to join his lab and allowing me to work with the most wonderful people one could ever ask for. His words of wisdom and genuine will for his students to succeed professionally are things that I will appreciate for the rest of my life. I would also like to thank Dr. Andrew Shreve for his invaluable support, time and constructive comments.

I would like to thank the faculty that acted as co-mentors from whom I learned an incredible amount of skills, Dr. Linnea Ista, Dr. Sofia Babanova, Dr. Andrew Schuler and Dr. Kateryna Artyushkova, I will always appreciate your time for insightful discussions and ideas. I always felt honored to work and collaborate with you.

I would like to acknowledge old and new friends that made this a richer and gratifying experience. Specially, Dr. Akinbayowa Falase, Dr. Pablo de la Iglesia, Dr. Ulises Martinez, Dr. Jared Roy, Dr. Carlo Santoro, Dr. Claudia Narvaez, Dr. Alexey Serov, Matteo Grattieri, Santiago Rojas, Anicet Zadick, Ryan Lopez, Ciana Lopez, Lydia Stariha, Noel Dawson, Shannon Landry, Dr. Patrick Murphy, Catherine Williams and Sean Williams. Thank you all for your friendship.

This study was in part funded by the Army Research Office and the Bill and Melinda Gates Foundation.

Microbial Biofilm Development and Electron Transfer in Electrochemical Systems

by

Jose Alberto Cornejo

B.S., Chemical Engineering, University of New Mexico, 2009
M.S., Chemical Engineering, University of New Mexico, 2013
Ph.D., Engineering, University of New Mexico, 2015

ABSTRACT

Energy harvesting from microorganisms has created vibrant research efforts for the past 20 years that has lead to the development of emerging topics such as microbial electrochemistry, biofilm formation in electrochemical systems and alternative energy technologies applied in environmental processes. In this study we present procedures that aim for further understanding of bacterial physiological conditions in electrochemical systems and interactions between biofilms and solid surfaces, particularly, for the facultative anaerobe *Shewanella oneidensis* MR-1. These systems consist of microbial fuel cells (MFCs) whose anode component will be evaluated with regards to performance, electrical current generation, and microbial coverage and biofilm development.

A better understanding of how anode surface properties affect growth, development, and activity of electrogenic biofilms has great potential to improve the performance of bioelectrochemical systems such as MFCs. A combination of spectroscopic, microscopic, and electrochemical techniques was used to evaluate how electrode surface chemistry influences morphological, chemical, and functional properties of wild type *S. oneidensis* and motility-impaired mutant strains, as well as mixed cultures found in wastewater treatment plants. This was done with an effort to develop improved electrode materials by studying structure-to-property relationships. 3D morphological features of biofilms that were directly linked to functional properties of the biofilm during growth during polarization were directly connected to the efficiency of electron transfer from the bacteria to the anode.

Table of Contents

List of Figures

List of Tables

Chapter 1 – Introduction

Bacterial communities play a crucial role in many biological processes, which include natural cycling, waste removal and gut microbiota processes. Therefore, these microorganisms present a tremendous impact to our ecosystem and the lives of all eukaryotes. While microbes utilize a various metabolic strategies in order to obtain nutrients and thus thrive in a given environment, we would like to focus our attention on a particular metabolic pathway. It is known that all metabolic processes require diverse sets of redox reactions to complete the demands from these microorganisms. The particular scenario involving organic carbon compounds as electron donors and inorganics such as metals as electron acceptors has attracted the attention of researchers that further study bacteria that possess the capabilities to utilize this specific pathway. This is due to the electron transfer pathway that resides in the electron accepting metals can be used for the harvesting of electrical energy [1]. This phenomenon has opened the door to a line of research that looks at electrogenic bacteria and couples them environmental and alternative energy technologies such as water remediation, waste removal and biofuel cells. The latter application comes to importance due to its promising capabilities in the conversion of chemical energy to electrical energy at considerably low costs and high portability (i.e. ubiquity of microbial communities).

Scientists in the field of research of microbial electrochemical systems have extensively explored several species of bacterial organisms due to their high compatibility for the advancement of microbial fuel cell (MFC) research. The two species that stand out are *Shewanella oneidensis* and *Geobacter sulfurreducens,* with the former being a facultative anaerobe and the latter an obligate anaerobe. This dissertation focuses on the electrogenic

capabilities of S. oneidensis, its incorporation in bioelectrochemical systems, and several subcellular structures that play an important role in the electron transfer process.

1.1 – Shewanella oneidensis as a Model Organism

S. oneidensis is a Gram-negative ϒ-Proteobacteria facultative anaerobe. It possesses the ability to oxidize organic compounds such as lactate, formate, certain amino acids and hydrogen [2,3]. In terms of reductions, *S. oneidensis* is known to reduce a broad range of substrates such as nitrate, nitrite, manganese, iron, thiosulfate, sulfite tetrathionate and fumarate. Prof. Kenneth Nealson diligently exposed the phenomenon of biological reduction of metal oxides in 1988 with his work on bacterial manganese reduction and manganese oxide as the sole electron acceptor [2]. This work fortified the hypothesis for biological metal cycling in stratified bodies of water and the important role that *S. oneidensis* has on the biogeochemical cycling processes of iron and manganese oxides, where oxygen is limited [3]. Furthermore, these studies opened new doors of research dedicated to the advancement of alternative energy technologies.

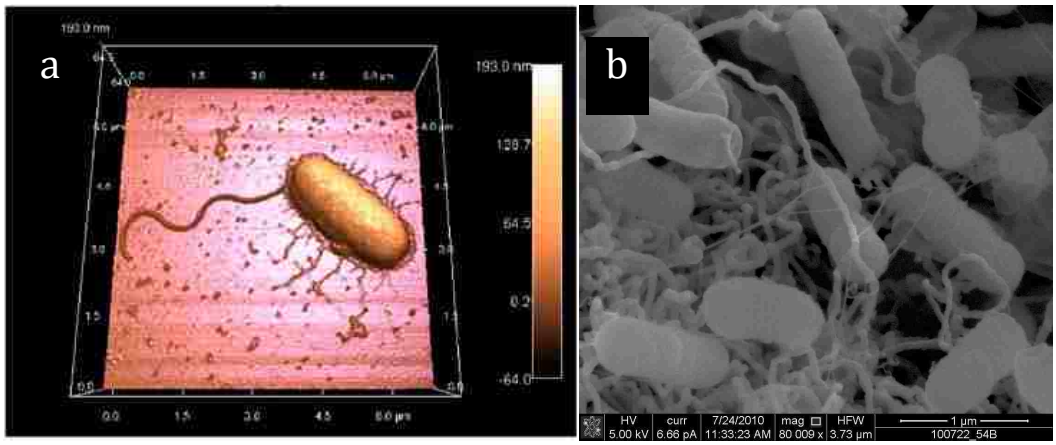

Figure 1.1: Images of *Shewanella oneidensis* showing its different appendages used in electron transfer: a) Flagellum (long tail) and pili (short appendages) [4]. b) Nanowires.

Electron flow mechanisms are essential in the bacterial cell metabolism. Terminal electron acceptors are important because they allow electrogenic bacterial cultures to continue cell growth and thrive in anaerobic environments. The specific mechanism of electron transfer in *S. oneidensis* has been subjected of extensive studies for many years. The consensus regarding this process has designated the electron transport between electron acceptors and the cell membrane as extra-cellular electron transfer (EET). Three subcategories have been identified which occur collectively: direct electron transfer (DET) via outer membrane-bound cytochromes [5], mediated electron transfer (MET) by soluble redox compounds such as flavins [6-9], and electrically conductive biological filaments or nanowires [10,11].

S. oneidensis will express cytochrome production in the cell membranes; where it has been postulated that these proteins may come in direct contact with metal oxides [5,12]. In particular, genetic knockout studies have identified MtrA, MtrB, MtrC, and OmcA

cytochromes as the components in the dissimilatory reduction of insoluble metal oxides [12]. These proteins comprise the "metallothermic reduction (Mtr) pathway" and they orchestrate the delivery of electrons from the inside of the cell to the outer membrane. (Figure 1.2)

CymA is thought to serve as the starting electron transfer protein in the Mtr pathway; this protein serves as an intermediate between the quinol pool of the inner membrane space to the Mtr pathway and the fumarate reductases [13]. The decaheme MtrA is a soluble c-type cytochrome located in the periplasm [14], it provides an important link through the between the periplasm and the outer membrane cytochromes. The MtrB cytochrome is essential for oxide reduction [15] and in the placement and insertion of the MtrC/OmcA outer membrane complex [17]. These two later cytochromes also contains contain 10 hemes, and are bound to the extracellular side of the outer membrane [18]. (Figure 1.2) In addition, MtrF (not pictured) has also been identified as a cytochrome that presents similar features and roles as MtrC [19] and therefore, an important component in EET studies.

Active metabolites mediating electron transfer to insoluble electron acceptors have been identified and widely studied in *S. oneidensis*. Riboflavin and flavin mononucleotide (FMN) specifically, are known to be electrochemically active molecules implicated in metal oxide reduction [8]. Their roles in electricity production have also been studied in *S. oneidensis* while incorporated in bioelectrochemical systems (BES) [20,21]. In these studies we take further analysis of the role of flavins in EET by utilizing electrochemical characterization techniques with the intent of understanding the flavin-cytochrome interactions at the molecular level and thus, EET efficiency.

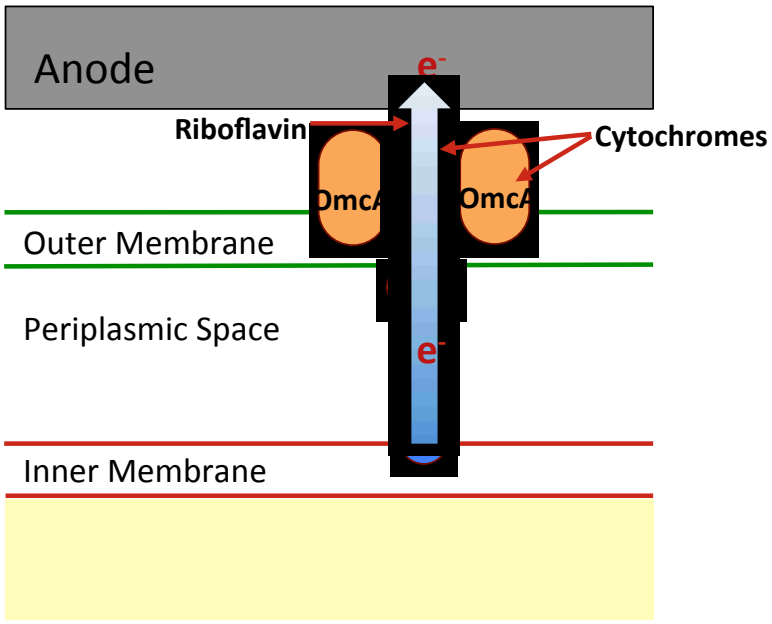

Figure 1.2: Schematic representation of the major cytochromes and soluble redox compounds (riboflavin) involved in EET in *S. oneidensis*. Cytochromes represented in this figure are: outer membrane cytochrome A (OmcA), metallothermic reduction A, B and C cytochromes (MtrA, MtrB, MtrC), and cytoplasmic membrane-bound A (CymA) cytochrome.

1.1.1 Biofilm formation and cell motility

In nature, *S. oneidensis*, like many other types of bacteria, are capable of secreting extracellular polymeric substance (EPS) as the building element for biofilm formation and stability [22]. For MFCs, biofilms are essential for effective organic substrate oxidation, EET and therefore current production. It is also through biofilms that S. oneidensis is capable of forming long filaments deemed nanowires, which are designed to facilitate electron transfer when bacterial cells not places in proximity with the electron reservoir (electron acceptor limitation) [23].

Other components that play an important role in substratum attachment and cell motility consist of appendages at the outer region of the bacterial cell known as flagella and pili, whose primary purpose are to provide movement to the cell. Specifically, these substructures are responsible for swimming, twitching and swarming. As shown in Figure 1.1, two different types of components can be identified: the flagella (long appendices) and the pili (short appendices). The pili have been associated to twitching motility whereas the larger flagellum has been linked to swimming in planktonic environments and swarming motility in solid substrata [23]. Further studies suggest their implications in surface attachment and electron transfer [24].

1.2 – Electrochemical Studies of Microbial Communities

Given the properties and processes inherited by *S. oneidensis*, this organism has been thoroughly utilized as a model for the development of bioelectrochemical systems, which includes MFCs (Figure 1.3). These electrochemical devices are capable of converting chemical energy stored from organic material into electrical energy utilizing electrogenic capabilities from microorganisms. This clean, renewable type of energy technology presents growing interest among researchers that aim for developing self-sustainable biological wastewater treatment systems [25]. Particularly, MFCs present the potential of significantly lowering costs in the operation of commercial, industrial and municipal wastewater treatment facilities.

The use of single cultures like those of *S. oneidensis* simplifies the intricacies related to genetic composition, bacterial metabolomics, culturing conditions and bacterial-electrode

interactions. Simplifying these subjects allows us to focus on important parameters that are related to the electrode material, surface properties and morphology due to their high impact on the performance and cost of MFCs. Specifically bacterial anode design becomes a key component that directly influences MFCs efficiency. Some characteristic requirements include chemical stability, mechanical strength, biocompatibility, high surface area and good conductivity. These parameters will in turn influence bacteria-electrode interactions and biofilm formation. For these reasons, a wide array of carbonaceous materials with different morphologies has have been studied as suitable anode materials [26-29]. Further examination on anode material morphology and surface treatment will be presented in chapters 4 and 5.

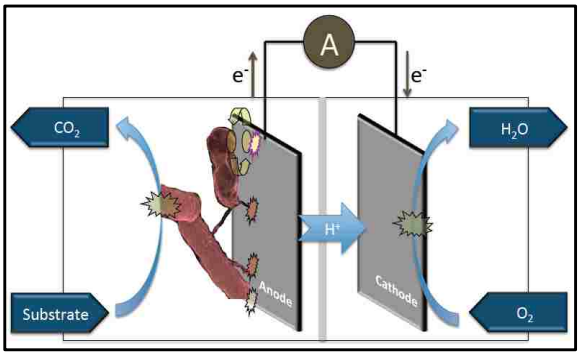

Figure 1.3: Basic schematic of a microbial fuel cell.

Once single bacterial cultures are thoroughly investigated, one can adopt the results obtained into mixed cultures. Diverse types of microbes work together to degrade biomass content from human waste, thus significantly easing waste removal. Part of this process is attributed to those organisms that are found in activated sludge. Several studies have provided empirical evidence for certain types of electrochemically active bacteria present in activated sludge [30]. Such bacteria are capable of harvesting electrons from

the oxidation of organic substrates and grow in biofilms on solid surfaces, which allows them to transfer electrons to these surfaces. Because of this, there has been growing interest in incorporating of electrogenic bacteria in fuel cell anodes, which can serve as solid platform for bacterial attachment and biofilm formation. Subsequently, electrons can then be carried from the anode side to the cathode side in which oxygen reduction takes place thus yielding water as a product, as shown in Figure 1.3.

Chapter 2 – Problem Statement and Objectives

The development and improvement of microbial electrochemical systems present challenges from several perspectives. These involve the design and development of microbial electrochemical systems capable of contributing towards the technology in renewable energy alternatives. On the other hand there are several questions that remain elusive regarding the fundamental understanding of microbial communities and their interactions with given substrates that are necessary for the conversion of chemical energy into electrical energy. Model organisms allow for the development of methodologies that provide important assistance to answering such questions.

This work focuses on the interactions that occur between electrochemically active bacteria and the electrode surface. Electrode material, morphology, design and surface chemistry have been taking into consideration in order to improve the electrical output in a microbial fuel cell system. Particularly we have focused our attention in the development and biocompatibility of anode materials. In addition to identifying and reducing the intricacies related to anode design, electrical current generation, and MFC performance, we have also quantified and characterized bacteria-to-anode surface attachment, biofilm growth and related morphological parameters. The electrochemically active organism *Shewanella oneidensis* has been used as a pure culture model in these studies. In addition, we have utilized mixed cultures extracted from municipal wastewater processes in order to characterize the specific bacterial population that can be considered as electrogenic. The challenges pertaining to understanding the diverse surface-to-microorganism interactions have lead to the following objectives that will be addressed in this dissertation:

- **Objective 1:** Establish electrochemical characterization methodologies to analyze extracellular electron transfer in *Shewanella oneidensis* biofilms when in contact to anodes.

Electrochemical cells will be used to cultivate *S. oneidensis* following given standard growth curves that correlate to the optimal bacterial development stages. Current generation will be measured by chronoamperometric studies in which the anode material of interest will be subjected to an applied constant potential. MFC performance and metabolomics studies will follow by using polarization curves and cyclic voltammetry.

- **Objective 2:** Identify the important molecular interactions in the *S. oneidensis* outer membrane components that affect electron transfer and current production.

It has been established that both DET and MET occur concurrently. This is due to the molecular interactions between specific types of cytochromes and flavins. Therefore, further viewing of the structural arrangement between these two molecules is of high importance in order to better understand the EET pathway in *S. oneidensis.* To achieve these goals, both experimental work and computational simulations have been done. These computational simulations have the capability to predict non-covalent binding of small molecules, such as flavins to macromolecules like cytochromes and provide information about the affinity of the interaction, predict the binding pocket in the cytochrome molecule for flavins, and identify specific hemes responsible for EET.

- **Objective 3:** Evaluate surface-treated anodes for optimal *Shewanella oneidensis* biofilm development and electrochemical performance.

Biofilm formation is essential for *S. oneidensis* to carry out efficient EET. This heavily relies on the type of solid substratum to which bacteria attaches to. Therefore, for the purpose of advancing MFCs, it is crucial to study the electrode material, structure and biocompatibility. For the fulfillment of this objective, a simple, fast and effective surface modification method for enhanced biofilm formation, increased electron transfer rate and higher current density generation from microbial fuel cell (MFC) will be tested. This method consists of partial oxidation of carbon felt material by UV/O_3 treatment.

- **Objective 4:** Elaborate quantifiable parameters that characterize the morphology of *S. oneidensis* biofilms on 2-D anode structures with defined surface chemistries.

A combination of spectroscopic, microscopic, and electrochemical techniques will be used to evaluate how electrode surface chemistry influences morphological, chemical, and functional properties of *S. oneidensis* MR-1 biofilms in an effort to develop improved electrode materials and structures for MFCs. We will investigate several conditions that influence electrode surface charge in order to find the optimal surface for MFC improvement.

- **Objective 5:** Develop microbial fuel cells for mixed culture organisms involved in water remediation based on previous single culture anodic evaluations.

Taking the gathered information from the studies in objective 4, we will elaborate methodologies to analyze MFC performance, power generation and biofilm characteristics using mixed cultures. Activated sludge contains a diverse pool of microorganisms that are crucial for organic waste processing in wastewater, a standard process that is currently applied in municipal reclamation facilities. We will also examine the phylum and class of bacterial composition from electrodes varying in hydrophilicity and surface charge.

- **Objective 6:** Assess the role of *S. oneidensis* outer membrane motility structures in EET, electrochemical performance and biofilm formation.

Extracellular appendages have been suggested be involved in motility and attachment in *S. oneidensis*. Therefore, it is important to identify and characterize the different roles of such appendages. In this study we will utilize motility mutants of *S. oneidensis* that lack key proteins involved in the secretion of type IV pili and flagella in order to identify the importance of their roles in biofilm development and current generation. Electrochemical characterization techniques previously introduced will be used to compare performance and current generation in each tested mutant as well as in wild type *S. oneidensis*. In addition, we will quantify the anodic biofilm 3D morphological characteristics based on microscopic techniques.

Chapter 3 – Experimental Methods

3.1 – Electrochemical Studies

All electrochemical experiments, unless otherwise noted, were done with a three-electrode half-cell setup consisting of a working carbon felt electrode for bacterial attachment and biofilm formation, a platinum counter electrode, and a Ag/AgCl reference electrode. The reference electrode is used as a stable standard with which the potential of the working electrode is measured against. No current passes through the reference electrode. The counter electrode balances the reaction occurring at the working electrode by passing current.

3.1.1 Chronoamperometry

Chronoamperometry (CA) measurements are, for the purposes of this study the first polarization technique employed. A potentiostat applies a given potential and is held constant, with current being measured and recorded over a given period of time. The amount of current generated depends strongly on the metabolic stage of the bacteria, the amount of bacterial coverage at the surface of the electrode, and the EET efficiency rate. These factors that contribute with current generation are in turn dependent on the culturing specifications regarding their growth medium and the amount of organic compounds that act as electron donors and acceptors. Upon completion of the CA measurements, polarization curves can be built.

Polarization curves are a useful tool for evaluating an electrocatalyst's performance, in this study; this corresponds to the outer membrane components from electrogenic bacteria. For this method, the open circuit potential of the electrode of interest is obtained. Then, the electrode is subjected to polarization values of equal increments where each potential is applied for 5 min until a maximum current is achieved. These curves offer the possibility to evaluate the anode, the cathode and a full cell. A power curve can be obtained from the polarization curve my multiplying the current by the potential. This methodology allows us to evaluate ohmic losses form the system.

3.1.2 Cyclic voltammetry

Cyclic voltammetry (CV) is a very useful electrochemical characterization technique that determines the behavior of oxidation-reduction reactions that occur on an electrocatalyst. A potentiostat applies a potential that varies with time. The potential follows a triangular waveform that varies as a function of the potential range as well as the rate of change of the potential. (Figure 3.1) For microbial electrochemical system characterization, the presence of specific current peaks within the CV provides useful information on the amount of electrochemically active compounds from the bacteria in question. Thus, one can characterize the EET efficiency rate, which heavily depends on the activity of outer membrane cytochromes and flavin cofactors.

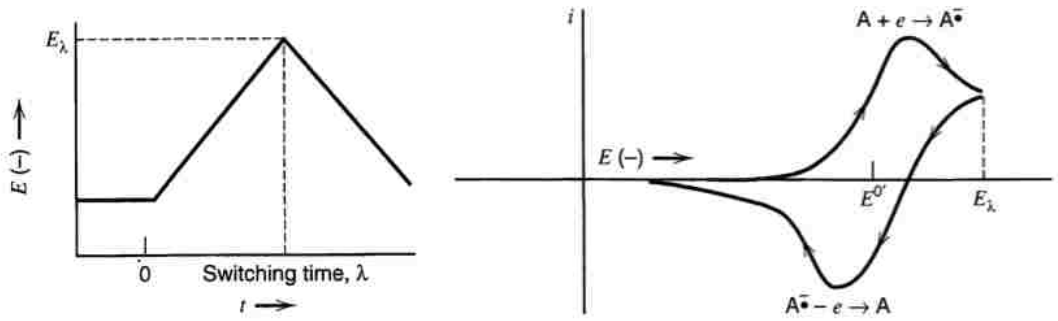

Figure 3.1: Cyclic voltammetry sweep (left). Resulting cyclic voltammograms (right).

3.2 – Structural Analysis

Several qualitative and quantitative analytical tools have been used to study bacterial biofilm characteristics and to characterize the surface of the electron material of interest. These include scanning electron microscopy (SEM), confocal laser scanning microscopy, x-ray photoelectron spectroscopy (XPS), contact angle measurements, and computational characterization tools. Correlations from these findings and those from electrochemical measurements will be elaborated by principal component analysis (PCA). Each technique will be described with further detail in each chapter according to their use.

3.3 – Biological Methods

Basic cultivation of the microorganisms will be described in detail within each chapter. Sterilization protocols were followed to ensure sample purity and to contribute to data reproducibility.

Chapter 4 – Extracellular Electron Transfer in *Shewanella oneidensis* Occurs via Outer Membrane/Flavin Interactions

4.1 – Introduction

It has been determined that bacteria such as *Shewanella* spp. can interact with solid electron acceptors, exploring three mechanisms of extracellular electron transfer (EET): mediated (MET) and direct (DET) electron transfer as well as long distance ETT through nanowires [20]. At the same time it was proposed that for *Geobacter* spp., which has been considered as the most active electrogenic bacteria, the only possible EET mechanism involves DET from outer membrane cytochromes (OMCs) [12,31]. The MET ability of *S. oneindesis* has been entirely correlated to the endogenous production and extracellular expression of flavins, which are then participating as electron shuttles enhancing the extracellular electron transfer rate [8,20, 32-34]. The two types of flavins excreted by Shewanella are flavin mononucleotide (FMN) and riboflavin (RF), where the amount of FMN secreted over-exceeds the RF content almost five times in both anaerobic and aerobic conditions [20]. Kotloski, et al. have demonstrated the importance of such flavins in EET mechanisms by analazyng flavin-deficient mutants of *S. oneidensis,* which lacked its bacterial FAD exporter (bfe) in biolectrochemical systems [32]. When flavins were not supplemented to the system, the bfe mutant generated 75% less current than the wild type, while once the same concentration of flavins was artificially introduced to both samples, they produced comparable currents.

The hypothesis of the mediating role of flavins has been stated and proved many times in the last 10 years [20,32] until recently when Okamoto et al. dramatically changed the

vision of the EET mechanism by providing a strong evidence for the role of the flavins not only as shuttling mediators but as cofactors associated with the OMCs [35-38]. In addition Okamoto et al. demonstrated the "preferences" of the flavins toward different outer membrane cytochromes, FMN specifically interacts with MtrC, while RF associates with OmcA [37]. The reasoning behind such specificity, according to the authors, lies in the differences in flavins' redox potential (-0.11 V for bound RF and -0.15 V for bound FMN, both versus SHE) and OMCs' pH dependence, which allows the utilization of various terminal electron acceptors as a survival strategy. At low potentials (-0.2 V vs. SHE) the FMN-MtrC association outperforms dramatically the RF-OmcA, which on the other hand has higher enhancement factor at lower pH (pH 6) [37]. The potential of the redox reaction of the bonded flavins appeared to be at least 0.1V more positive than the free flavins in solution, which decreases the potential difference between flavins and the OmcA-MtrC complex [36]. The bound flavins undergo one electron reduction by OMCs forming a semiquinone [36,37]. It is believed that the formation of the OMCs-flavin complexes leads to stabilization of the semiquinone along with the positive shift in the redox potential. Okamoto et al. demonstrated that the enhancement of the EET at the Shewanella/electrode interface is due not only to the previously proposed shuttling mechanism but to the redox activity of the oxidized flavin/semiquinone redox couple explicitly when the flavin is associated with a particular OMC, RF with OmcA and FMN with MtrC [36]. They further expended their work by demonstrating that *S. oneidensis* and *G. sulfurreducens* share common EET mechanisms with the involvement of flavins [20]. The molecular modeling of the interactions between macromolecules and small ligands has been presented elsewhere [39-41], which can be applied towards the further

understanding of the specific binding between cytochromes and flavins. This can provide information about the affinity of the interaction, predict the position in the cytochrome molecule where the flavin binds, and reveal which heme in the protein molecule is carrying out the EET. Based on the flavin-heme distance a qualitative evaluation of the EET rate can also be performed. Revealing the molecular-level flavin-OMCs interactions may provide a strategy for controlling the rate of EET, which could be important for versatile EET related applications not just microbial fuel cells but microbial corrosion protection, and bioremediation. The AutoDock Vina Software was used in this study, because, in contrast to other common docking simulation packages, it treats molecular docking as a stochastic global optimization of the scoring function on a precalculated grid maps [39]. This scoring function estimates the standard chemical potential of the system, which in turn determines the bound conformation preference and the free energy of binding.

In addition to molecular computational simulations, in this work, we utilize electrochemical methods such as cyclic voltammetry (CV) to probe the electrochemical interactions between a developing *S. oneidensis* MR-1 biofilm and an electrode surface in an anaerobic environment. We propose that riboflavin is secreted by MR-1 (potentially as a stress-response to changes in environment) and has the capacity to sense redox changes within its environment and lead the culture into the formation of conductive biofilms on the surface of an electrode, corroborating the findings of Li et al [42]. We investigated the effect of different potentials applied to the electrode in respect to the attachment and subsequent electrochemical interaction of an MR-1 biofilm. The applied potentials were based on the theoretical electrochemistry of riboflavin, with comparison to non-polarized

electrodes as control studies. The findings herein provide insight into the initial phases of biofilm attachment and development for *S. oneidensis* MR-1.

4.2 – Materials and Methods

4.2.1 Strains and culturing conditions

Frozen stocks of *Shewanella oneidensis* MR-1 were stored in a glycerol solution at −80◦C. Cultures were maintained on Triptic Soy Broth (TSB) agar plates and incubated for 24 hours at 30°C. Isolated colonies were subcultured into TSB and incubated aerobically at 150 rpm and 30°C for approximately 18 hours corresponding to late exponential growth/early stationary phase and an optical density (OD600) of approximately 4. A 250 mL, 3-neck flask, was modified to fit a 3-electrode electrochemical cell configuration. *Shewanella oneidensis* MR-1 (MR-1) was subcultured from the initial TSB stock into 50 mM sodium phosphate buffer and continuously sparged with nitrogen to achieve anaerobic conditions. 30 mM sodium fumarate and 100 mM sodium lactate were also added prior to electrochemical measurements. Fumarate is essential for initial accumulation of biomass in cultures under anaerobic conditions, thus achieving exclusive respiration with the electrode by the attached biomass.

4.2.2 Electrochemical testing

Large surface area electrodes consisting of 1 cm^3 of graphite felt (Morgan AM&T Grade VDG) were used in bioelectrochemical systems to examine the current density of relevant *S. oneidensis* MR-1 biofilms. The graphite felt electrodes were wired with 10 cm Ni wire

as a current collector. All measurements and applied potential experiments were done on a Gamry Reference 600 potentiostat. CVs were measured between −0.8 V (vs. Ag/AgCl) and 0.8 V at a scan rate of 10 mV/s. Polarization curves were first measured by potentiostatic polarization based on the open circuit potential after biofilm formation. Galvanostatic polarization were subsequently measured based on the current obtained under potentiostatic polarization. Galvanostatic polarization curves are reported within this study. All voltammograms reported are representative of experiments performed in triplicate.

4.2.3 Scanning electron microscopy

SEM analysis was used for visual confirmation of biofilm formation on the graphite felt electrodes after electrochemical characterization. Cells were chemically fixed to the electrode using a 2.5% glutaraldehyde solution for approximately 12 hours and then exposed to increasing concentrations of ethanol (30, 40, 50, 60, 70, 80, 90%) ending in 3 separate washes of 100% ethanol. The samples were then exposed to critical point drying using an automated critical point dryer (Seevac Inc.) before coating with ~5 nm layer of gold-palladium using an Emitech K950X sputter coater. Electron microscope manufactured by FEI Company (model Quanta 3D FEG microscope) was used to image the samples at 5 to 10 kV accelerating voltages.

4.2.4 Microbial cell viability assay

Upon the completion of the electrochemical studies, graphite felt electrodes were rinsed with phosphate buffer and submerged in a solution containing 7.5μM of Syto 13 green

fluorescent nucleic acid stain (Life Technologies Corporation) and 7.5 μM propidium iodide red fluorescent nucleic acid stain for 15 minutes. These indicators were used in order to discriminate living and nonliving cells, respectively. The electrodes were then mounted on a glass microscope slide and analyzed with an Axio Imager A1 fluorescence microscope (Carl Zeiss, Ltd.) at 40x magnification.

4.2.5 Spectrophotometric determination of riboflavin content

Spectrometry was used as a fast and simple method for the determination of riboflavin concentration in the electrolyte at the end of the electrochemical measurements. Standard addition methodology was used for the determination of the analyte concentration. The planktonic bacterial samples were centrifuged and the produced supernatant was later filtered through Nylon syringe filters (Fisherbrand, 0.2 μm, 25 mm, sterile). The filtrate was spiked with riboflavin solution with known concentrations (0.2, 0.8, 1 and 2 μM). The absorbance of the filtrate with and without the riboflavin additions at 420 nm was measured using a spectrometer (SpectraMax M5). The wavelength was selected based on the fact that riboflavin dissolved in 50 mM PBS has a maximum absorbance at 420 nm.

4.2.6 Molecular docking simulations

AutoDock Vina was used to perform the docking simulations providing nine possible models for each run of the simulation. The models are arranged in a descending order of the protein-substrate binding affinity. To increase the reliability of the docking, in each case the simulations were performed three times. The biologically meaningful complex candidates were further selected using two criteria: (1) high frequency of the model

appearing based on a histogram of the frequencies of the given output models from the three simulation runs, and (2) the minimum flavin-heme distance (N5 from the flavin molecule and the Fe in the nearest cytochrome heme) to be less than 11 Å, to support rapid EET. For the docking simulations, the proteins crystallographic structures were used (4LMH for OmcA [43] and 4LM8 for MtrC acquired from protein data bank). The structure of riboflavin was optimized using B3LYP/6-31G level of theory and the polarizable continuum model as implemented in the Gaussian 09 quantum chemical package [44]. AutoDock tools from MGL tools software were used for setting up the input files for AutoDock Vina and for visualization of the docking models.

4.3 – Results and Discussion

4.3.1 Biofilm development

An applied potential corresponding to that of riboflavin (near −0.450 V vs. Ag/AgCl) was applied to the working electrode under anaerobic conditions for ~36 hours (corresponding to reduced riboflavin on the electrode surface). The CV of the resulting electrode, however, exhibited little evidence of biomass accumulation or the presence of electrochemically-active metabolites (Figure 4.1a, −0.45 V biofilm). The experiment was repeated, with an applied potential of −0.3 V on the working electrode (this time, corresponding to a greater concentration of oxidized riboflavin on the surface). The CV obtained for this system (Figure 4.1a, −300 mV biofilm) provided evidence for the accumulation of biomass on the electrode surface, based on higher capacitance relative to the abiotic CV. Interestingly, a non-reversible oxidation peak centered at 0.2 V was also

observed and this oxidation species was investigated using further experiments (described below). As a point of reference, a further experiment was performed with an applied positive potential of 0.1 V vs. Ag/AgCl. The CV obtained (Figure 4.1a, +100 mV biofilm) for this system also lacked any evidence for biomass accumulation on the electrode surface. In all four cases, no oxidation or reduction species near −0.45 V vs. Ag/AgCl was detected via CV, indicating the lack of riboflavin or a concentration below limits of detection for *S. oneidensis* biofilms [45]. The lack of riboflavin after 36 hours of polarization without a subsequent addition of lactate may be due to the dissimilation of riboflavin from the cells. Clear riboflavin presence was observed (Figure 4.2) after 36 hours of poised potential (−0.30 V vs. Ag/AgCl).

The specific response of the MR-1 culture to an applied potential of −0.3 V led us to speculate that redox gradients may play a role in biofilm formation under anaerobic conditions. It is plausible that cell-to-cell signaling may be utilized by Shewanella to form biofilms, triggered by the release of specific metabolites under changes in environmental conditions. Electrochemically active metabolites, such as riboflavin, may be retained at the electrode surface and thereby create a redox gradients that directs cell attachment to insoluble electron acceptors. This taxis-like behavior has been previously reported for *S. oneidensis* in response to riboflavin gradients [45].

4.3.2 Electron transfer mechanism in anaerobic biofilms

Building on the evidence that MR-1 can form biofilms under specific growth conditions, the nature of EET was explored, with possible connections to the oxidation species observed at 0.2 V (Figure 4.1a, −300 mV biofilm). A mutated form of MR-1

(ΔMtrC/OmcA) contains a double deletion mutant lacking the MtrC/OmcA multi-heme cytochrome complex. MtrC/OmcA is the terminal protein in the Mtr pathway of *S. oneidensis*, proposed as the electron pathway for DET, linking the metabolic system of the cell to an insoluble electron acceptor [46-48]. When cultured in the electrochemical cell at an applied potential of −0.3 V vs. Ag/AgCl for 36 hours, the ΔMtrcC/OmcA provided compelling insight into the involvement of specific cytochromes in EET. First, there was only a minor change in capacitance between the abiotic electrode and the electrode populated by the ΔMtrcC/OmcA mutant MR-1 (Figure 4.1b), indicating a lack of biomass attachment at the electrode surface. This puts into question the ability for the biofilm to electrochemically communicate with the electrode when lacking this terminal protein.

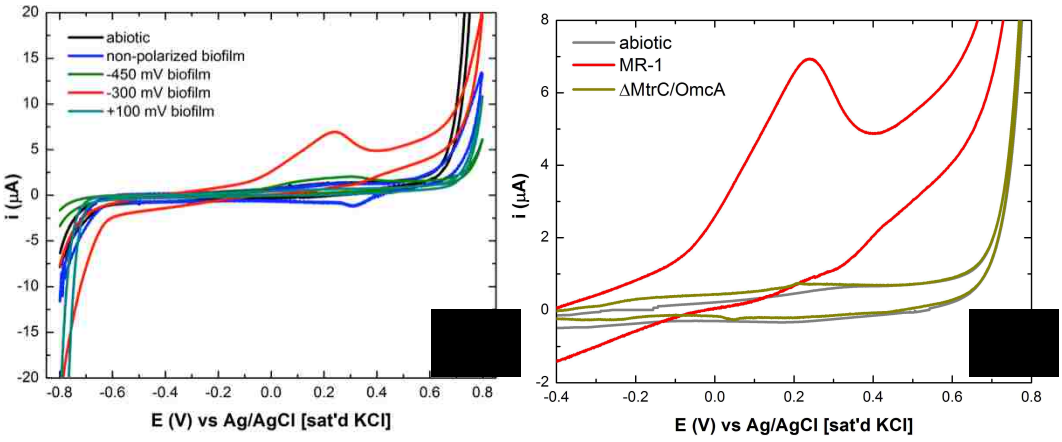

Figure 4.1: a) Cyclic voltammograms of *S. oneidensis*-electrode interaction after 36 hours at different applied potentials, abiotic samples (black), and non-polarized samples (blue). b) Cyclic voltammograms of wild type strain *S. oneidensis* (red), the ΔMtrC/OmcA mutant (green), and abiotic control (gray) after 36 hours of applied potential at −0.3 V vs. Ag/AgCl [49].

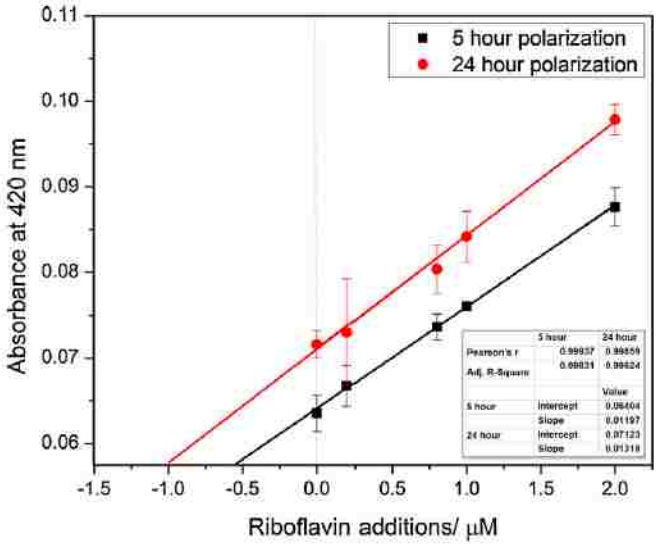

Figure 4.2: Standard addition plots showing the dependence of the electrolyte absorbance at 420 nm from the concentration of the riboflavin additions (spiked samples µM). The absolute value of the x-intercept is equal to the unknown concentration of riboflavin in the tested samples. The red line corresponds to samples taken after 24 hours of electrode polarization. The black line corresponds to samples taken after 5 hours of polarization [50].

4.3.3 Riboflavin docking simulations

Riboflavin was docked first on OmcA since Okamoto et al. demonstrated experimentally that this cytochrome interacts with riboflavin [37]. Figure 4.3 shows the two most probable docking positions for riboflavin (RF). The affinity of the OmcA-RF interactions at the two positions is similar (-7.4 kcal/mol for position 1 and -7.3 kcal/mol for position 2), indicating identical probability for the two models. In the first position RF docks close to heme 5 (RF-heme 5 distance of 5.8 Å) and in the second position, it is located in the proximity of heme 7 (RF-heme 7 distance of 11.2 Å). The closer distance between RF and heme 5 would suggest lower activation energy for the electron transfer and thus faster and more efficient RF reduction by OmcA.

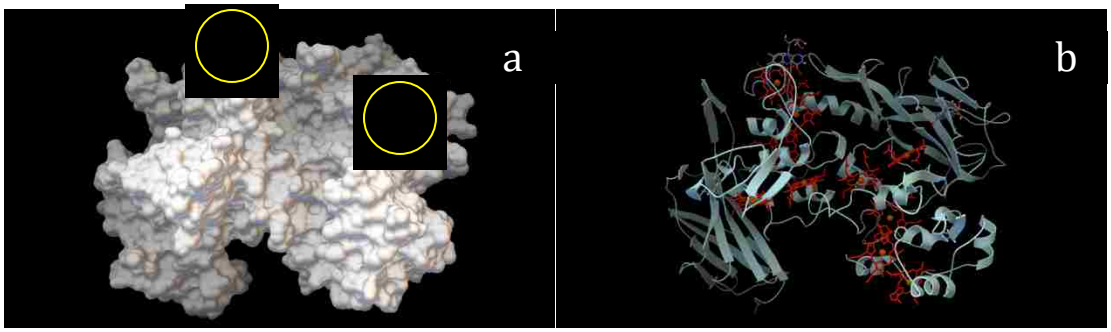

Figure 4.3: Docking of RF on OmcA, where in a) the van der Waals surface of the protein is represented with the two most probable docking positions for RF are circled, and in b) the OmcA cytochrome is represented with its secondary structure with the hemes colored in red. The RF is colored based on the element composition with N in blue, O in red and C in gray.

The binding event of ligands on macromolecules occurs by intermolecular forces, such as ionic bonds, hydrogen bonds, van der Waals or electrostatic forces. When the electrostatic potential was mapped on the van der Waals surface of OmcA, no indication for electrostatic attraction between OmcA and RF was observed (Fig. 4.4a). At the same time plotting the van der Waals surface for both RF and OmcA it can be seen that RF binds on the surface of the protein and does not penetrate the protein molecule (Fig. 4.4b). In addition looking into the shape of the protein surface where the RF docks, it can be speculated that the interactions between RF and OmcA are based on stereo-specificity for both of the docking positions. The same conclusion can be made for the interactions of RF and MtrC (data not shown), where in a similar manner RF occupied protein surface pockets after the docking.

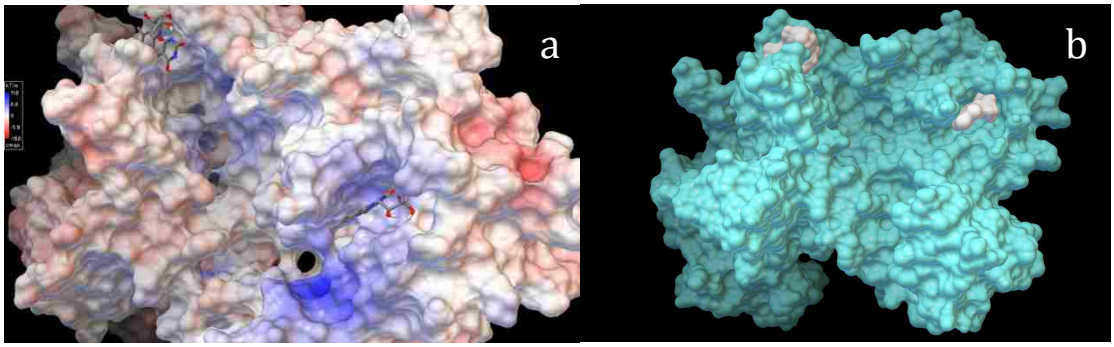

Figure 4.4: a) Docking of RF on OmcA, where the electrostatic potential was mapped on the van der Waals surface of the protein. RF is color coded according to the atom type. b) Docking of RF on OmcA, where the van der Waals surface of the protein is represented in cyan and the van der Waals surface of RF is in white.

4.3.4 Visual confirmation of biofilm and viability

SEM was used to confirm the presence of attached biomass on the electrode surface. For the non-poised anaerobic biofilm (Figure 4.5a), minimal biomass is visible on the electrode surface and even with increasing magnification the presence of biological nanowires is not observed. In contrast, the biofilm formed anaerobically with applied potential at −0.3 V yields significantly greater coverage of biomass on the electrode surface (Figure 4.5b). These SEM images provide further visual confirmation to the electrochemical data suggesting preferential biomass attachment and biofilm formation on the surface of the electrode when a potential of −0.3 V vs. Ag/AgCl is applied during anaerobic culturing.

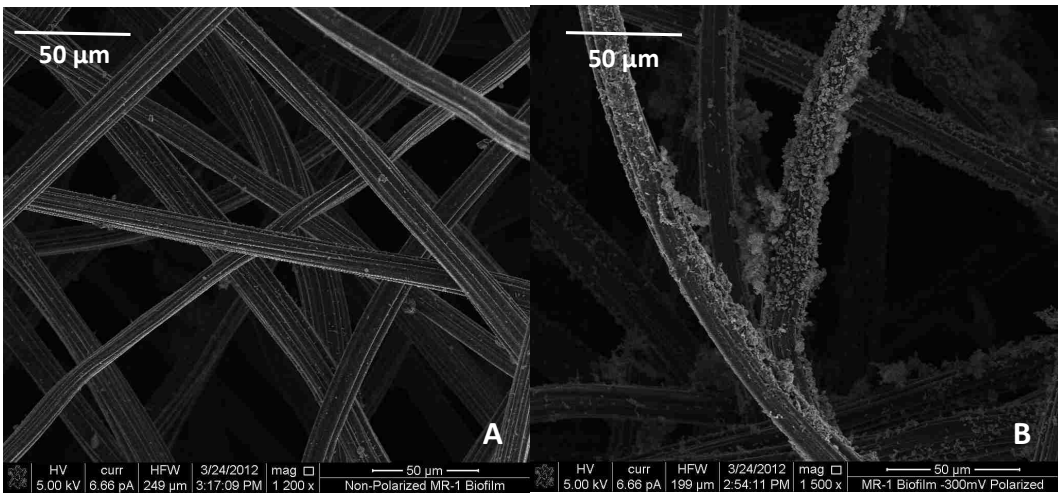

Figure 4.5. SEM images of *S. oneidensi*s under A) non-poised potential biofilm formation and B) applied potential (−0.3 V vs. Ag/AgCl) biofilm formation [49].

Figure 4.6 shows SEM micrographs of *S. oneidensis* attached to the anodes after 5 and 24 h of electrode polarization. Few cells are observed attached at 5-hour polarized electrodes indicating that this anode is at the initial stage of biofilm development. The 24-hour samples have fully formed biofilm coverage with abundant exopolymeric substance encasing attached cells.

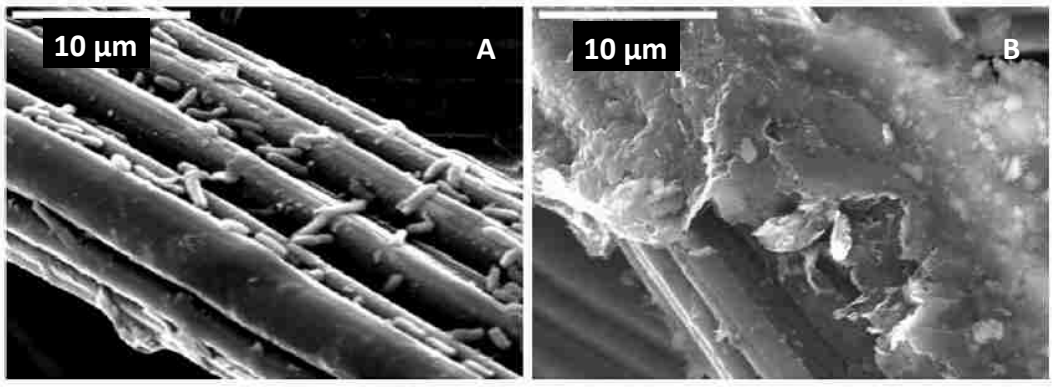

Figure 4.6: SEM images of electrodes after A) 5 hours and B) 24 hours of polarization subjected to a constant potential of −0.30 V vs. Ag/AgCl and image acquisition accelerating voltage of 15 keV [50].

Fluorescence microscopy images of carbon felt electrodes poised at −0.30 V were taken after the electrochemical measurements (Figure 4.6). Syto 13 green fluorescent nucleic acid stain was used to stain live cells and propidium iodide red fluorescent nucleic acid stain to detect unlived bacterial cells. The image shows abundance of live *S. oneidensis* cells attached to the fibers of the carbon felt electrodes, which indicates that the formed biofilm contains functional bacterial cells. The background of the fluorescence image is green due to the thickness of the carbon felt material and the amount of attached bacterial cells surrounding it.

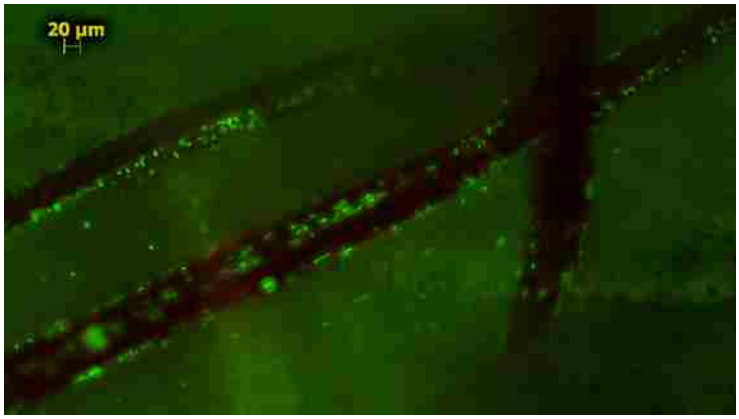

Figure 4.7: Fluorescence microscopy images of carbon felt electrodes after 36 hours of polarization at −0.3 V vs. Ag/AgCl [49].

4.4 – Conclusions

A docking program has been explored as a tool of revealing the OMCs-flavin interactions, predicting various possible docking positions for RF on OmcA and MtrC. It was suggested that OmcA could interact with RF through hemes 5 and 7, where the

binding affinity of RF-OmcA complex is slightly higher than the FMN-OmcA along with a shorter flavin-Fe-heme distance. Both of these parameters indicate better interaction of OmcA with RF in regards to FMN. Three identical docking positions were identified for RF on MtrC (close to hemes 2, 9 and 7). A hypothesis for the MtrC-OmcA complex and OMCs-flavin interactions has been stated. According to this hypothesis OmcA can interact with RF through heme 7.

These simulations were coupled with electrochemical, microscopy and spectrophotometric analysis that evaluate the role of RF when *S. oneidensis* is in contact with an electrode surface in which EET can occur. The amount of secreted RF were calculated at different stages of biofilm formation and compared. It was deduced that the amount of RF secretion was more abundant when the anodes are subjected to an applied potential of -0.3 V vs. Ag/AgCl reference electrode for a period of 24 to 36 hours. In addition, MtrC/OmcA cytochrome-lacking mutants showed the importance of this macromolecular complex in EET and MFC performance by showing poor bacterial electrochemical activity in comparison to their wild type counterpart.

Future studies will consist of similar simulations work regarding FMN and its interaction with OmcA and MtrC. Similarly, experimental work will be focused on the quantification of FMN in a MFC system under varying electrochemical parameters in order to verify the assertion that FMN secretion exceeds RF [20].

Chapter 5 - Surface Modification for Enhanced Biofilm Formation and Electron Transport in *Shewanella oneidensis* Anodes

5.1 - Introduction

The possibility to directly convert the energy of chemical bonds into electricity has been recognized as an alternative and effective approach for energy transformation. This quest has been embodied in electrochemical devices including batteries and fuel cells. Commonly used batteries and fuel cells employ inorganic catalysts and harmful, costly electrolytes. In order to overcome the limited reserve of noble metals usually used and avoid the use of harmful compounds, a new avenue of electrochemical systems has been developed. These new systems rely on bio-catalytic ability of enzymes and microorganisms in fuel cells [51]. The latter has gained attention of researchers, government agencies and industry driven by, among other things, the potential for combining efficient wastewater purification with concomitant electricity production. This achievement will provide an opportunity for the development of portable, self-sustaining wastewater treatment units. The electrode material and its properties are a key component, determining the performance and cost of Microbial Fuel Cells (MFCs) [52]. Therefore, electrode design is one of the greatest challenges in making MFCs a cost-effective and scalable technology [53–58]. Among the general requirements, such as good conductivity, chemical stability, mechanical strength, high surface area and low cost, anode materials should posses several key characteristics that will determine the rate of bacteria-electrode interactions. These are, but not limited to: i) high surface roughness; ii) biocompatibility; and iii) surface chemistry that enhances bacterial attachment and

electron transfer [51-59]. Based on these requirements, various surface modification techniques have been explored and recognized as a new avenue for MFCs optimization. In addition, it has been established that increased biofilm formation and bacterial coverage leads to increased MFCs current generation [55,59–61]. At the same time, the electron transfer rate from bacteria towards the electrode surface was proven to be one of the most important factors determining the performance of those systems [8,38,62]. Both of these factors strongly depend on the electrode material properties, such as real surface area, conductivity, hydrophilicity and surface chemistry.

Commonly used materials for supporting bioelectrodes include a vast variety of carbonaceous materials that differ significantly in morphology, surface area and hydrophilicity [27,29,61,63]. These materials can be modified to provide higher bacteria adhesion and increased biofilm formation and development [52]. Modification techniques include surface treatments with physical or chemical methods, immobilization of conductive and electro-active polymers, as well as deposition of various metals or metal seeds [53,57,58,64]. In addition, surface chemical or electrochemical oxidation can also be an effective treatment method for enhanced bacteria-electrode interactions [59]. Surface chemistry modification techniques such as benzene diazonium treatment [65] and ammonia gas treatment [65] provide a positively charged electrode surface, which as been speculated to be beneficial for bacterial attachment [53,59,61,65]. In addition, simultaneous utilization of nitric acid and sulfuric acid, provide surface oxidation and introduction of oxygen containing groups. This modification approach increased the ratio of saturated/unsaturated carbon on the surface and consequently decreased the electrode resistance, which also had a positive effect on bacteria attachment and biofilm formation

[59] Another example of electrochemical oxidation of the electrode material resulted in a significant increase in current produced from MFC graphite anodes over MFCs containing untreated anodes [66]. These methods, however effective, are not optimal for large-scale applications due to cost, safety chemical handling and technical requirements. Therefore, we propose a simple, fast and effective and therefore low-cost surface modification method for enhanced biofilm formation, increased electron transfer rate, and thus higher current density generation. This method focuses in lowering the degree of hydrophobicity of the anode material and consists of partial oxidation of carbonaceous material by UV/O_3 treatment [67]. In this process, a UV/O_3 irradiation chamber utilizes UV light to excite ambient O2 molecules, thus lowering their activation energy and moving them into a more reactive state. The interaction between highly reactive oxygen and carbon atoms from the carbon felt structures leads to the formation of different functional groups at surface, including –OH, –COOH, =O, =CO and –CO. The introduction of such functional groups allowed for the increase in the surface wettability of the material [68-70]. The procedure provides a type of surface treatment that can be carried out at atmospheric pressures thus, lowering treatment cost, and minimizes damaging effects inherent in other treatment techniques such as strong acid oxidation [66]. The influence of the UV/O_3 time of exposure to the material surface chemistry and morphology was examined and correlated with the electrochemical performance of these electrodes when explored in Shewanella oneidensis MFCs.

It is known that the degree of hydrophobicity/hydrophilicity and surface charge of the material are very important parameters regarding the enhancement of bacterial anode attachment and thus, improved extracellular electron transfer (EET). [REF] The latter

leads to higher MFC overall performance with both pure and mixed cultures [61,64]. The current start up time in MFCs is a crucial parameter that is highly influenced by the EET rate and is therefore carefully taken into consideration in our electrochemical characterization methods. We have shown that the start up time of MFCs inoculated with wastewater was also decreased by electrochemical oxidation of the anode, introducing different surface chemistries [59,61].

S. oneidensis utilizes several biomolecules that take part in EET. It is know that metabolites such as flavins along with and even in association with outer membrane proteins (cytochromes) play an important part in this process [8,36]. In particular, riboflavin molecules secreted by *S. oneidensis* present electrochemical activity at the biofilm-electrode interface [8] and more importantly play the role of a cofactor for the outer membrane cytochrome OmcA. In these studies, we verified the importance of riboflavin in the EET by showing a direct correlation between riboflavin-enriched anodes and anodic performance.

5.2 – Experimental

5.2.1 Electrode surface modification

Surface modification relied on partial oxidation of carbon material by UV/ozone treatment. Carbon felt disks with 1.2 cm in diameter were treated at different UV/ozone exposure times ranging from 0 to 60 minutes using a UV/O_3 cleaner 144AX (Jelight Company, Irvine, CA). As a benchmark, a carbon felt electrode was treated with Isopropyl alcohol (IPA) for 10 min and rinsed 3 times in sterile buffer.

5.2.2 Electrochemical testing

The electrochemical experiments were conducted in a three-electrode electrochemical cell with a reference electrode (saturated Ag/AgCl), a platinum wire counter electrode and a carbon felt as the working electrode (1.2 cm in diameter) [50]. *S. oneidensis* MR-1 suspended in 50 mM phosphate buffer was introduced in the cells prior to electrochemical experiments. All electrochemical tests were done using a Gamry Reference 600 potentiostat (Gamry Instruments, Warminster, PA). Chronoamperometry studies were performed for 24 hours at a constant potential of −0.30 V vs. Ag/AgCl. Potentiostatic polarization curves were carried out based on several chronoamperometry steps starting from open circuit potential to 0.30 V vs. Ag/AgCl with a step of 0.05 V. The electron transfer mechanism was examined via cyclic voltammetry in the potential region of −0.45 V to 0.40 V vs. Ag/AgCl at a scan rate of 10 mV s−1. The electrochemical cell was purged with nitrogen and sealed with Parafilm (Sigma) throughout the experiments to maintain micro-aerobic conditions [50].

5.2.3 Determination of riboflavin content

Cyclic voltammetry measurements of the *S. oneidensis* anodes after 24 hours of potentiostatic polarization were carried out at various scan rates. A couple of redox peaks associated with the riboflavin oxidation/reduction was observed, and a linear dependence of the peak currents from the scan rate was detected. This analysis indicates surface confined electrochemistry, which allows the utilization of the following equation for the

calculation of the riboflavin surface coverage (Γ_o^*, mol cm^{-2}) [71]:

$$i_p = (n^2F^2/4RT)\vartheta A\Gamma_o^* \qquad \textbf{Equation 5.1}$$

where i_p is the peak current (A), n is the number of electrons necessary for riboflavin redox transformation, F is the Faradaic constant, R is the universal gas constant, T is the temperature in K, A is the surface area of the electrodes (cm^2) and " is the scan rate (V s^{-1}). The riboflavin surface coverage was calculated first based on the geometrical surface area and then normalized to the electrochemical accessible surface area (ECSA).

5.2.4 Scanning electron microscopy

Scanning electron microscopy (SEM) analysis was used for visual confirmation of biofilm formation on the carbon-felt electrodes after the electrochemical characterization. Upon completion of these studies, bacterial cells were fixed to the electrode using a 2.5% glutaraldehyde solution for 24 hours and then exposed to increasing concentrations of ethanol (50, 60, 70, 80, 90, 95, and 100%) ending in 3 separate washes of 100% ethanol. The samples were then dried by immersion in 50% (v/v) hexamethyl-disilazane (HMDS) in ethanol for 15 min, followed by 15 min in 100% HMDS and finally air exposure overnight. The samples were then coated with a 15 nm layer of gold-palladium using an Emitech K950X sputter coater. A Hitachi S-5200 Nano SEM was used to capture the samples' images at an accelerating voltage of 10kV.

5.2.5 X-ray photoelectron spectroscopy

Surface chemistry of the carbon felt materials modified through partial oxidation by different times of exposure to UV/O_3 were characterized using XPS analyses. XPS measurements were performed with a Kratos Axis Ultra DLD X-ray photoelectron spectrometer using a monochromatic Al Kα source operating at 225W. Survey and C1s, O1s and N1s high-resolution spectra were acquired at 80 and 20 eV pass energy, respectively. Charge compensation was not necessary. The data obtained are average of 3 different areas per sample.

Data analysis and quantification were performed in CasaXPS software. A linear background was used for quantification. Quantification utilized sensitivity factors that were provided by the manufacturer. High-resolution C 1s spectra were curve-fitted using individual peaks with 70% Gaussian / 30% Lorentzian (GL (30)) peak shape and 1.0 +/- 0.2 eV full width at half maximums (FWHMs).

5.2.6 Evaluation of electrochemical accessible surface area (ECSA)

The ECSA of the carbon felt electrodes after their modification was evaluated based on changes in materials capacitance [72]. Cyclic voltammetry of the electrodes in 50 mM phosphate buffer was carried out to determine the capacitance of the modified carbon felts experimentally. The ECSA was determined using the following equation:

$$ECSA = i/(2 * \upsilon * C_{sp}) \qquad \textbf{Equation 5.2}$$

where C_{sp} is the specific capacitance, *i* is the difference in the anodic and cathodic current at a chosen potential, and υ is the scan rate in V s^{-1}. The specific capacitance for the carbonaceous material was taken to be 35 μF cm^{-2} only for electrode comparison, and *i* under nitrogen conditions was taken at a scan rate of 10 mV s^{-1} to calculate the ECSA.

5.3 – Results and Discussion

As stated previously, *S. oneidensis* MR-1 is a model organism in MFCs due to its capability to transfer electrons across the outer cell membrane to reduce the number of alternative electron acceptors beside oxygen. Among the terminal electron acceptors for *S. oneidensis* are Mn (IV) and Fe (III) oxides, which can be replaced by solid supports such as electrodes and exploited in the development of MFCs [73-75]. Previous studies have shown that, after 24 h of polarization, when an *S. oneidensis* biofilm is covering the electrode surface, the number of cells attached to the surface was defined mostly by the ECSA and the expanded uncertainty of the anode's response decreased significantly when the current was normalized to that parameter [50]. At the same time, our group has also demonstrated the importance of the hydrophilicity and surface morphology on bacteria attachment and the dynamics of biofilm formation determining the start up time of MFCs [29]. Therefore in this study the important parameters related to the properties of the electrode material have been examined. These include electrochemical accessible surface area of the electrodes, their resistance and surface chemistry as well as *S. oneidensis* biofilm formation, riboflavin accumulation, and anode performance.

5.3.1 Surface chemistry and morphology

X-ray photoelectron spectroscopy (XPS) was used to study the changes in the surface composition of the materials as a result of the oxidative etching. Table 1 summarizes the evaluated chemistry. According to XPS data, the performed modification procedure led to several oxygen content variations. That is, a linear dependence between the time of UV/O_3 exposure and the amount of carboxyl and hydroxyl groups was observed as shown in Figure 5.1a. At the same time, a decrease in the amount of sp2 carbon was also seen (Figure 5.1b).

Table 5.1: XPS data for carbon felt electrodes exposed to UV/O_3 at different treatment times.

Sample	C 1s %	N 1s%	O 1s %	C=C %	C-O %	C-OH %	C=O %	COOH
0 min	88.4	0.9	10.7	46.5	12.0	4.7	7.8	4.0
2 min	87.6	0.7	11.6	45.7	14.9	5.3	8.0	3.8
5 min	86.5	0.7	12.8	46.4	13.8	5.0	7.9	4.6
10 min	90.5	0.6	8.9	41.3	13.2	5.4	7.5	4.1
20 min	87.8	0.6	11.6	34.0	12.0	6.4	9.4	3.7
30 min	82.1	0.6	17.3	39.4	14.9	7.0	10.8	5.4
60 min	82.1	0.7	17.2	22.6	13.2	8.4	13.2	4.8

The increase in oxygen containing functional groups should most likely cause an increase in the hydrophilicity of the electrodes and thus enhance the biofilm formation and development. It was also suggested that the decrease in C=C bonds leads to a decreased

resistance as was observed before, [59] but no such observation can be made here. The resistance of the modified electrodes in this study, determined via electrochemical impedance spectroscopy, increased with the increased time of UV/O_3 exposure or with the decreased amount of C=C bonds. The resistance of the untreated carbon felt electrode was 24 Ω increasing to 136 Ω after 20 min of UV/O_3 exposure, reaching 285 Ω and 366 Ω after 45 and 60 min of UV/O_3 exposure, respectively. This observation, besides being controversy to previous studies, is expected since the electrons in carbonaceous materials are being transferred through the C=C bonds. The oxidative etching of carbon materials creates defects and holes in their structure increasing their specific surface area. The electrochemical accessible surface area was calculated using electrode capacitance. It is important to clarify that the ECSA determined from this study can only be used for relative comparison of the studied materials. From the increase in the amount of oxygen with longer exposure time, we can assume that the ECSA will also increase. Figure 5.1c shows the dependence of the electrode ECSA on the time of UV/O_3 exposure. The increase of the ECSA with the treatment time confirmed our assumption and raised another hypothesis that increased surface area available for bacteria attachment and biofilm growth will improve the anode performance. It is well known that more porous materials typically produce higher current densities per geometrical surface area compared to their smoother counterparts. It has been also established that electrochemical accessible surface area of carbon felt is a limiting factor when *S. oneidensis* biofilms are formed [50]. Therefore we expected increased anode current densities at higher UV/O_3 exposure time besides the increasing electrodes resistance.

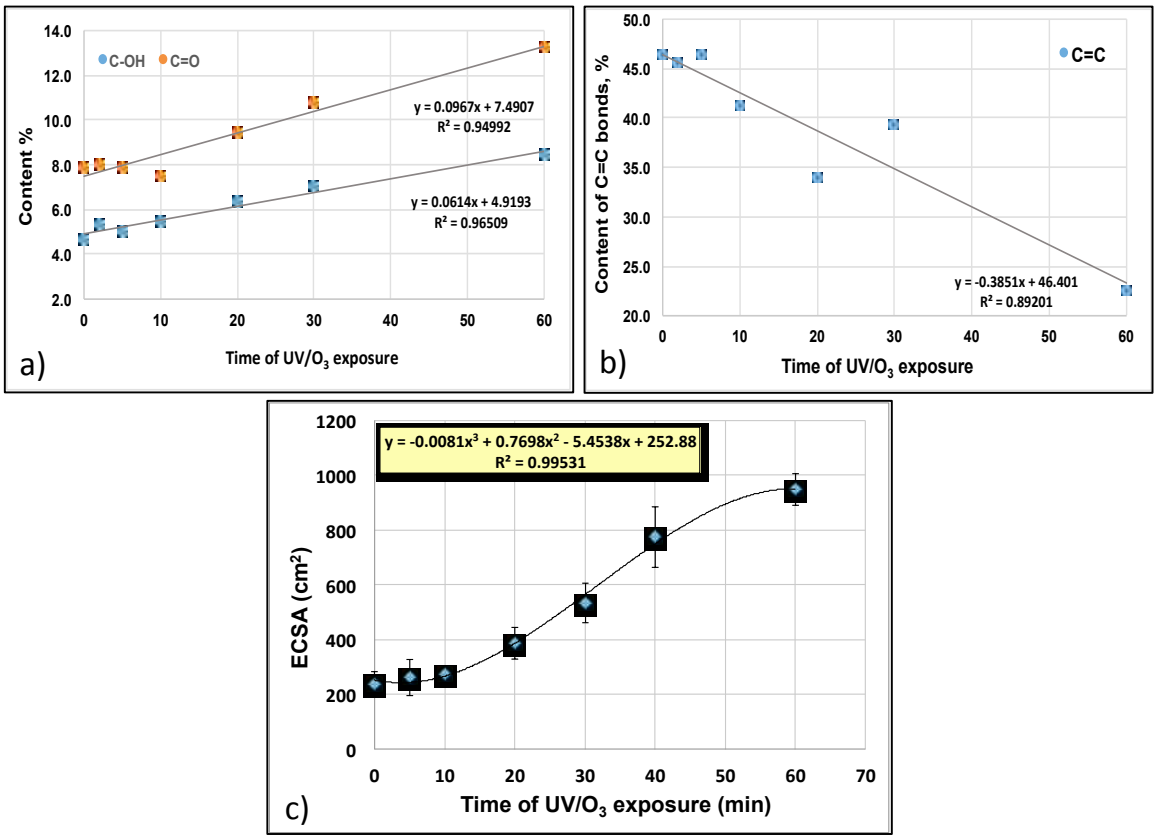

Figure 5.1: Dependence of a) C-OH, C=O, b) C=C bonds from the time of UV/O_3 exposure and c) Electrochemical accessible surface area of carbon felt electrodes treated at different UV/O_3 times of exposure.

5.3.2 Electrochemical performance and biofilm coverage

It has been established that biofilm formation for Shewanella oneidensis MR-1 occurs preferentially on an electrode polarized with a constant potential of −0.3 V vs. Ag/AgCl [50]. Biofilms formed under these conditions yield behavior indicative of mediated electron transport (MET) at lower potentials and direct electron transport (DET) from outer membrane-bound multiheme cytochromes at potentials above 0.00 V vs. Ag/AgCl [50]. All electrodes were subjected to a constant potential of −0.3 V for 24 hours while current production was recorded (Figure 5.2a).

Additional lactate was introduced into the electrolyte after 10 hours of operation to ensure fuel excess. The observed maximum current for 20 and 45 min treated electrodes reached roughly 32 μA after 24 hours. At the same time, the electrode treated by 60 minutes of UV/O_3 exposure exhibited maximum current similar to those of IPA-treated carbon felt, used as a benchmark, which was notably lower then the rest of the modified electrodes. No significant current was detected when using untreated carbon felt. The increase in generated current for the 45 min treated electrode after 7–8 hours of polarization was an indication of initial biofilm formation as it has been observed previously [50]. The start up time for 20 min treated electrode was significantly higher than the 45 min electrode indicating slower biofilm development. After 24 hour of constant electrode polarization we expected that the 20 and 45 min treated electrodes would possess higher bacterial coverage than all electrodes studied.

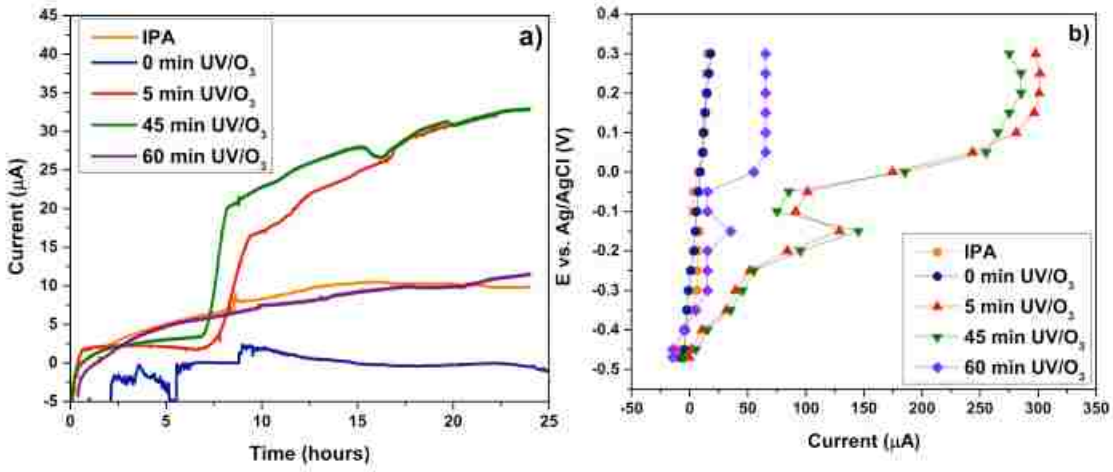

Figure 5.2: a) Chronoamperometry measurements of *S. oneidensis* on treated and non-treated carbon felt electrodes at applied potential of -0.3 V and b) Polarization curves of *S. oneidensis* on treated and non-treated carbon felt electrodes after 24 hours of applied potential of -0.3 V.

The polarization curves taken at the end of the chronoamperometry measurement showed a similar trend in anodes performance, where 45 min time point presented the highest performance among all samples (Figure 5.2b). The shape of the recorded polarization curves is in accordance with previous studies of *S. oneidensis* anodes, demonstrating the ability of these bacteria to exhibit both MET and DET at the proper potentials. It is clear that the electrode modification through UV/O_3 partial oxidation promotes DET and provides higher surface for direct contact between bacterial cells and electrode surface which may be due to both increased hydrophilicity [67-70] of carbon felt and increased ECSA (Figure 5.1c and Figure 5.3). SEM of the ozonized carbon felts demonstrated the highest bacterial coverage on samples treated with 45 min of UV/O_3 (Figure 5.3), whereas untreated electrodes supported the lowest amount of bacterial attachment. Although the electrode subjected to 60 min of UV/O_3 oxidation had the highest ECSA (Figure 5.1c), the bacteria coverage was lower than the 45 min treated anode (Figures 5.3 and 5.4). In contrary to the highest ECSA the 60 min treated electrode possessed the highest resistance (366 Ω), which was 1.3 times higher than the resistance of 45 min treated carbon felt and 2.7 times higher than 20 min treated electrode. The latter suggests that the increased electrode resistance is additional factor regulating bacteria attachment and biofilm growth and development. The order in which the current densities generated by the electrodes increase follows the order in which the bacterial coverage changes, demonstrating an expected correlation between MFC performance and biofilm formation on the surface of the anode [29,55,60].

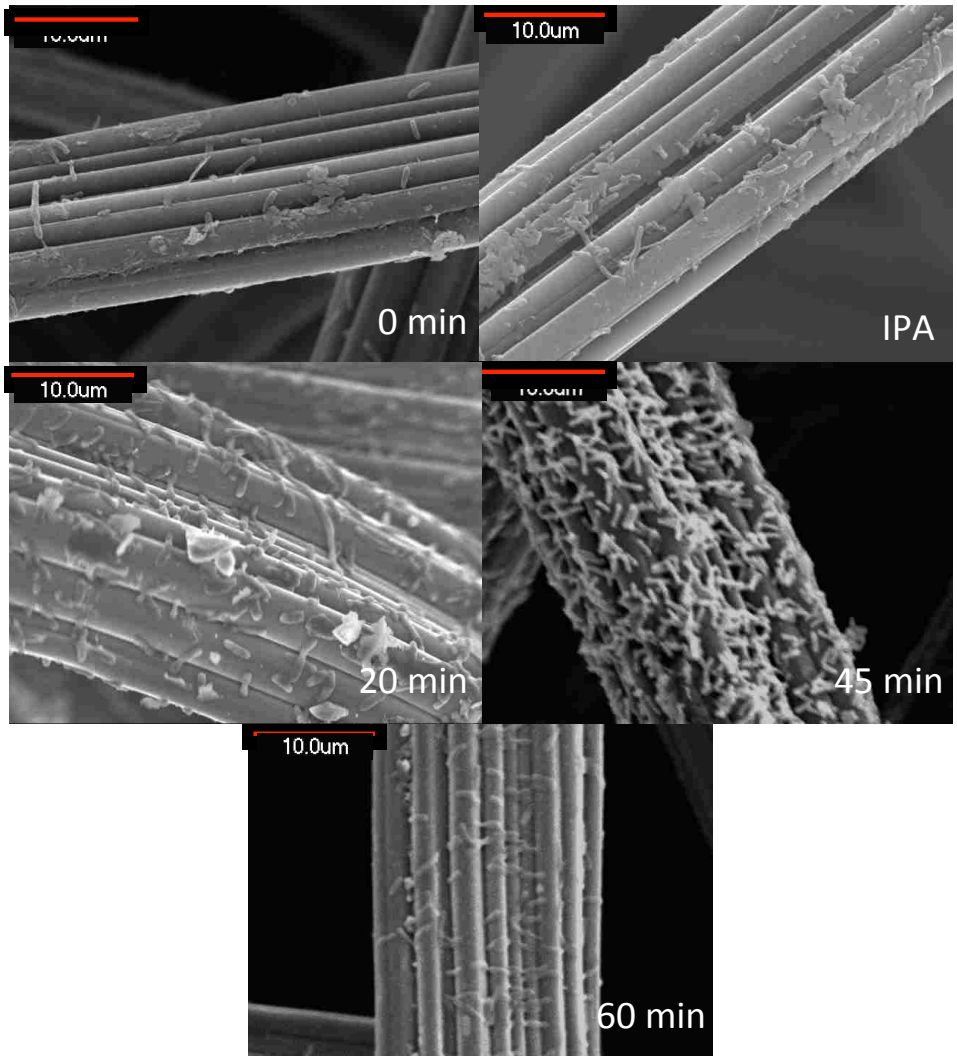

Figure 5.3: SEM images of carbon felt electrodes subjected to different times of UV/O_3 exposure taken after electrode polarization and electrochemical characterization.

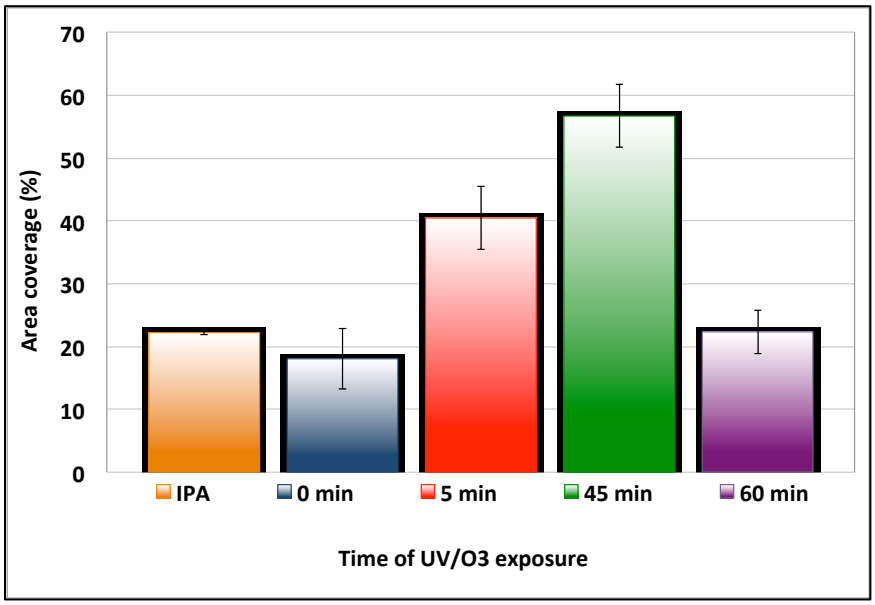

Figure 5.4: Bacterial surface area coverage on carbon felts treated at different UV/O_3 times. The area coverage was calculated after processing SEM images through Image J.

5.3.3 Detection of metabolites implicated in extracellular electron transfer

Cyclic voltammograms of the tested *S. oneidensis* anodes (Figure 5.5) demonstrate increasing capacitance with the increasing time of UV/O_3 exposure, which can be explained by the increasing ECSA of the treated electrode materials. One can also identify peaks that can be attributed to both MET and DET as it has been observed before [50]. The first couple of redox peaks with formal redox potential ($E^{\circ`}$) of approximately -0.45 V vs. Ag/AgCl can be assigned to the reversible electrochemical transformation of riboflavin, a metabolic product known to play a key role in the extracellular electron transfer in *Shewanella spp* [8]. The catalytic wave with half wave potential ($E_{1/2}$) at 0.02 V vs. Ag/AgCl is due to DET carried out through the outer surface cytochromes. And the

irreversible oxidation peak at potentials at 0.40 V vs. Ag/AgCl was ascribed to cytochromes' oxidation at the electrode surface [49, 50]

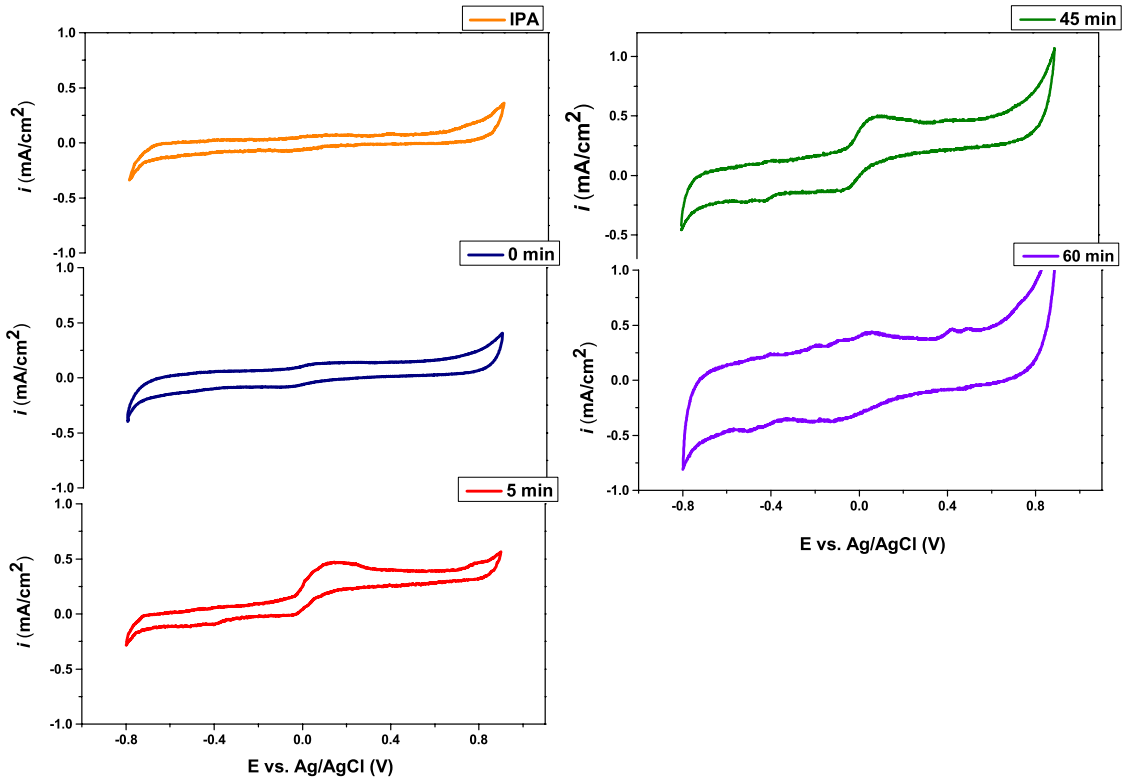

Figure 5.5: Cyclic voltammograms of carbon felt anodes treated through UV/O_3 for various time of exposure.

In order to quantify the amount of riboflavin secreted by bacteria in contact with the anodes, cyclic voltammograms were generated at scan rates varying from 5 mV s^{-1} to 200 mV s^{-1}. Plotting the peaks current associated with the riboflavin redox reaction versus the scan rate, a linear trend line was found, which indicated surface confined reaction of riboflavin reduction. Therefore, we can claim that the peaks observed at potentials around -0.30 V vs. Ag/AgCl are due to riboflavin oxidation/reduction, when it is adsorbed on the

electrode surface as previously demonstrated when electrodes were colonized with *S. oneidensis* biofilms [8].

Riboflavin molecules are implicated in DET pathway of *Shewanella* anodes [36], with flavins enhancing the electron transfer through the outer membrane cytochromes as bound cofactors, not as free-form flavins. This concept for EET is also found in the model organism *Geobacter sulfurreducens*, which secrete flavins at concentrations comparable to those of *S. oneidensis* and exploits these for enhanced communication with an electrode [38]. For *S. oneidensis* bioelectrodes, flavins adsorbed on the anode interact with MtrC or OmcA proteins found on the outer membranes and nanowires and enhance the enzymatic reaction [49].

Riboflavin secretion by *S. oneidensis* is a sensor and response to redox changes, and as such, it promotes cell attachment and biofilm formation [49]. In this model, riboflavin is retained at the electrode surface and we hypothesize that by that it creates a redox gradient that can be sensed by bacteria and directs cell swimming towards the electrode surface and attachment.

The amount (nmol cm^{-2}) of riboflavin adsorbed on the electrodes was determined based on the response of the peak current to riboflavin concentration [71]. Since the geometrical surface area is not representative of the specific surface area of the materials, the amount of riboflavin adsorbed was calculated based on both the geometrical surface area and the ECSA (Figure 5.1c). During flavin-mediated electron transfer, one electron is transferred between the outer membrane cytochromes and flavin mononucleotide (FMN), resulting in the formation of semiquinone rather than fully reduced FMN [36]; therefore we based our model on such a 1-electron transfer. Figure 5.6a shows a linear correlation between

the riboflavin coverage and the UV/O_3 treatment time when the riboflavin coverage was normalized to the geometrical surface area of the electrode. In contrast, when the riboflavin coverage was normalized to the ECSA a polynomial dependence was observed with highest amount of riboflavin adsorbed on 45 min treated electrodes, followed by 20 min oxidized one (Figure 5.6b), which also showed the highest current densities (Figure 5.2b). This observation is in accordance with the hypothesis that flavins are involved in DET and that respiratory current from dissimilatory metal reducing bacteria is strongly coupled to the amount of electrochemically active flavins.

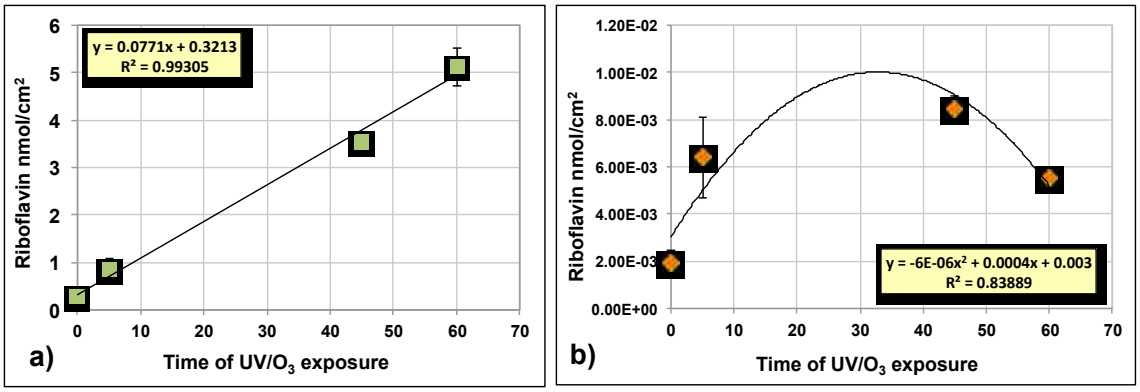

Figure 5.6: Riboflavin coverage at the electrode surface, calculated based on: a) the electrode geometrical surface area; b) the ECSA.

It has previously been shown that oxidized graphite can adsorb and retain higher amounts of mediator, most likely due to the increased specific surface area of the electrodes [63]. The same observation can be made in this study. Increasing the time of UV/O_3 exposure provides higher electrochemical accessible surface area, increased amount of oxygen containing groups and thus increased amount of adsorbed riboflavin.

EET via MtrC-bound flavins present a more efficient electron transfer rate as opposed to free-flavin molecules [8.38]. This is due to the ability of soluble flavin to be adsorbed at

the surface of the electrode. Our reports corroborate these findings after performing further electrochemical studies. These consisted of non-treated UV/O_3 carbon felt electrode incubated in a solution of 1 mM riboflavin for 24 hours prior to electrode polarization in the MFC. The results were compared to measurements in the absence of additional riboflavin from non-treated carbon felt.

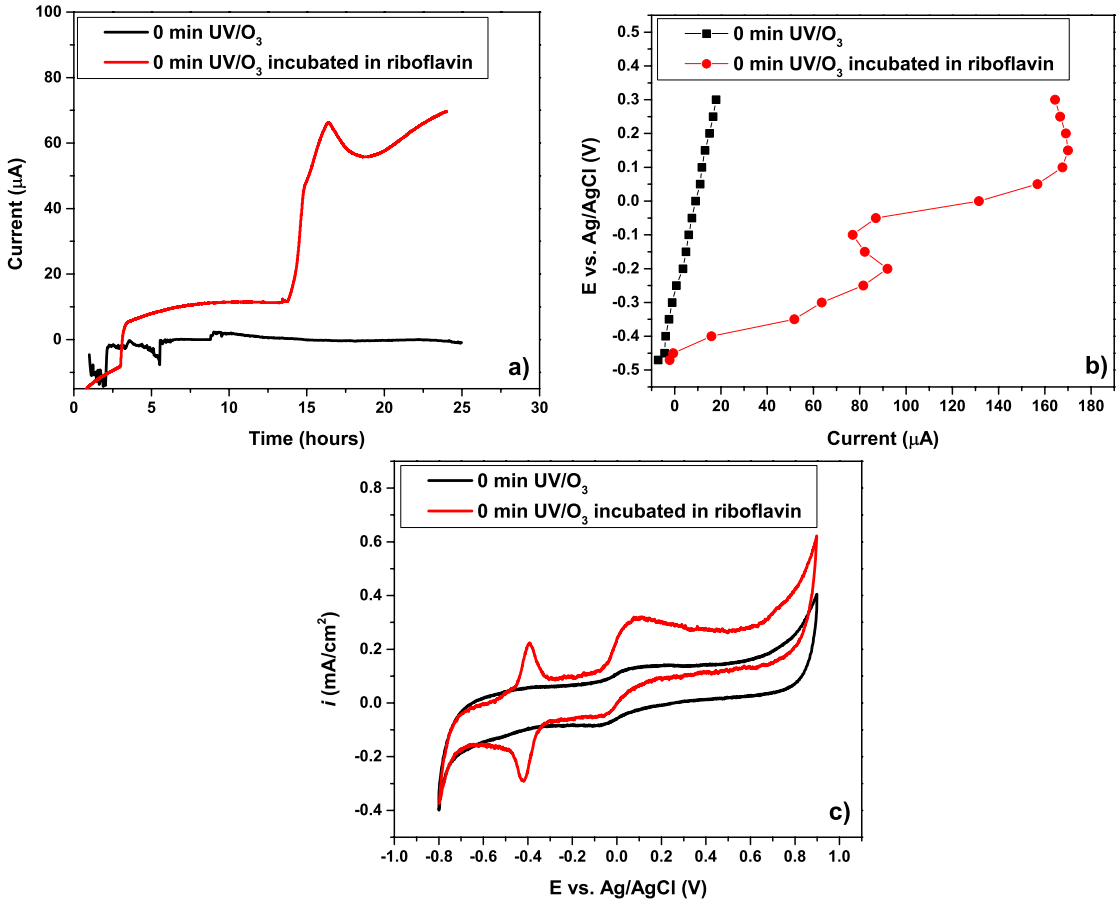

Figure 5.7: Electrochemical measurements from non-treated carbon felt electrodes (0 min) incubated in riboflavin solution prior to Shewanella inclusion (red trace) and when no additional riboflavin is included (blue trace). a) Chronoamperometry of *Shewanella*. b) Polarization curves c) Cyclic voltammograms.

We found that the electrode incubated in riboflavin for 24 hours prior to electrochemical experiments demonstrated higher current generation during the polarization step, greater anode performance and higher CV peaks associated with riboflavin oxidation/reduction in comparison to the unmodified anode (Figure 5.7). We speculate that by introducing additional riboflavin molecules to the electrode surface, which are readily available to interact with the outer membrane cytochromes and leads to enhance electrochemical behavior.

5.4 - Conclusions

Electrochemical studies have been performed on *S. oneidensis* utilizing UV/O_3 treated carbon felt electrodes. The proposed treatment is a simple, low-cost, and effective method, which can be easily exploited for modification of high surface anode materials. Carbon electrodes exposed to 45 min of surface treatment provided the best electrochemical results and richer bacterial cell attachment. This was further confirmed via SEM imaging and analysis. In addition, we have shown that enrichment of the electrode surface with flavin correlates with the increased anodic performance. This observation is in accordance with the hypothesis that flavins are involved in DET.

Chapter 6 - Relationship between surface chemistry, biofilm structure, and electron transfer in *Shewanella oneidensis*

6.1 – Introduction

Optimization of underlying MFC processes is critical for efficient and cost-effective bioelectrochemical system operation and practical commercialization. Particularly with respect to improving biofilm development and the rate of electron transfer from bacteria to the electrode [3,76]. Both biofilm formation and electron transfer rates are strongly dependent on electrode material properties, including surface chemistry and morphology, surface area, and conductivity [8,52,76]. A better understanding how electrode properties affect biofilm performance is, therefore, likely to guide development of improved bioelectrochemical system designs.

Several surface modification techniques have been explored to enhance bacterial adhesion and increase biofilm formation, including physical (thermal) and chemical treatments, immobilization of conductive and electroactive polymers, and deposition of various metals or metal seeds [52,53,59,77,79]. Attachment surface charge and wettability (hydrophilicity/ hydrophobicity) may be particularly important to the growth, development, and properties of bacterial biofilm and optimization of MFC performance [55]. Positively charged and hydrophilic surfaces were shown to improve attachment of the electrogenic Geobacter, and therefore improved electroactive biofilm growth and development [55]. We previously reported the importance of hydrophilic moieties and surface morphology on bacterial attachment, dynamics of biofilm formation, and MFC performance [29]. While previous studies have significantly expanded our understanding

on how anode surface modifications affect power output, the influence of different functional groups on biofilm properties, and, therefore, subsequent MFC performance is still not well understood [52,58,79-81]. We used self-assembled monolayers (SAMs) as electrodes to systematically evaluate well-defined surface chemistries' influence on MFC performance [55]. SAM-modified gold electrodes were used to eliminate the morphology effects associated with conventional 3D structured carbonaceous electrodes.

Angle-resolved XPS (ARXPS) can be utilized for collecting information from different depths of biofilms grown on solid supports without removing the top surface layers [82]. Biofilm chemical composition and its overall thickness can be discerned from ARXPS analyses. ARXPS has been also widely used to study SAMs and biomaterials [83-88]. ARXPS was applied in the current research to study substratum surface chemistry before, after, and during biofilm development. Biofilm thickness and heterogeneity, as determined by confocal laser scanning microscopy (CLSM), have also been shown to vary with electrode surface chemistry [55]. However, CLSM and similar techniques are usually presented qualitatively. Thus, further analysis on the relationships between morphological and performance parameters are necessary in order to achieve quantification of microscopic images [89-91]. Previously, we demonstrated a methodology for extracting quantitative morphological information from microscopic images by digital image processing and correlating this information with the activity of electrodes in MFCs [29,58,59].

To compare biofilm structures, researchers have used different parameters, such as biofilm volume, thickness, volume to surface ratio, and roughness. A set of more comprehensive parameters that describe heterogeneous biofilm morphology in three

dimensions was recently recommended [89-91]. CLSM is suitable calculating parameters related to three-dimensional morphology and other critical dimensions of biomass, as it allows acquisition of images of fully hydrated biofilms at high spatial resolution in lateral and vertical directions. This study relates biofilm areal, volumetric, and textural parameters properties to electron transfer rates and efficiency. Areal metrics, such as cluster size, inter-cell distances, and orientation of cell clusters, may be responsible for transport properties. The variability of biofilm clusters as captured by fractal dimension (FD) might be associated with hydrodynamics. Volumetric parameters include biofilm volume, i.e., a total volume of biomass in the biofilm, and biomass roughness describing thickness variation in biomass. Textural parameters show variations in image gray level, which can be caused by local biofilm density, thickness, and color variations. Textural parameters measure the properties of the cell clusters and inter-cluster spaces based on the likelihood that pixels of similar or dissimilar types are neighbors. The majority of reported studies performed so far have been done using mixed culture bacteria, in which case correlation of bacterial attachment and biofilm development with the current produced is potentially complicated by changes in bacterial populations. Consequently, the study of a single species of bacteria may provide a clearer understanding the attachment processes and current generation as a function of biofilm development. In this study we utilized anode structures consisting of SAMs of ω-substituted alkanethiolates on gold, terminated with the functional groups $–N(CH_3)_3^+$, –COOH, –OH, and $–CH_3$ were used as anodes. It has been reported elsewhere that NMe_3^+ terminated SAMs have a positive effect on MFC start up time and its overall electrochemical performance from biofilms formed from natural mixed cultures bacterial populations [53]. In this study, we

concentrated on the effects on *S. oneidensis*, to simplify the bioelectrochemical system and provide direct correlation between biofilm structure and physiology with energy production.

The aim of this research was to derive guidelines for the development of better electrode materials and structures by characterizing the surface properties of an anode and resulting *S. oneidensis* MR-1 biofilms, along with MFC performance, by a combination of analytical spectroscopic, microscopic, and electrochemical techniques. The interplay between electrode surface chemistry, the resulting morphological and chemical properties of *S. oneidensis* MR-1 biofilms, and biofilm electrochemical properties were the main focus of this study. This multianalytical study provides a large set of data describing properties of biofilms, chemical composition and 3D morphological parameters; which can be related to anode electrochemical performance. Dealing with this large number of variables (parameters), finding correlations between them and classifying samples (in this case different types of biofilms grown on different SAMs) was addressed using principal component analysis (PCA). We showed that positively charged, highly functionalized hydrophilic surfaces are optimal for growth of a uniform biofilm with the smallest cluster size and inter-cluster diffusion distance correlating to the most efficient electron transfer. Moreover, we followed the evolution of biofilm morphology during its growth and after electrode polarization. It was found that biofilm thickness was not as important as biofilm heterogeneity. Finally, we propose metrics describing the loss of biomass, change in intercell properties and overall biofilm morphology, based on quantifying biofilm properties from 3D CLSM images directly related to biofilm electron transfer efficiency and stability.

6.2 – Materials and Methods

6.2.1 Making of Self-assembled monolayers

Microscope glass coverslips (24 X 60 mm, #1, VWR, USA) were used as mechanical support for sample preparation. The coverslips were first cleaned using 1 h UV ozone treatment and then placed into the chamber of a VE-90 electroevaporator (Thermionics, Hayward, CA, USA), and evacuated to approx. 10^{-6} mTorr. An initial layer of 15 Å Cr was deposited on the glass face followed by 30 nm gold. After gold deposition, samples were immediately submerged in 1 mM ethanolic solutions of 1-mercaptoundecyl trimethylamine (NMe_3^+ SAM; Prochimia, Poland), 1-mercaptoundecanol (OH SAM; Aldrich, St. Louis, MO, USA), 1-undecanethiol (CH_3 SAM; Aldrich, St. Louis, MO, USA), and 1-mercaptoundecanoic acid (COOH SAM, Aldrich, St. Louis, MO, USA).

6.2.2 Bacterial cultures and electrochemical setup

S. oneidensis culturing methodologies were applied as previously described. Biofilm growth was analyzed prior to SAM anode polarization as well as at the completion of all electrochemical measurements. The SAM surfaces were submerged in Petri dishes containing phosphate buffer with *S. oneidensis* and biofilm coverage was monitored using CSLM (LSM 510-Meta, Zeiss, Jena). The electrochemical experiments were carried out in membraneless single chamber MFCs [80] and were modified to incorporate three electrodes. These consisted of a reference electrode (saturated Ag/AgCl), a platinum wire counter electrode, and the working electrode, which included two SAM

gold coverslips clipped together with nickel wire, with the functionalized sides facing the buffer solution. All four SAM types were tested separately. All electrochemical tests were performed using Gamry Instruments. Chronoamperometric tests were done at a constant potential of -0.30V vs. Ag/AgCl over a period of 24 h. Cyclic voltammetry was performed at a scan rate of 10 mV/s varying the potential from -0.8 to 0.9 V in order to examine distinctive peaks related to the metabolic activity of *S. oneidensis* [50]. The electrochemical cells were purged by nitrogen in order to maintain a micro-aerobic environment.

6.2.3 Angle resolved XPS

XPS measurements were performed with a Kratos Axis Ultra DLD x-ray photoelectron spectrometer using a monochromatic Al Ka source operating at 225 W. Survey and high resolution C1s, O1s, N1s, and Au 4f were acquired at 80 and 20 eV pass energy, respectively. Three take-off angles (TOAs) were used for angle resolved studies: 90^{O}, 60^{O}, and 30^{O} with respect to the surface. Times of acquisition were: 3 min for O, C, and Au and 6 min for N at 90^{O} TOA; 6 min for O, C, and Au and 12 min for N at 60^{O} TOA; and 10 min for O, C and Au and 20 min for N at 30^{O} TOA charge compensation was accomplished using low energy electrons. As shown before, minimal x-ray degradation occurs when analysis is performed for 1–2 h per sample [84,92]. Standard operating conditions for good charge compensation were -3.1V bias voltage, -1.0V filament voltage, and filament current of 2.1 A. The data presented are averages of three different areas per sample. SAMs grown on gold and biofilms grown on SAMs for 2, 24, and 48 h were analyzed at the same time. Data analysis and quantification were performed using

the CASAXPS software. A linear background was used for quantification. Quantification utilized sensitivity factors that were provided by the manufacturer. A 70% Gaussian/30% Lorentzian [GL (30)] line shape was used for the curve-fits. All the spectra were charge referenced to the Au 4f at 84 eV. Full width at half maximums used for curve fits of C 1s spectra was constrained to 1.0 +/- 0.2 eV. The thicknesses of SAMs on the gold substrate and of biofilms on SAM were calculated using the substrate/overlayer model in Arctick. For SAMs thicknesses, area under the C peak was used as signal from the overlayer, while for biofilms thicknesses, area under the peaks for N was used to represent the overlayer, and, in both cases, area under the Au peak was used to represent the substrate.

6.2.4 Confocal laser scanning microscopy and image acquisition

Upon completion of the electrochemical measurements, microscopic observations on the SAM surfaces were done using a Zeiss LSM-510 Meta confocal fluorescence microscope (Carl Zeiss Microscopy, Jena). Prior to microscopy, SAM samples with biofilms were fixed using 2.5% v/v glutaraldehyde in phosphate buffer for a minimum of 8 h. Samples were then rinsed with water and placed in a solution of 5 μM Syto 21 green fluorescent nucleic acid stain (Life Technologies, Grand Island, NY, USA) for 15 min. The stained samples were viewed using a 63X/0.95W Achroplan water immersion objective and a 505–530 nm band pass filter. A compatible Argon/2 laser, 488 nm, was used to excite the green Syto 21 stain. Z stacks were acquired with a slice separation of 0.72 μm for all samples. The resulting slices were processed using ZEN software (Carl Zeiss Microscopy) and further analyzed using MATLAB.

6.2.5 Biofilm structure and multivariate analysis

Digital image processing was done using the graphical user interface (GUI) in MATLAB [93] based on the algorithm introduced by Beyenal et al. [89,90]. An in-house written GUI for thresholding of image stacks was used. The GUI is available at the Mathworks File exchange website [93]. Areal and volumetric parameters describe the morphology of biofilms, i.e., they describe size and shape/orientation of the constituent parts. Each parameter measures a unique characteristic feature of the biomass cluster and intercluster space in the biofilm. First, the images were thresholded, which separated cell clusters from inter-cluster voids. The following volumetric parameters (Figure 6.1) were then calculated: (1) Biofilm volume is the total volume of biomass in the biofilm measured as the total number of pixels where biomass present (value of 1 in the thresholded image).
(2) Biomass roughness Ra is variation in biomass thickness. (3) Cluster size measured as average run (AR) length, which is the number of consecutive biomass pixels representing cell clusters in a given directions. AR in both X and Y directions was very similar, so cluster size in a horizontal direction (ARX) was used to represent the average cluster size.
(4) Average diffusion distance is the average distance from a cluster pixel to the nearest void pixel in the image. This is a measure of closeness of individual cell clusters to each other. (5) FD is a measure of the roughness of the boundaries of cell clusters or irregularity of cell cluster surface.

Texture provides information about the spatial distribution of intensity levels. Textural features, based on gray scale co-occurrence matrices (GLCM), provide measures of homogeneity, randomness, or directionality [94-98]. The GLCM is a tabulation of how often different combinations of pixel intensity values (gray levels) occur in an image.

Uniformity and entropy were calculated from GLCM texture. Uniformity, also called energy, represents the homogeneity or orderliness of image. Smaller uniformity values are observed for frequent and repeated patterns of pixel clusters while more homogeneous image structure with fewer repeated patterns has higher uniformity. Entropy measures degree of randomness. Complex textures and more heterogeneous images have higher entropy, which increases with the number of cell clusters.

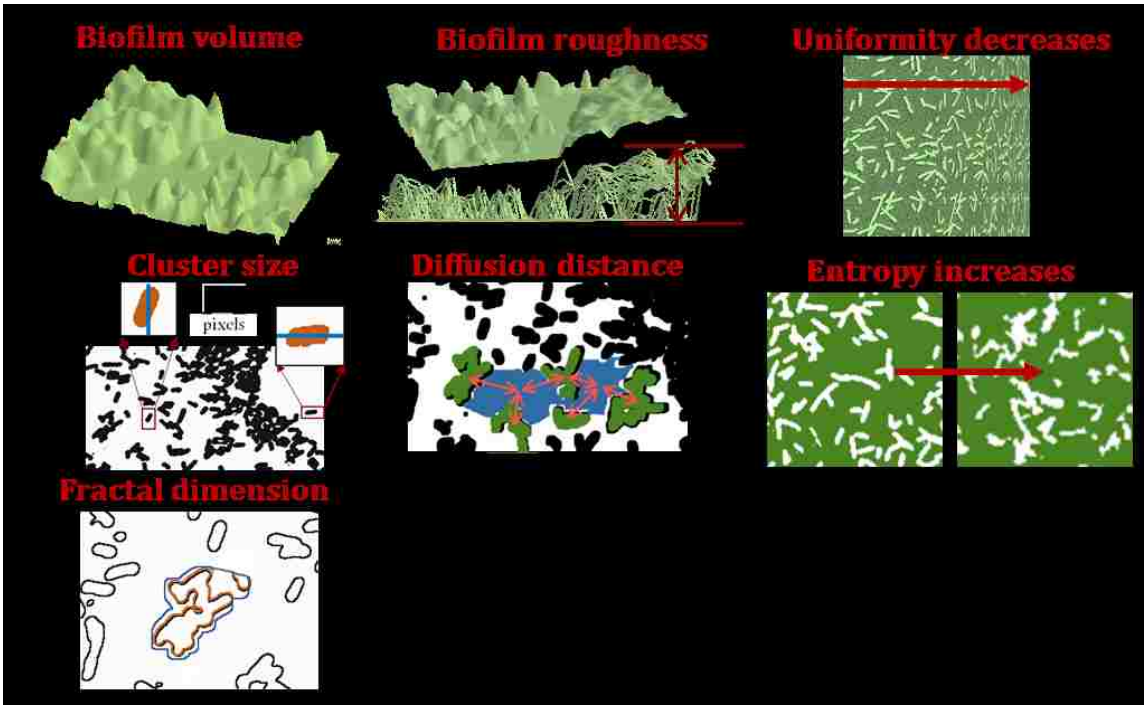

Figure 6.1: 3D metrics extracted from confocal laser scanning microscopy 3D stacks.

Multivariate analysis was done using PLS_Toolbox 7.9 for MATLAB.36 Principal component analysis, using an auto scaling as a preprocessing option (mean centering and scaling to unit variance), was the default method of data analysis. PCA transforms original variables into new uncorrelated variables called principal components. Auto scaling ensures that parameters having very different magnitudes have the same statistical

contribution in the model. The first principal component (PC1) contains the maximum variance. The second principal component (PC2) is calculated to have the second most variance, and, importantly, is uncorrelated with the PC1 and so on. The first output from PCA is loadings, which are the coefficients of the linear combinations of the original variables that generate the principal components. The second output, scores, shows the relationship between samples. Biplots displaying both loadings for each variable and scores for each sample in a single plot for the PC1 and PC2 were produced to visualize the clustering of samples with respect to parameters that were the most or least important for separating samples based on their activity. Correlated variables and samples are located in the same quadrant on a biplot.

6.3 - Results and Discussion

6.3.1 Electrochemical testing

The cell was inoculated with a suspension of *S. oneidensis* in buffer with lactate as the electron donor. The SAM-modified gold electrodes were exposed to the conditions mentioned above, during which the current generated as a result of lactate oxidation by *S. oneidensis* was recorded via chronoamperometry (Figure 6.2a). The NMe_3^+-terminated SAM electrode generated the highest current reaching 442 μA during the initial 7–8 h of polarization, while the CH_3-SAM electrode exhibited the lowest current, reaching only 67 μA at the same time point. These observations were in agreement with previous results, indicating that NMe_3^+ moieties are related to higher current generation than are CH_3 [53]. This can be explained by the hydrophobicity of the CH_3-SAM surfaces having a negative

impact on biofilm development and thus on the current generation [99]. Upon completing the chronoamperometry experiments, the SAM-modified bioanodes were analyzed by cyclic voltammetry (CV) (Figure 6.2b). The CV of the NMe_3- terminated SAM demonstrated oxidation peaks usually assigned to flavin oxidation, where the more negative peak at potential lower than -0.3V was due to oxidation of riboflavin dissolved in the electrolyte and the second, more positive peak at potential between -0.3 and -0.2, was a result of riboflavin oxidation when riboflavin is bound to bacteria outer membrane cytochromes [36]. These results demonstrated favorable conditions for biofilm development and electron transfer on NMe_3^+ -SAMs surfaces. Based on previous electrochemical studies, Figure 6.2b shows that the cyclic voltammograms from NMe_3^+-SAMs also have maximum capacitance and electron transfer peaks [50].

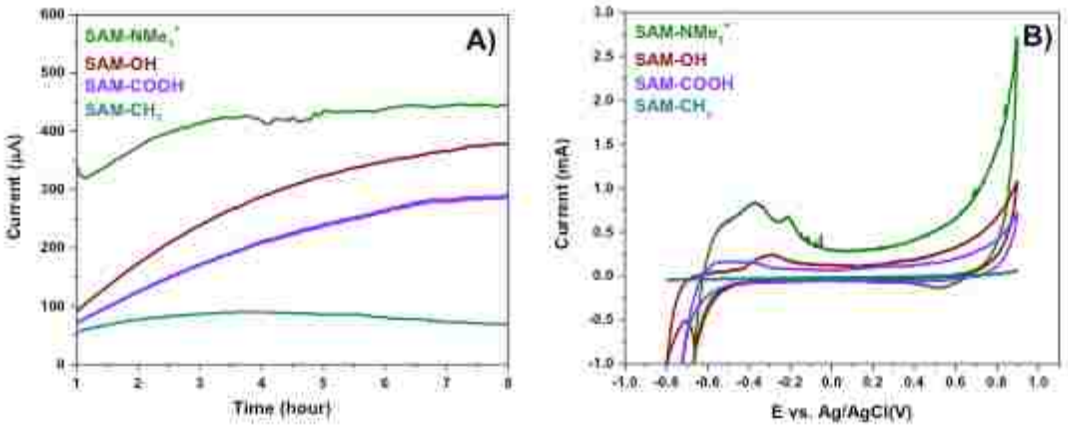

Figure 6.2: A) Chronoamperometry of the different SAM-modified anodes performed at a constant potential of -0.30 V vs. Ag/AgCl. B) Cyclic voltammograms of the different SAM anodes at a scan rate of 10 mV/s.

6.3.2 XPS results

ARXPS was used to analyze both SAMs on gold and biofilm samples grown at different times. Figure 6.3 shows high-resolution C 1s spectra representative of four SAM samples

at 90^{O} TOA. Three areas per sample were analyzed at three take-off-angles, and substrate-overlayer model was used to calculate the thickness of SAM overlayer on the gold substrate. In the substrate-overlayer model, the intensities of two peaks, one coming from the substrate and another from the overlayer, as a function of take-of-angle, were used to calculate thickness at known inelastic mean free path (IMFP) of photoelectrons. This model assumes that IMFP of the electrons in the substrate and overlayer are identical and that the overlayer is homogeneous and continuous [100,101]. This assumption is valid for the system of SAMs on gold, in which intensities of Au and C are used to calculate the SAM thickness. IMFP were obtained from Penn [102]. The range of SAM thicknesses between 1.3 and 1.7 nm was in good correspondence with reported values [103-105]. Peaks in C 1s spectra were representative of chemistries expected from the termination groups, including a peak due to C–N at 287 eV in SAM-NMe_3^+, a peak at 287.2 eV due to C–OH and some amount of higher oxidation state was detected for SAM-OH at 289 eV, peaks due to C–O (287.2 eV) and C=O (289 eV) from carboxyl group were detected for SAM-COOH, and finally, SAM-CH_3 had a C spectrum consisting of single symmetrical peak at 285 eV with negligible amount of C–O (286.8 eV) contamination from adventitious carbon. For the biofilm thickness calculations, we have used signal from N 1s from biofilm versus gold substrate in the ARCTICK overlayer-substrate model. The assumption of a homogeneous and continuous overlayer may not be valid for biofilm samples. For SAM-NMe_3^+, the signal was adjusted by the nitrogen amount that was present in the NMe_3^+ SAM itself, and the thickness was adjusted by the thickness of underlying SAM layer. Figure 6.4 shows N at. % and thickness calculated as a function of time of biofilm growth. For films grown for 2 h, the

SAM-CH_3 and SAM-COOH have largest amount of N while NMe_3^+ has the smallest amount of N from the biofilm detected. The thickness of the biofilm grown on SAM-NMe_3^+ was relatively constant, and it was the smallest among all the samples. The largest continuous growth occurred on the SAM-COOH, which corresponded to increased N with time. For SAM-CH_3, the biofilm increased by roughly 25% from 2 to 24 h, and then plateaued. The SAM-OH biofilm increased and then decreased, suggesting that some biomass detachment occurred. Interestingly, the hydrophilic, positively charged surface (NMe_3^+) yielded the highest current and also had the least biomass, and there was no increase in biomass thickness. ARXPS provided an integrated composition and thickness from a large area of 300 X700 μm, so heterogeneities smaller than this area of analysis were overlooked. Also, the overlayer-substrate model did not take into account that the overlayer may be porous and rough, and so the biofilm thicknesses provided by ARXPS may not represent total biomass or reflect surface heterogeneity [106].

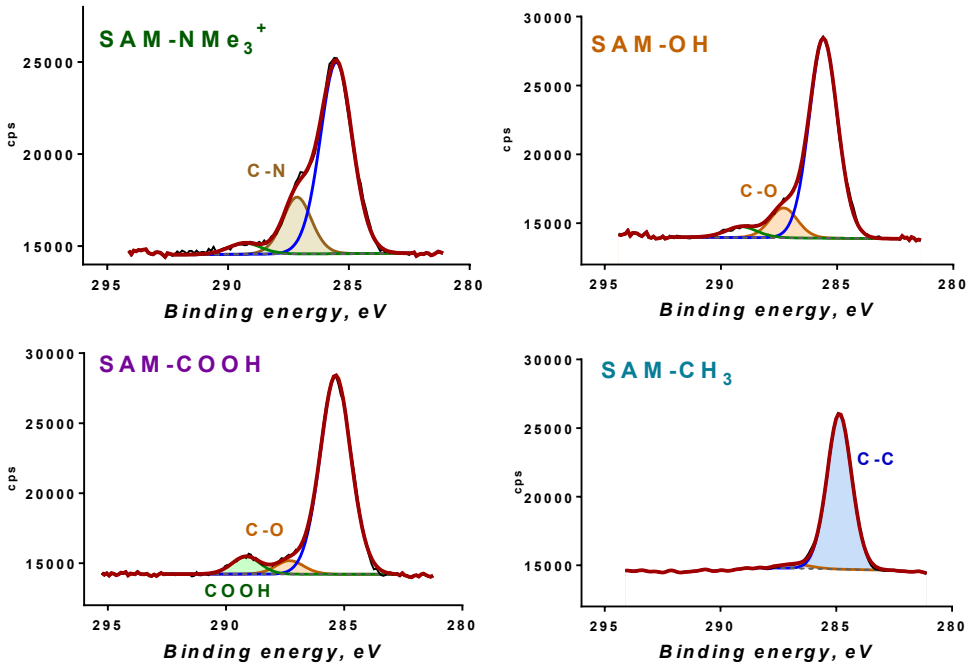

Figure 6.3: High-resolution C 1s spectra from SAMs on gold substrates.

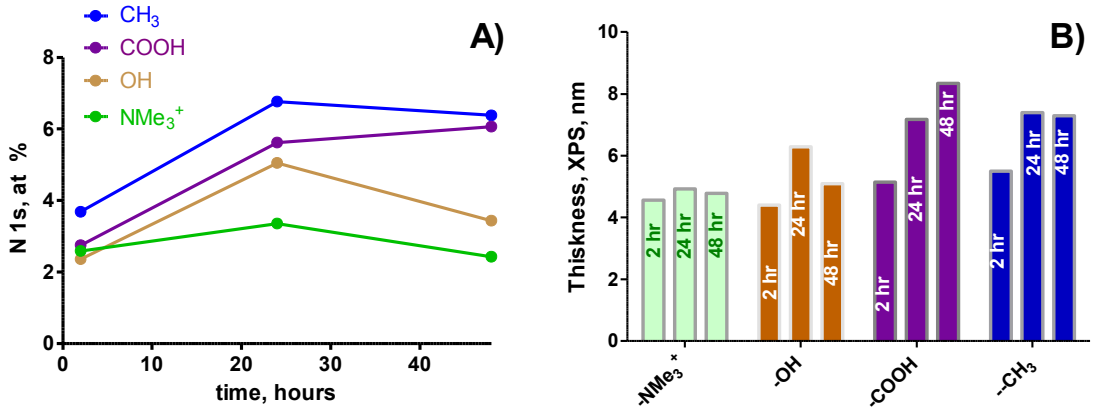

Figure 6.4: A) Atomic % of N and B) thickness in nm for biofilms growth at SAMs at three different times.

6.3.3 Confocal microscopy results

Figure 6.5 shows CLSM 3D image stacks displayed in the orthogonal view for all biofilms and as volumes for biofilms grown on SAM-NMe_3^+ for 2 and 24 h. At 2 h, SAM-NMe_3^+ and SAM-OH exhibited the most homogeneous morphology of the four electrodes, with the smallest spacing between biofilm clusters. Biofilms grown on SAM-COOH for 2 h had the highest heterogeneity with the largest number of pores visible. At 2 h, the SAM-CH3 biofilm was less homogeneous with less uniformity and more pores visible than for SAM-NMe_3^+. The morphologies changed during biofilm growth from 2 to 24 h on some SAMs. Increased contrast, clustering of cells, and growth of pores was visible in SAM-NMe_3^+ at 24 h, while the SAM-OH and SAM-CH3 biofilms did not demonstrate obvious loss of structure according to the CLSM images. On SAM-COOH substrata, the biofilm was highly deteriorated by 24 h. This observation contradicts the information obtained from ARXPS, indicating than some N deposited on the electrode transferred from the film that was not present anymore. This highlights the limitations of XPS for studying systems that undergo changes upon transfer from humidified to the dry environment. The nitrogen signal that was used in XPS analyses as a metric of the biofilm presence may not accurately represent the live biofilm on the surface. This demonstrates the utility of multianalytical studies, such as presented here, to provide a more complete picture of biofilm structures.

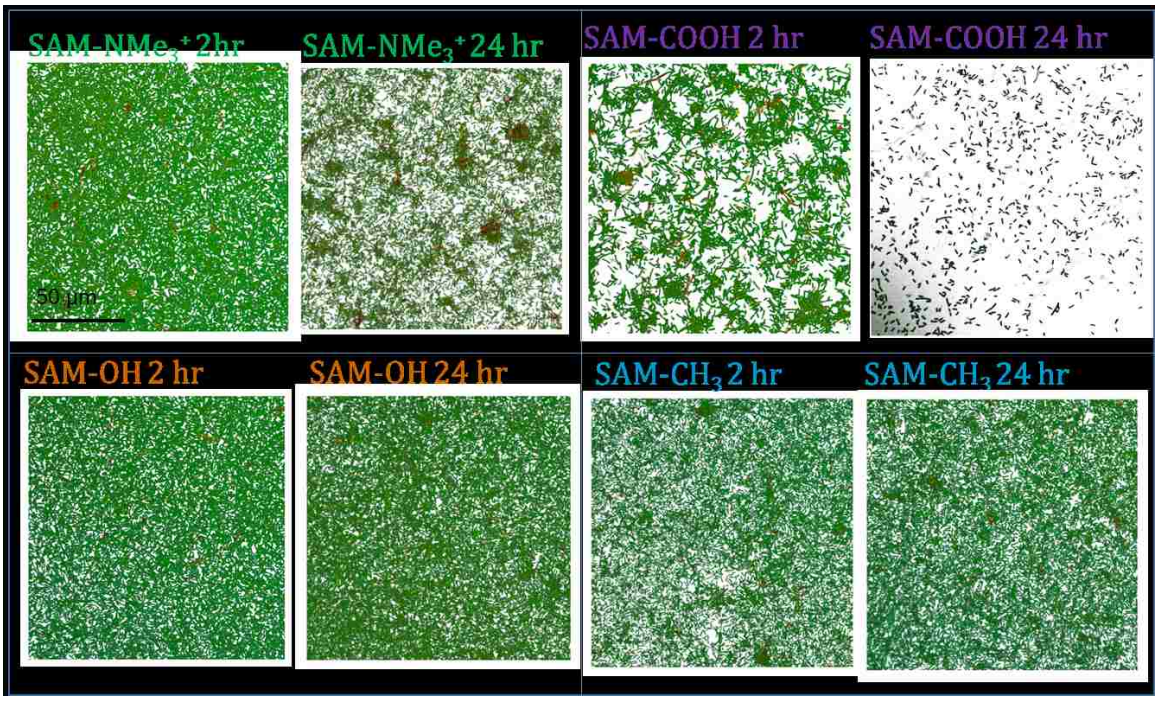

Figure 6.5: Confocal images of biofilms grown on SAMs for 2 hours and 24 hours.

6.3.4 Structure-to-property correlations

This multianalytical approach provides a large set of parameters. In order to develop correlations between results of microscopic and spectroscopic methods and performance characteristics of the engineered material, we need to correlate information from multiple analytical methods. Dealing with the large number of variables (parameters) and finding correlations between them and classification of samples is an important challenge. Application of multivariate analysis methods such as PCA allows for fast and efficient way to find correlations between samples and parameters from large datasets combining information from multiple analytical methods. Structural biofilm parameters were extracted from the confocal 3D stack images representing total biofilm volume, biofilm roughness, cluster size, the diffusion distance, fractal dimension, entropy, and uniformity

as described in Sec. II. These morphological parameters were then combined with parameters of electrochemical performance, XPS composition, and XPS thickness of the film into one dataset, as shown in Table 6.1. Figure 6.6 shows a PCA biplot obtained from this multivariate dataset. PC1 separates samples by their electrochemical performance, with better performing samples contributing positively to PC1, and worse performing samples contributing negatively to PC1. PC2 separated samples by the amount of the biofilm grown. Quadrant I contains the SAM-NMe_3^+ sample, with the best electrochemical performance, and highest amount of N and O. The SAM-NMe_3^+ sample was positively charged and hydrophilic surface, and produced the most uniform biofilm with the smallest cluster size and diffusion distance between clusters. This morphology apparently enabled the most efficient electron transfer to the electrode surface. Overall thickness of the biofilm was not as important as biofilm heterogeneity. Quadrant II includes the SAM-COOH biofilm, which exhibited good electrochemical performance, and had high roughness but at the same time high uniformity of the cell clusters. Uniformity decreases with more frequently repeated patterns of pixel clusters, and so structures that have fewer repeated cell clusters may result in higher biomass roughness. SAM-CH_3, the worst performing sample, is located in Quadrant III. This sample has the largest amount of carbon, the smallest amount of functionalization, the largest cluster size, and the largest diffusion distance between cell clusters.

Table 6.1: Morphological parameters, XPS surface chemical composition and performance parameters combined in one dataset for principal component analysis.

	Entropy	Uniformity	Biomass roughness	Cluster size	Diffusion distance	Fractal dimension	Biomass volume
SAM-CH_3	5.71	0.019	0.042	11.3	2.05	2.57	23957000
SAM-COOH	5.50	0.023	0.077	9.5	2.01	2.52	20514322
SAM-NMe_3^+	7.07	0.005	0.045	9.7	1.94	2.65	23876871
SAM-OH	6.48	0.009	0.042	11.1	2.06	2.64	27016639
	XPS thickness (nm)	C 1s (%)	O 1s (%)	N 1s (%)	C–C (%)	C–N/C–O (%)	COOH (%)
SAM-CH_3	5.5	95.4	4.4	0.1	93.6	6.4	0.0
SAM-COOH	5.1	85.0	14.8	0.2	88.3	5.1	6.6
SAM-NMe_3^+	5.9	83.2	12.2	4.7	78.8	16.5	4.7
SAM-OH	4.4	82.7	17.2	0.1	83.2	12.7	4.1
	I at 5 h (μA)	I (oxidation peak) (μA)					
SAM-CH_3	85.4	−13.7					
SAM-COOH	238.5	53.5					
SAM-NMe_3^+	433.7	298.9					
SAM-OH	323.4	77.0					

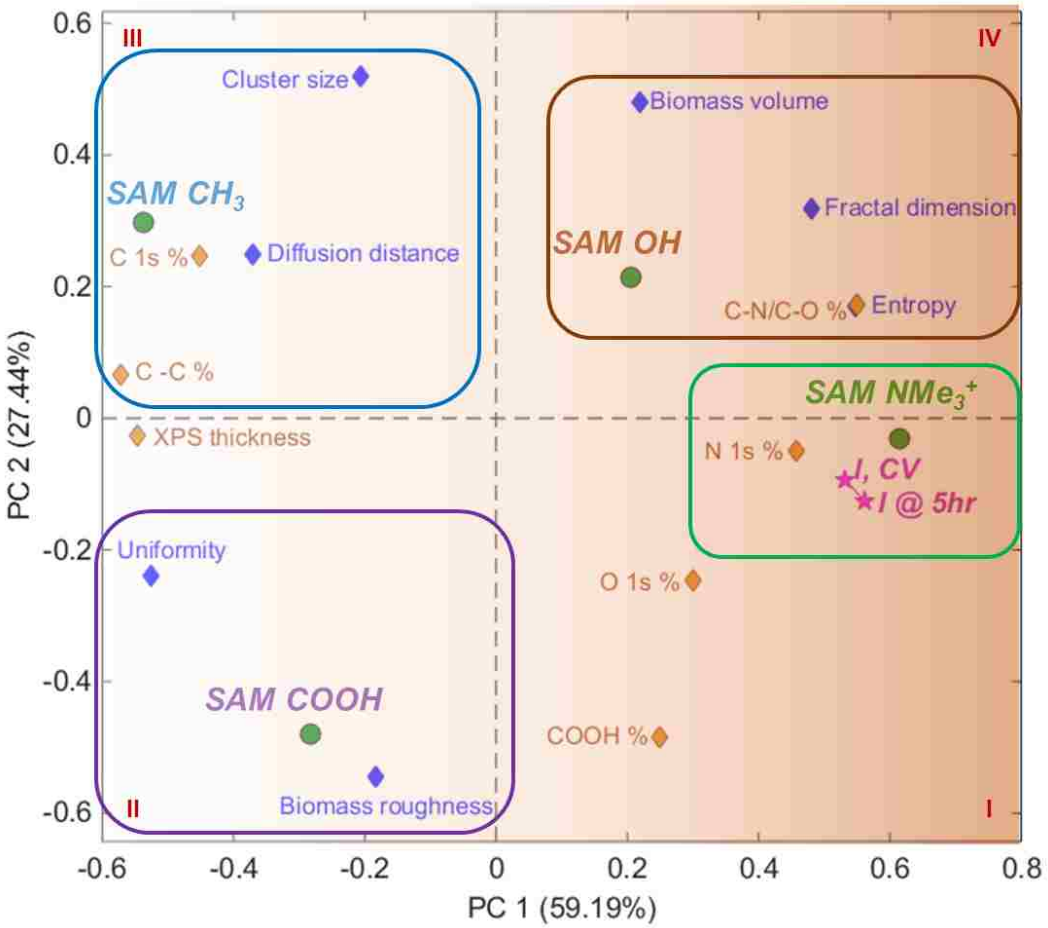

Figure 6.6: PCA biplot for data set combining 3D metrics from CLSM, XPS composition, XPS thickness and electrochemical performance.

Figure 6.7 shows representative SEM images from polarized SAM-CH_3 and SAM-NMe_3^+ illustrating the different morphologies with SAM-CH_3 sample having larger cells cluster size than SAM-NMe_3^+. This difference in morphology was captured by the metrics obtained from confocal microscopy. As a result of the higher surface tension observed in SAM-CH_3, there can be conglomeration of dead bacterial cells at the surface. Further verification of this phenomenon can be observed in the electrochemical results where the cyclic voltammetry peaks corresponding to the SAM-CH_3 are negligible, suggesting poor electron transfer, which is attributed to abiotic components at the anode surface. The hydrophobic SAM-CH_3 chemistry apparently resulted in a thick biofilm with high volume, but the poorest morphological aerial properties for electron transfer. Quadrant IV includes the SAM-OH biofilm, which had largest biofilm volume, but poor performance that may be related to its relatively large cell cluster size and higher diffusion distance than the SAM-NMe_3^+ biofilm. This biofilm also had the highest degree of irregularity in the cluster structure and entropy.

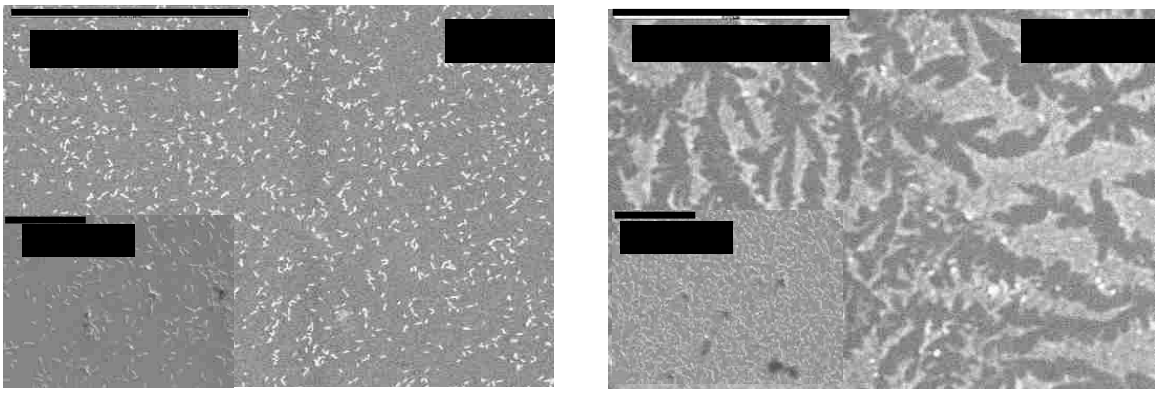

Figure 6.7: SEM images from biofilm on A) SAM-NMe_3^+ and B) SAM-CH_3.

6.3.5 Quantifying biofilm structure

The parameters biofilm volume, biofilm roughness, cluster size, the diffusion distance, and fractal dimension can be important for stability and performance of the bacterial biofilms. The evolution of biofilm morphologies were analyzed by image analysis of 3D confocal depth stacks acquired for biofilms grown at 2 and 24 h, as well as after electrochemical polarization for 24 h (Figure 6.8). For all but SAM-COOH, the biofilms grew continuously without changes in overall roughness. This was not true after samples were subjected to electrochemical polarization, when a significant loss of biofilm was observed, accompanied by a notable increase in biofilm roughness. This may be attributed to the fact that the development of thick biofilms hinders the electron transfer from bacteria toward the electrode surface and creates diffusional limitations for the bacteria electron donor. Although it was suggested that Shewanella cells are capable of external cell-to-cell electron transfer, [107] the growth of thicker biofilms may impose resistance that decreases the efficiency of the electron transfer and, consequently, the generated current. At the same time, thicker biofilms create diffusional resistance to electron donor transport (lactate in this case), so it cannot access the deeper layers of the biofilm, and therefore, bacteria located farther away from the solution and closer to the solid surface die and get separated from the surface. Since the development of thick biofilms is not beneficial for MFC operation, the polarized samples with thick biofilms do not allow for development of cellular communication with the surface as reflected by the diffusion distance and clustering as reflected by the cluster size. The best electrochemically performing sample had the smallest roughness after polarization, indicating higher uniformity of the biofilm. This may explain its higher electrochemical

response since the bacterial cells communicating directly with the electrode surface were the ones participating effectively in the current generation.

The changes in cell cluster dimensions and intercluster diffusion distances over time are also shown in Figure 6.8. The SAM-COOH biofilm demonstrated very different behaviors from the other biofilms. The cluster size and diffusion distance decreased, which was consistent with the overall loss of biomass (Figure 6.5). Under the nearly neutral pH of biofilm growth, the acidic groups of SAM-COOH (pKa=6.5) are only partially deprotonated, so there is no strong repulsion between COO^- and bacteria [108]. Interactions between carboxylic groups and (currently unidentified) components on the bacterial surfaces drive attachment of bacteria and growth of biofilm is observed at initial times of growth. However, with further growth time, and in the polarization test, the biofilm morphology changes profoundly, due to cell detachment cells or increased clustering. This may be the result of chemical changes at the cell–substratum interface, such as weak strength of the hydrogen bonding, possible effects of H-bonding on local pH creating zones of negatively charged COO^- bonds repelling bacteria [108] and steric effects due to hydrogen bonding between carboxylic groups of SAM [109]. Alternatively, the SAM surface could have triggered phenotypic changes in attached bacteria, leading to detachment or surface motility processes known to occur during biofilm development [110].

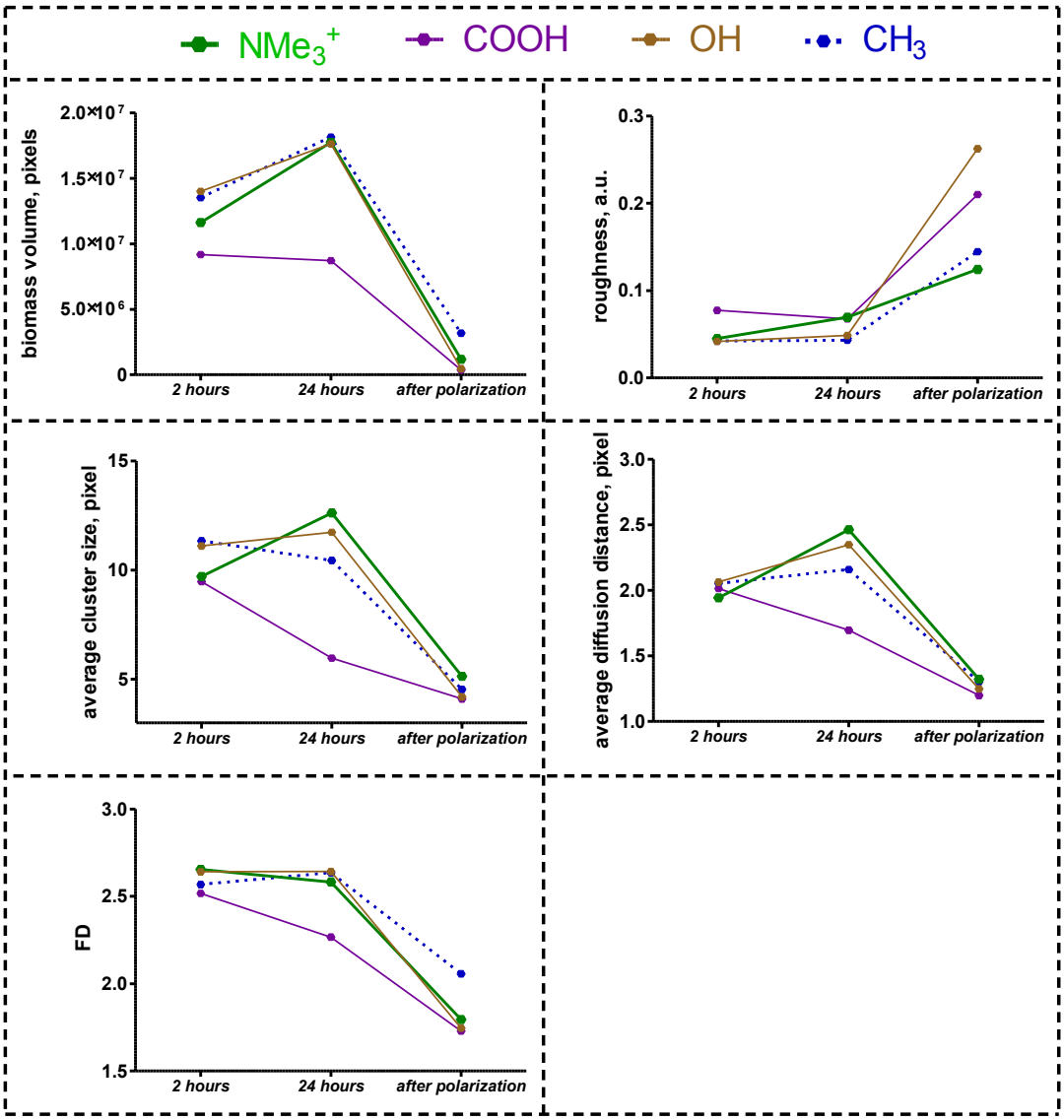

Figure 6.8: Evolution in 3D biofilm parameters from biofilm frown for 2 to 24 hours and after applied polarization.

The most significant change in cell-to-cell morphology was evident for the best performing biofilm on SAM-NMe_3^+ under both polarized and nonpolarized conditions. During biofilm growth from 2 to 24 h, cells become larger and farther apart. There was a smaller increase in cell clusters in both SAM-CH3 and SAM-OH samples, but there was also an increase in diffusion distance for both of them. After polarization, all biofilms

become very similar to each other in terms of areal properties. The decrease in cluster size and diffusion distance was accompanied by the overall loss of biomass. Irregularity of the cell structure expressed as a fractal dimension did not change during film growth for any of the biofilms. However, it decreased after polarization, suggesting that major loss of biomass occurs from peaks protruding from the outer part of the cell cluster, resulting in a smoother surface after the polarization. The SAM-CH3 had the lowest biomass loss as expressed in the largest preserved biological volume and the lowest loss of fractality of the cell structure, supporting this hypothesis.

Texture parameters, entropy, and uniformity were used to evaluate changes in biofilm morphological properties. The smallest change in these properties with growth and after polarization was observed for the worst performing biofilm grown on SAM-CH3. The least stable biofilm that formed on SAM-COOH had the highest increase in uniformity, due to the loss of cells during development. Biofilm grown on SAM-OH had relatively stable morphology, as manifested by little change in entropy and uniformity, but after polarization the loss of cell clusters resulting in lower entropy and higher uniformity exceeded that for biofilm grown on SAM-COOH. For SAM-NMe_3^+, the best performing biofilm, biofilm morphology changed during growth, but the resultant morphology after polarization was more preserved than for the other two biofilms grown on hydrophilic SAMs. The two ratios the distance between cell clusters to the size of the cluster, which serves as a measure of connectivity between cells facilitating electron transfer, and the ratio of uniformity to entropy, which is a measure of overall loss of biomass are shown in Figure 8.9. For NMe_3^+-SAM, there is a little change in the diffusion distance/cluster size ratio during biofilm growth. As the biofilm grows, the distance between cell clusters

increases proportionally to the cell cluster size, potentially resulting in more efficient electron transfer in comparison with biofilms grown on other SAMs, in which this ratio increased, potentially resulting in less efficient electron transfer. The highest instability of the SAM-COOH biofilm was evident from the largest change in both ratios during biofilm growth on this SAM. The highest loss of biomass after polarization occurred on SAM-OH, corresponding highest values of both ratios. Biofilms grown on the best performing (SAM-NMe_3^+) and worst performing (SAM-CH_3) surfaces were the most stable, with the smallest loss of biomass for SAM-CH_3 and the smallest change in cell-to-cell properties for SAM-NMe_3^+.

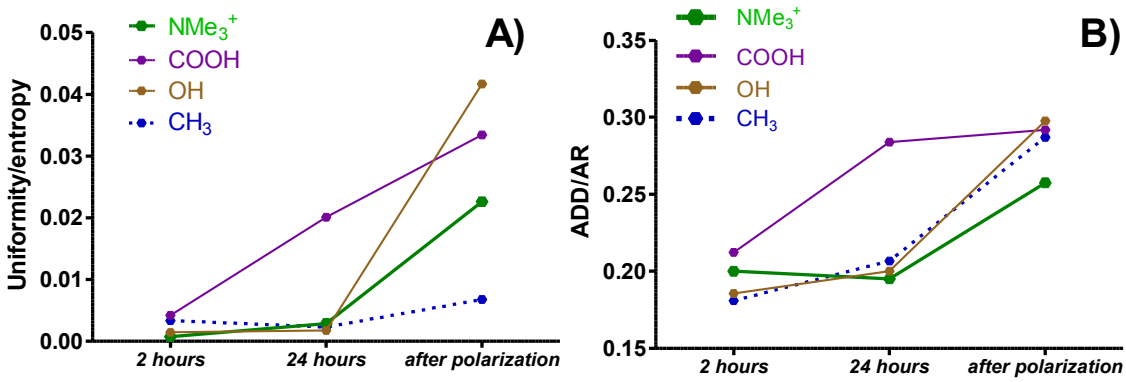

Figure 6.9: Ratio of A) uniformity to entropy and B) diffusion distance /cluster size for biofilms grown at 2 hours, 24 hours and after polarization.

The effects of surface chemistry on biofilm structure are part of an important subject of study. Isolated observations suggest that attachment substratum chemistry can affect subsequent cell–cell interactions [111], exopolymer production, [112] and ultimately adhesion properties of biofilms [113]. The conventional wisdom, however, is that substratum properties affect on the initial attachment phase of biofilm formation, with little effect on subsequent biofilm development or morphology [113,114]. Biofilm

development [115] ultimately involves many interactions between the bacteria and attachment substratum; these include the ability of exopolymers to expand and adhere on surfaces, [116] bacterial surface motility [117], persistence [118], and detachment. Our results indicate that the substratum chemistry affects not only primary attachment but also potentially other processes such as surface motility. For static immersion systems (without mixing), like the one used in this study, the decrease in biofilm observed on SAM-COOH is likely driven by biological processes within the biofilm (leading to bacterial detachment or programmed cell death, for example) [119]. Such processes may be promoted by changes in the cells morphology as a result of the attachment [120].

6.4 – Conclusions

The multianalytical approach used in this study allowed the monitoring the perturbations in biofilm structure and development in different environments (surface chemistry) and in response to environmental changes (electrical potential). Surface chemistry can be used to modulate subsequent biofilm processes, including EET, enabling a new paradigm in biointerface design. This study provided the first demonstration of differences in biofilm responses when subjected to external polarization, which previously was hypothesized but never clearly demonstrated. The present study is a significant contribution toward further understanding and optimization of MFCs systems as it addresses the effect of biofilm growth and development, as well as its structure and morphology on MFC operation.

Chapter 7 – Influence of Anode Surface Chemistry on Mixed Culture Microbial Fuel Cell Operation

7.1 – Introduction

The rate-limiting step in MFC operation is the electron transfer rate at the biofilm/electrode interface, which determines the maximum current and power output under steady state conditions. Therefore, it is critical to optimize the electrode morphology and chemistry to promote fast electron transfer rate. This goal can be achieved through selection of specific electrode materials, enrichment with anode-respiring bacteria, morphological or chemical modifications of the electrode surface [55, 121, 122]. The electrode material and morphology should facilitate bacterial attachment and subsequent biofilm formation. At the same time, anode surface chemistry along with the biofilm formation should enhance electron transfer from bacteria to the electrode [52-123,124]. Several thermal or chemical treatments have been described to reduce MFC start-up time by facilitating rapid cell attachment and biofilm development for enhanced power output in MFC [121,125,126]. Thermal treatment of the electrodes leads to modification of the surface roughness and porosity and thus enhances cells concentration and biofilm development [53,78,127,128]. Depending on the gas atmosphere (e.g., nitrogen, oxygen, ammonia, etc.) used in thermal treatment, hydrophilic functional groups can be added on the electrode surface [129]. The main purpose of the chemical treatment is to introduce functional groups (typically nitrogen and oxygen containing groups) that improve cell attachment and biofilm development on electrode surface

[59,65,130,131]. Several compounds, such as nitric acid [59,65], ethylenediamine [65], ammonium nitrate [59], ammonium persulfate [59], polyaniline [130], 4(N,N-dimethylamino) benzene diazonium [131] have been used for surface chemical modification of carbonaceous electrodes. However, as previously shown [58], the chemical treatment of carbonaceous surfaces (e.g., carbon cloth) affect both the chemistry and morphology (e.g., roughness and porosity) of said surfaces, thus a clear discrimination of the benefits provided by chemical and surface effects is not straightforward. [58]. The inability to distinguish the influence of only one parameter from the whole set of parameters that are usually altered through the commonly used surface modification techniques is a result of the intercorrelation between the introduced variances in the parameters' magnitudes [132]. Therefore, the impact of the anode surface chemistry on current and power output in MFC should be studied using flat electrode material, thus de-coupling chemical effects from change in surface morphology. In addition, proper statistical interpretation of the data sets should be provided. This statistical tool should have the ability to identify correlation between particular factors and the final output of the studied system. Such a statistical technique is Principal Component Analysis, which application in MFCs and material analysis has been successfully demonstrated.

Recently, Guo et al. [55] studied the influence of the surface charge and hydrophobicity on the current output of anodes operated in half-cell bioelectrochemical systems. They modified glassy carbon electrodes through electrochemical grafting with aryl diazonium salts. As a result, the surface of each anode has been altered distinctively to be hydrophilic (-OH, SO3-, -N(CH3)3+) or hydrophobic (-CH3) with positive, negative or

neutral charge [55]. All anodes were immersed in the same electrochemical cell with the identical electrolyte and polarized at a constant potential (-0.2 V vs. Ag/AgCl, 3.5 M KCl). Higher biomass attachment was measured on hydrophilic and positively charged surfaces, which was directly related to the current output [55]. The microbial biofilm on the best performing anodes was enriched in electrochemically active microorganisms (e.g., *Geobacter* spp). The same conclusion has been reported by Picot et al., who also observed significant increases in anode current output when the surface was amended with positively charged phenylphosphanium cations [133].

While these studies have added new knowledge relative to how anode surface modifications improve current and power output, the specific effects of given functional groups on MFC startup time, current and power output are still not well understood. In this study, ω-substituted alkanethiolates on gold terminated with functional groups (-$N(CH_3)_3$+, -COO-, -OH and -CH_3) are used for the modification of gold anodes. We have previously shown that SAMs improve cells attachment and early biofilm formation and extend this model surface to electrochemical studies [64,134-136]. Here, SCMFC equipped with activated carbon air cathodes are used. The correlation between the surface chemistry of the anode and the SCMFC current and power output is investigated. SAMs-modified gold electrodes are employed as anodes to eliminate the morphology effects associated with conventional carbonaceous electrode. Instead of polarizing all electrodes in the one and the same electrochemical cells and same solution simultaneously, in this work, each anode material was tested in a separate SCMFC in order to: i) avoid undesired shunt-current losses, ii) avoid interaction among the different electrodes exposed to the same electrolyte, iii) evaluate the microbial community developed on the different

electrodes starting from the same initial solution. Following electrochemical characterization for 45 days, DNA from anodic biofilms is sequenced to characterize the electrogenic communities and identify any phylogenetic differences that might have occurred as a function of the unique surface modifications.

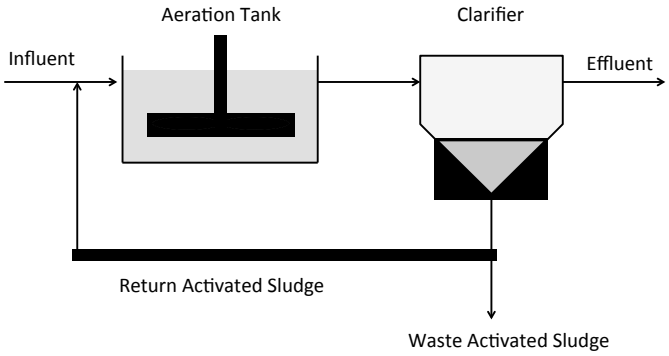

Figure 7.1: Schematic of the secondary wastewater treatment commonly used in municipal treatment plants.

7.2 – Materials and Methods

Self-assembled monolayers were prepared as previously described in Chapter 6. The four types of alkanethiolates (CH_3, OH, COOH and NMe_3^+) as previously mentioned were utilized in these studies as bioanodes.

7.2.1 MFC configuration and cathode material preparation

Single chamber microbial fuel cells (SCMFC) with a volume of 130 mL were assembled as described elsewhere [137]. The anolyte was 50% 0.1 M phosphate buffer solution

(PBS) with 0.1 M KCl and 50% of activated sludge from the Albuquerque Wastewater Treatment Plant. Sodium acetate ($C_2H_3NaO_2$, 5 g L^{-1}) was used as a substrate and introduced periodically in each MFC to maintain non-limiting substrate concentration. The pH of the anolyte was 7.4-7.5 and remained constant along the entire experiment [58]. SAM-modified gold anodes (geometric area 14.4 cm^2) were assembled with two coverslips using a titanium wire with the functionalized surface facing the medium solution. The anode was connected to the cathode through an external resistance of 1000 Ω. The cathode used in this work has been previously described [138]. Briefly, activated carbon (Calgon, USA) with a surface area of 802 $m^2 g^{-1}$ was grinded with 20%wt PTFE (60% dispersion in water, Sigma Aldrich). 60 ± 2 mg cm^{-2} of the obtained mixture were pressed at 1400 psi for 2 minutes on a carbon cloth (30% wt. wet proof, Fuel Cell Earth) used as the electron collector. The cathode assembly was then heated at 200 ºC for 1 h before utilization. The cathode had a geometric surface area of 3.5 cm^2 directly exposed to the electrolyte [138]. The SMFCs were operated in duplicate for each SAM-modified anode material at room temperature (21±1ºC).

7.2.2 Electrochemical testing

The overall single chamber microbial fuel cell (SCMFC) potential was recorded every 25 min using a datalog system (Personal DAQ/56, USA) connected to a PC for over 45 days. At the end of the experiment, anode and cathode potentiodynamic polarization curves were taken using a three-electrode configuration as previously described using a VersaStat potentiostat (Princeton Applied Research, USA) [139]. Briefly, the electrode

under investigation (anode or cathode) was used as the working electrode, Ag/AgCl 3M KCl (+0.21 V vs. SHE) was used as the reference electrode and a stainless steel A316 mesh with the same area of the working electrode was used as a counter electrode. The anode potential was scanned from open circuit potential (OCP) to 0 V vs Ag/AgCl 3M KCl. The cathode potential was scanned from OCP to -0.3 V vs Ag/AgCl 3M KCl. The scan rate utilized for the potentiodynamic curve was 0.2 and -0.2 mV s^{-1}, respectively. The cell polarization curves were carried out after the single electrode polarizations in two electrode mode, connecting the anode as working and the cathode as counter and reference electrode. The polarization was started after the OCP stabilized (approximately one hour), and then the polarization curve was measured from the open circuit cell potential (OCP) to 0.01 V (vs Ag/AgCl 3M KCl). The power (P) was obtained using the equation $P = V \times I$ where V and I are the SCMFC voltage and current, respectively. Power and current are normalized to the anode geometric surface area (14.4 cm^2).

7.2.3 Anodic biofilm characterization

At the end of the 45 days of experiments, anodic and cathodic biofilm were removed by scraping the electrodes. Pyrosequencing was done on one anode per each electrode material and on the planktonic biomass of the SCMFC equipped with $N(CH_3)_3^+$ - modified anode. DNA was extracted using sucrose lysis/cetyltrimethylammonium bromide (CTAB) as previously described [140], and its purity was evaluated from the ratio of absorbance at 260 and 280 nm. Samples were shipped on ice for DNA pyrosequencing by Research and Testing Laboratories (Lubbock, TX, USA). Bacterial tag-encoded FLX amplicon pyrosequencing was performed as described previously [141]

with small modifications to utilize the Titanium sequencing platform (Roche Applied Science, Indianapolis, IN). A single 35-cycle PCR step with Again HotStar master mix and addition of 0.5 U of HotStar HiFidelity polymerase were used in each reaction (Qiagen, Valencia, CA). The primers were 28f (5'-GAG TTT GAT CNT GGC TCA G-3') and 519r (5'-GTN TTA CNG CGG CKG CTG-3') (Escherichia coli 16S gene numbering). Pyrosequence reads were analyzed at UNM using AmpliconNoise 1.25 [142] to remove low quality sequences, which included sequences less than 200 bp in length, with an average quality score of less than 25, containing ambiguous characters, and/or without the correct primer sequence. A workflow script in QIIME 1.80 was used to pick operational taxonomic units (OTUs) at the 97% sequence identity level. Representative sequences from each OTU were identified by the Ribosomal Database Project44 classification method using QIIME, with assignment of taxonomic identities using the Greengenes 16s rRNA gene database [143].

7.3 – Results and Discussion

7.3.1 Overall MFC voltage

Gold electrodes were modified with self-assembled monolayers (SAMs) having four different terminal groups, –CH3, -OH, -COOH and –N(CH3)3+. A stable molecular monolayer coated uniformly the surface as showed previously [139]. The SCMFC potential under constant external load (1000 Ω) was monitored for 45 days (Figure 7.2). As in many other MFC studies, the potential increased with time, indicating electrochemically active biofilm formation. However, the potential evolution with time

was different for each material, indicating differences in electroactivity and electron transfer rate [144].

MFCs fitted with –$N(CH_3)_3^+$–SAM anodes showed a rapid potential increase (after 15 d), followed by –COOH (17 d), -CH_3 (17 d) and –OH (20 d) (Figure 7.2). The -$N(CH_3)_3^+$-MFCs showed the fastest potential slope (170-195 mV d-1) and achieved stable conditions after roughly 18 days. COOH-MFCs showed a slower potential slope (75-96 mV d-1) and stabilized after 22-23 days. The potential slope of OH-MFCs could be divided in two different parts: i) at potential < 0.15 V, the slope was of 21-25 mV day-1; ii) at potential 0.42 > E > 0.15 V with the slope increased to 50-56 mV day-1. Finally, the E slope of CH_3-MFCs was much smaller than the other materials, only 2.2-2.3 mV day-1. These results show that anode coating affects both the start-up time of potential production and the rate of potential increase with time, which in turn correlates to the attachment and growth of electrochemically active biofilms.

Despite the different start-up times, the $N(CH_3)_3^+$-, COOH- and OH-MFCs reached a similar stable voltage output (0.41-0.43 V), as the external resistance chosen was higher than the smaller sustainable resistance [145]. However, the potential of CH_3-containing MFC increased slowly over time and stabilized after 40 days to 0.06 V (Figure 7.2).

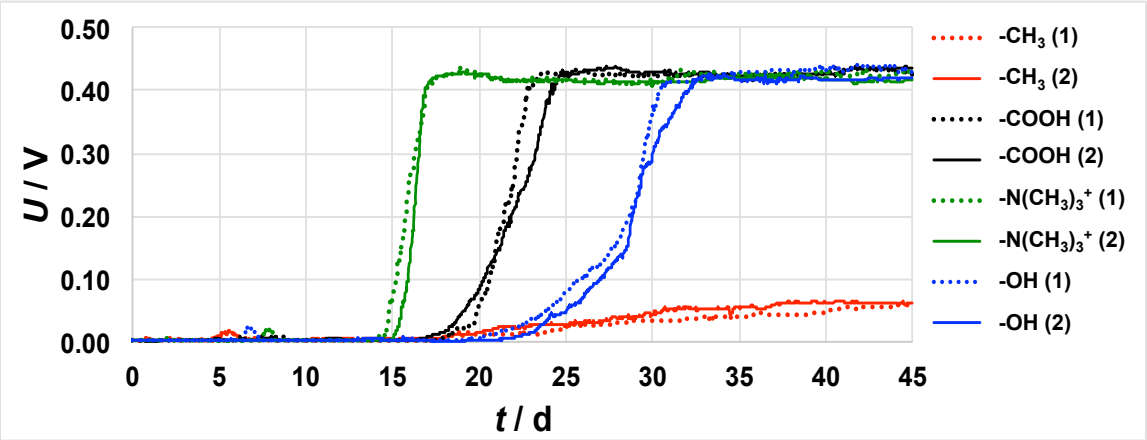

Figure 7.2: Voltage output of MFCs containing different SAMs as modified gold anodes over 45 days of operation. The numbers in the brackets indicate the number of the replicate sample.

7.3.2 Anodic polarization curves

To study the anode behavior independently of the cathode, the anode electrochemical response was measured using potentiodynamic polarization curves after 45 days of MFCs operation (Figure 7.3). Despite the fact that the voltage achieved at 1000 Ω external resistance after day 45 of MFCs polarization was approximately the same for $N(CH_3)_3^+$-, COOH- and OH-MFCs, the different surface chemistry of the anodes results in a different anodic polarization behavior. Maximum current densities of 225-230 μA/cm^2 were achieved by the $–N(CH_3)_3^+$ modified anodes at approximately -0.40 V vs. Ag/AgCl. The peak observed at -0.40 V is likely due to direct electron transfer at the biofilm/electrode interface. The same peak was observed in the polarization curves of all anodes studied except the CH_3-modified one. The $–N(CH_3)_3^+$-anode demonstrated another peak at higher anodic potential (-0.27 V vs. Ag/AgCl). The maximum current densities achieved for each SAMs-modified anode follow the same trends as the voltage startup conditions in

that the -$N(CH_3)_3^+$ systems showed the highest performance followed by -COOH, -OH and -CH_3, respectively (Figure 7.3).

The -$N(CH_3)_3^+$-MFCs showed the highest anode current densities and shortest start up time most likely due to bacteria preference towards hydrophilic and positively charged surfaces in agreement with previous studies [124].

It has been previously demonstrated that different bacteria exhibit different attachment responses to SAMs [64,134,139]. -COOH and -OH- SAM generated much lower current densities relative to the $N(CH_3)_3^+$-anodes. These data suggest that the surface chemistry directly affect biofilm formation and/or specific biofilm characteristics. Furthermore, the -COOH, -OH and -CH_3-modified surfaces may limit biofilm development and electron transfer rate [124]. Cathode polarization curves resulted in similar trends, showing that the cathode is not the limiting electrode. The performance of the cathodes decreased slightly after 45 days of operation for all SCMFCs tested. The decrease in the cathodic current might have resulted from biofilm development at the cathode, which also could introduce diffusional limitations and induce biofouling of the catalytic sites at the cathode-liquid interface.

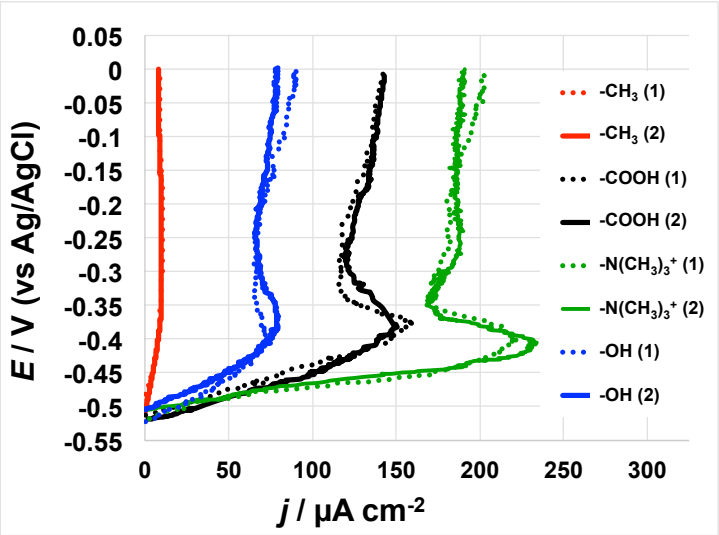

Figure 7.3: Anode polarization curves for duplicate MFC systems featuring different SAMs-modified anodes after 45 days operations. The numbers in the brackets indicate the number of the replicate sample.

7.3.3 Overall MFC performance

The overall performances of the MFCs were evaluated in terms of current and power produced to assess full system performance. The $N(CH_3)_3^+$-, COOH- and OH-MFCs had similar OCV values at 550-565 mV and similar current output at potentials close to OCP until roughly 70 µA cm-2 (Figure 7.4a). As the current densities increase, the I-E curves showed diffusion limitations going into overshoot conditions [146]. Particularly, the OH-MFCs showed mass transfer control at roughly 70 µA cm-2 while the COOH-MFCs showed diffusion limitations at roughly 125 µA/cm^2 and the $N(CH_3)_3^+$-MFC was limited by mass transfer at roughly 200 µA/cm^2.

The MFCs with $–CH_3$ modified anodes had significantly lower OCPs (450 mV) and significantly lower short circuit currents of 5-7 µA/cm^2. The $N(CH_3)_3^+$ MFCs had a maximum power density of 40-41 µW/cm^2 followed by COOH-MFC with 35-37

$\mu W/cm^2$ and by OH-MFCs with 25-28 $\mu W/cm^2$. The CH_3-MFCs had the lowest performances with a maximum power of only 1.2 $\mu W/cm^2$ (Figure 7.4b). Comparison between Figure 7.3 and Figure 7.4 shows that MFC polarization measurements followed the same trends of the anode polarization curves.

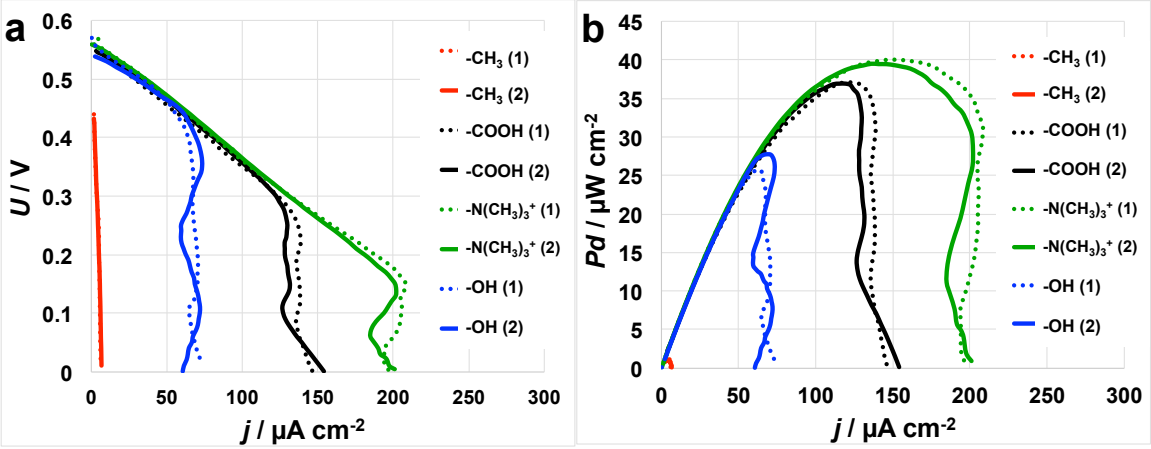

Figure 7.4: Cell polarization (I-V) curves (a) and power curves (b) of MFCs with SAMs-modified anodes. The numbers in the brackets indicate the number of the replicate sample.

7.3.4 Biofilm analysis

Pyrosequencing of 16S rRNA gene amplicons derived from the anode-associated biomass shows diverse bacterial populations at the anode surfaces (Figure 7.5). A phylum-level analysis (Figure 7.5a) indicates that phylum Proteobacteria comprised between 32 % and 37 % of the anode-associated biofilms. Specifically, the $-N(CH_3)_3^+$ modified surface featured Proteobacteria in a relative abundance of 36 %, the -COOH had 37 % relative abundance, and -OH had 32 % relative abundance. The $N(CH_3)_3^+$ bulk solution (labeled as WW in Figure 7.5) also showed 37 % relative abundance of Proteobacteria. However,

Proteobacteria only occupied approximately 6 % of the biofilm associated with the $–CH_3$ modified anode.

The phylum Firmicutes had a high relative abundance in all of the communities, between 21 % and 34 % of the biofilm. The biofilm associated with the $-CH_3$-modified electrode had the highest relative abundance of Firmicutes at 34 %. Interestingly, Firmicutes have been identified in many different microbial fuel cell reports, including a particular strain (Firmicutes Thermincola sp. strain JR) that was isolated from thermophilic microbial fuel cells and was able to directly transfer electrons to an anode surface [146].

The phylum Bacteroidetes was present in all of the communities with relative community abundance of 22 % ($-N(CH_3)_3^+$), 12 % (-COOH), 6 % (-OH), 13 % ($-CH_3$) and 15 % (WW). The $-CH_3$ modified anode also had a relatively high abundance of phyla Lentisphaerae (24 %) and Actinobacteria (19 %) as compared to the other samples.

The class-level analysis of the anode communities shows that the phylum Proteobacteria featured class δ-Proteobacteria, β-Proteobacteria, γ-Proteobacteria, ε-Proteobacteria and α-Proteobacteria. Class δ-Proteobacteria had the highest relative abundance in the $-N(CH_3)_3^+$, -COOH and -OH anode biofilms, and very low relative abundance in the -CH3 anode-associated biofilm and the $-N(CH_3)_3^+$ bulk solution (WW). Several members of class δ-Proteobacteria and γ-Proteobacteria have been reported as electrochemically active microbes in bioelectrochemical systems [144,145,148-150].

The high relative abundance of class δ-Proteobacteria in all of the biofilms that showed good current and power output ($N(CH_3)_3^+$, -COOH and -OH), suggests that these community members are active in electron transfer to the anode surfaces. The -COOH anode-associated biofilm and the WW also featured a small percentage of class γ -

Proteobacteria, which suggests that these community members might be active in multiple functions, including electron transfer to the anode and possibly fermentation of complex substrates in the bulk solution. The presence of class β-Proteobacteria in wastewater-enriched microbial fuel cells has also been reported by several MFC researchers [148-151]; however, the functional role(s) of these microbes have not been comprehensively defined, and members of this class may perform multiple functions within the biofilm.

Interestingly, all the reactors featured a high relative abundance of fermentative microbes including class Clostridia, Bacterioidia, Deferribacteres and Lentisphaerea. This result suggests that acetate was not the sole carbon source for the community and that residual complex carbon substrates from the activated sludge inoculum may also have been used as electron donors for the biofilm and planktonic communities. Members of class Clostridia, Bacterioidia, Deferribacteres and Lentisphaerea have been reported in several wastewater-enriched microbial fuel cells [148-152], and it is speculated that these organisms are critical for converting sugars and other complex substrates to simple volatile fatty acids that are the preferred carbons sources for electrochemically active δ- and γ- Proteobacteria .

A more detailed sequencing effort is required to identify strain-level associations with the various electrode surface chemistries; however, the class-level analysis suggests that there may have been different community members contributing to electron transfer at the various chemically-modified surfaces. The results strongly suggest that the surface chemistry (charge and hydrophobicity) of the -CH_3-modified anode had the most effect on microbial taxonomic enrichment, which negatively impacted the overall system

function. The lack of δ-Proteobacteria members and a higher relative abundance of diverse fermentative members (e.g. Bacilli, Lentisphaerae and Actinobacteria) correlates with the low electrochemical performance of the CH_3-modified system, and suggests that fermentation was the primary function of this community.

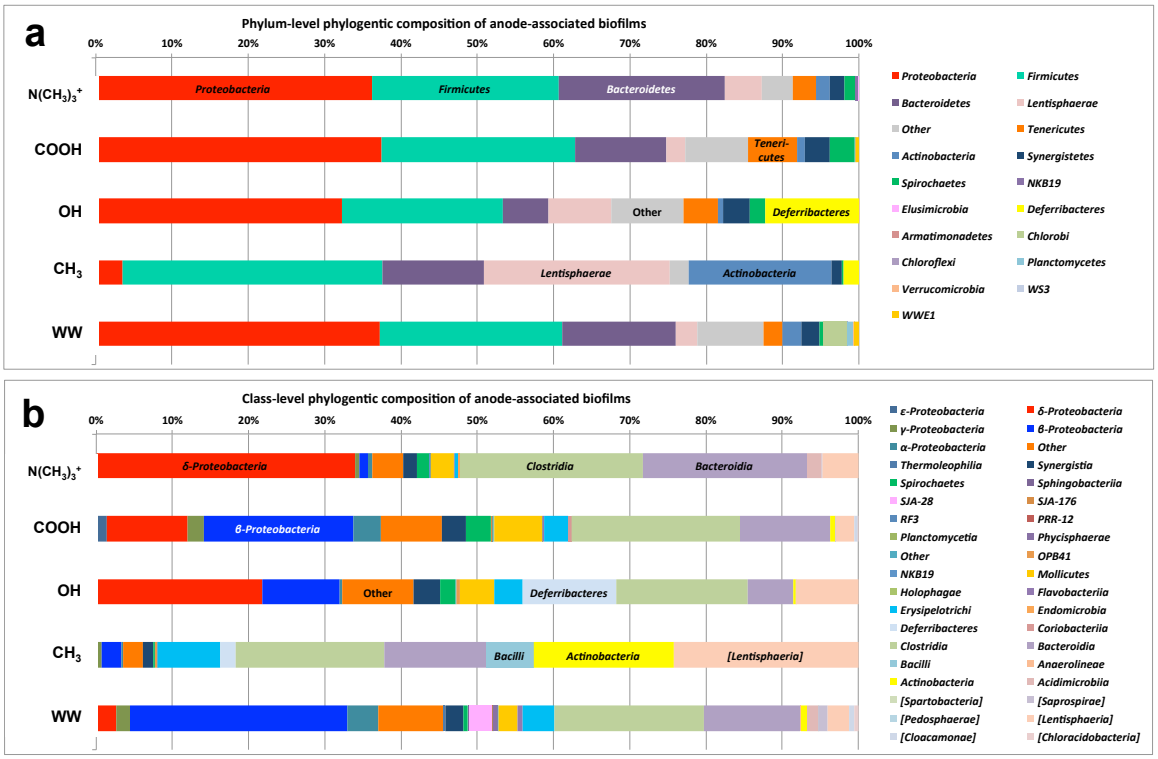

Figure 7.5: a) Phylum-level taxonomic distribution of 16S rRNA community profile within anode electrochemically active bacteria and b) class-level taxonomic profile of 16S rRNA community profile within anode electrochemically active bacteria.

7.3.5 PCA and parameter relationships

As it has been indicated in the Introduction section of the manuscript, due to the complexity of MFCs, the abundance of factors determining the overall system performance and their intercorrelation, ascribing the observable variations in the MFC

output to only one parameter is highly incorrect. Thus, although in this study we intentionally varied only one parameter (anode surface chemistry), the differences in the MFCs behavior cannot be addressed to the impact of only this variable. As we demonstrated, the variations in the anodes surface chemistry led to differences in surface hydrophobicity (Table 7.1), bacteria population on the electrodes (Figure 7.5) as well as variations in the interface electron transfer rate, all leading to different MFCs behavior.

Table 7.1. Contact angle measurements and electrode charge transfer ability. This was determined based on cyclic voltammetry of abiotic solutions of 10 mM $K_3[Fe(CN)_6]$, where the oxidation peak current from the CVs on the modified electrodes is normalized to the oxidation peak current of $K_3[Fe(CN)_6]$ on bare gold.

Anode	Contact Angle (°)	Charge transfer ability
$-CH_3$	102.5 ± 1.6	0.03
-COOH	19.2 ± 0.7	1.11
$-N(CH_3)_3$	51.4 ± 4.7	1.07
-OH	27.2 ± 1.6	0.67
bare Au	83.5 ± 2.3	1.00

Principal Component Analysis was used to find correlations between the different factors affecting the tested herein MFCs and their operational characteristics, such as current and power output, start up and steady-state time. Steady-state time is defined as the time necessary for the system to reach steady-state current when the MFC is subjected to a constant external load in abundance of a carbon source.

PCA separates the variables and the samples into three groups (Figure 7.6). The first group contains $N(CH_3)_3^+$ MFC with the highest current and power densities and the lowest start up and steady-state times. The parameters contributing to the higher performance of the $N(CH_3)_3^+$ anode and MFC, respectively, are the positive charge of the surface groups, the higher K_{ETapp}, the higher overpotential applied as well as the presence

of higher amounts of bacteria from the classes of δ-Proteobacteria and Clostridia. Among all tested surfaces deemed hydrophilic, the $N(CH_3)_3^+$ SAM was the least hydrophilic, however, as it can be seen, its positive charge further facilitate attachment of negatively charged bacteria at circumneutral pH. It is well known that an increase in the relative abundance of δ-Proteobacteria in the bacterial biofilm [55,148,149] leads to enhancement of the anodes electrical output, as this bacterial class includes several electrochemically active species. However, due to the complexity of the carbon compounds in wastewater, a consortium between Clostridia and δ-Proteobacteria result in increased electrochemical performance of the SCMFCs.

The second group contains –COOH and –OH modified MFCs. Both are characterized with high hydrophilicity but lower content of δ-Proteobacteria and Clostridia. Contact angles measurements in ultrapure water showed similar values for –OH (27±1°), -COOH (19±1°) and $-N(CH_3)_3^+$ (51±4°) SAMs despite having differently charged surface while the $-CH_3$ SAM had a much higher values (102±2°) (Table 7.1). At the pH of wastewater used in this study, it is not entirely clear if the -COOH group from the $SH(CH_2)_{10}COOH$ is deprotonated or not. The $pK_{1/2}$ of $HS(CH_2)_{10}COOH$ has been found to be 7.4 and the pH of the electrolyte in this study was 7.4-7.5. Crittenden, et al. suggested that the carboxylic acid terminus of SAMs can interact with the peptide bonds in proteins via strong hydrogen bonds [153]. Thus, -COOH could bind outer membrane cytochromes, which are responsible for electron transfer in model electrochemically active microorganisms.

The $–CH_3$ modified anode surface represents the third group. This group demonstrates the longest start up and steady-state times, no δ-Proteobacteria, and most importantly, a

hydrophobic character of the anode surface. The electron transfer rate at the biofilm/electrode interface along with the bacteria attachment depend on the hydrophilicity of the electrode surface. The variations in the surface hydrophilicity affect the electrolyte-electrode interactions, as shown by using a ferricyanide probe (Table 7.1), where increased hydrophobicity decreases the contact between the electrode and the electrolyte and thus lower the charge transfer rate at the bio-support interface. As a result of the decreased charge transfer ability of the electrode surface is also decreased subsequently leading to decrease in the generated current.

There is no clear separation between the impact of the microbial populations and the physical properties of the electrode surface on the MFC's final output. Therefore, it should be noted that both of these factors are present a significant impact on MFC design. It is also reasonable to mention that the physical properties of the electrodes have an effect on microbial community in the formed biofilms. Consequently the hydrophobic/ hydrophilic properties of the surface define the electrode–electrolyte contact and thus charge transfer ability as well as bacterial attachment and biofilm formation. Electrode surface charge on the other hand also influences bacterial attachment. Variation in charge transfer abilities of the electrodes implies the generated current and power densities. In parallel, the types of bacteria present in the wastewater microbial population will greatly influence biofilm formation and the types of bacteria able to participate in the electron transfer, both very important parameters for successful MFC operation.

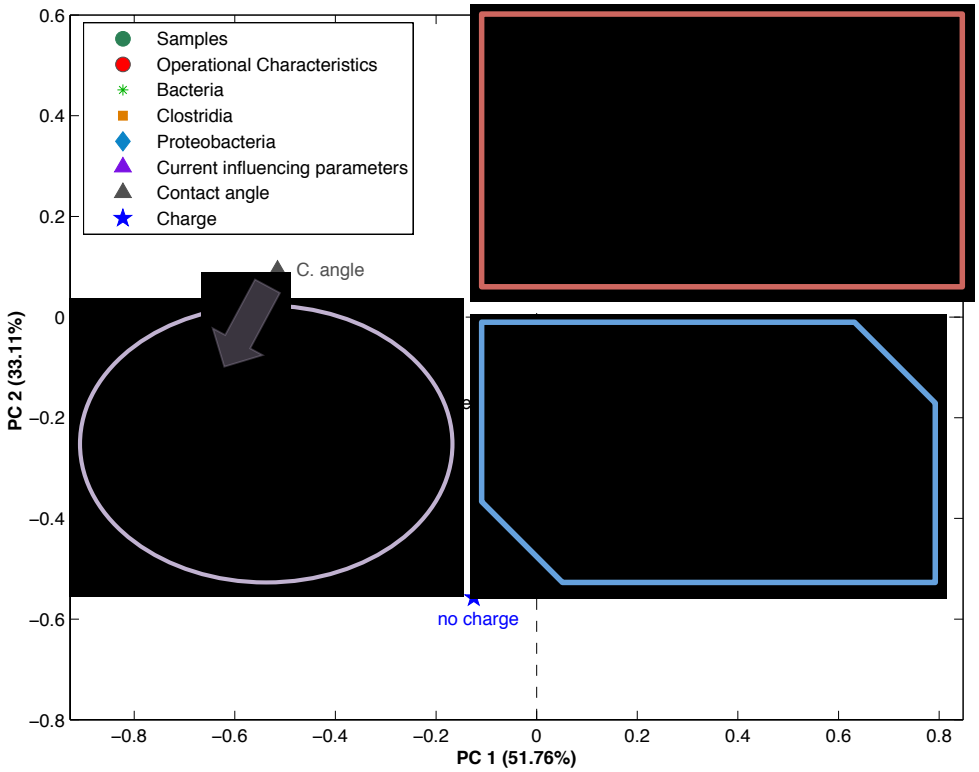

Figure 7.6: PCA biplot with scores (samples) and loadings (variables) for MFCs with different anode surface chemistries are plotted on the first two components, where Isc is the short circuit current of MFCs, SS time is steady-state time, C angle is contact angle, anode and cathode current and overall power generation.

7.4 – Conclusions

Hydrophilic/hydrophobic SAM-modified gold anodes, harboring positive or negative functional groups, determine the current and power output of SCMFCs. Electrochemically active microorganisms attach preferentially on hydrophilic and positively charged surfaces. In fact, $N(CH_3)_3^+$ -modified anodes showed the shortest start-up time, the highest current and power densities and the fastest electron transfer rates among the materials investigated. Pyrosequencing showed the highest percentage of

δ-Proteobacteria on -$N(CH_3)_3^+$ -modified anodes, most likely responsible for direct electron transfer at the biofilm/electrode interface. A consortium of Clostridia and δ-Proteobacteria was found on all anode surfaces, suggesting synergistic effect, which warrants further investigation. A clear separation between the impact of the microbial population and the physical properties of the electrode surface on the MFCs' final output cannot be made. Both of these sets of factors are equally important when MFCs are designed and studied.

Chapter 8 – Effects of *Shewanella oneidensis* Motility Structural Proteins on Electrochemical Performance and Biofilm Development

8.1 Introduction

The ability of *Shewanella oneidensis* to perform efficient electron transfer in microbial biofuel cells is dependent on the presence and structure of the associated biofilm [8,64]. Biofilm formation occurs through a series of discrete, yet overlapping steps: primary attachment, growth of attached cells and maturation. During the maturation phase, surface-associated cell motility is to be essential in many organisms, including *S. oneidensis* [154-156]. In the well-studied model organism, *Pseudomonas aeruginosa* PAO1, two forms of surface associated motility were required for biofilm formation: swarming, mediated by flagella and supported by type IV pili and twitching, mediated by type IV pili alone. Early investigations demonstrated that, while presence of an active twitching apparatus is necessary [156] for biofilm formation, absence of flagellar motility increased biofilm formation [157].

Twitching motility requires the result of extension, adhesion and retraction of type IV pili [158]. Prepilins are first processed by a pre pilin peptidase (PilD) located in the inner membrane of the bacteria cell. These precursors are then assembled into structural pili in an ATP-dependent manner by PilD. The pili extend through the cell wall (Figure 8.1b) and periplasmic space through a pore generated in the outer membrane by PilQ). This results in assembly of the mature pilin. While this process is required for the multiple functions of type IV [159], twitching requires retraction of the pili after they have

attached to the surface, moving the cell forward. This process is mediated via the ATPase PilT [23,160], which disassembles the protein, and shortens the pilus thus, pulling the organism toward the attached end of the pilus.

S. oneidensis contains two structural pili monomer types: a) PilA pili, which are similar to that found in *P. aeruginosa,* and b) another homologous to known mannose-sensitive hemagglutinin (Msh) pili in enteric bacteria. [24]. Biofilm formation on glass is unaffected by the loss of the Msh-type pilin [24], leading to the suggestion that it is responsible for attachment only, and that PilA-type pili are responsible for twitching in *S. oneidensis*. Figure 1a depicts both pili types and flagellum structures in a *S. oneidensis* cell. Figure 8.1b shows a representation of the different peptides that are responsible for ultimately secreting PilA peptides, which elongate beyond the cell's outer membrane. The transmembrane proteins involved in Msh-type pili secretion are represented best represented in the work by Fitzgerlad, et al. [160]

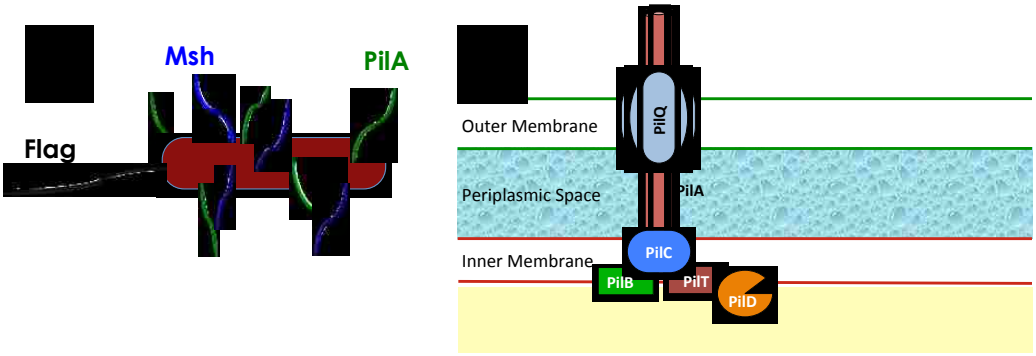

Figure 8.1: a) Schematic of appendages present in *S. oneidensis* MR-1, which consist of one flagellum, and Msh and PilA type IV pili. b) Schematic representation of type IV pili protein complex including the peptides PilQ, PilA, PilB, PilC, PilD and PilT.

Recently, we have demonstrated that variation of the chemistry of the substratum supporting biofilm formation and electrogenesis changes both biofilm structure and current production in wild type *S. oneidensis* MR-1. The morphological properties of the biofilm grown at substrates possessing different chemical and hydrophilic character were quite different and this resulted in different efficiency of electron transfer between the biofilm and electrode. [61,64] Because these differences occur and biofilm formation is dependent on twitching motility, it is important to investigate whether lacking either one or both of the structural pili in the mutant affects biofilm formation and current production. We have previously stated the importance of the anode surface chemistry and accessibility to microbial communities in MFCs. This is why in this study we utilize UV/O_3-treated carbon felt electrodes at the most optimal treatment time for current generation, anode performance and biofilm coverage [162].

Additionally, in this paper we explore the biofilm formation and electrogenic properties of mutants each of the type IV structural pili, and components of the twitching motor. We have found that twitching motility is required for both biofilm formation and electrogenesis under these conditions and is independent of the pilus structure.

8.2 – Materials and Methods

8.2.1 Bacterial strains and growth conditions

All strains of *S. oneidensis* were obtained from the Alfred M. Spormann Laboratory at Stanford University. Genotypic and phenotypic information on these strains and the chromosomal deletions of pilus biogenesis that resulted in the described mutants may be found in the work by Saville, et al. [24] PilA-type mutants consisted in the deletion of

transmembrane peptides involved in the secretion pathway of the PilA protein at several stages (Figure 8.1B). In the case of the Msh-type pili, we studied a mutant that only lacked the structural, extracellular component of the protein complex, which is elsewhere referred as ΔMshA-D [161].

All planktonic cultures of *S. oneidensis* strains were suspended in 50 mM phosphate buffer (pH of 7.4) to which 30 mM of sodium fumarate (Sigma) and 80 mM of sodium lactate (Sigma) were added as oxidizing and reducing agents respectively.

8.2.2 Electrochemical characterization

All electrochemical experiments were conducted in a half-cell configuration consisting of a three-electrode with a reference electrode (saturated Ag/AgCl), a platinum wire counter electrode and a carbon felt as the working electrode (1.2 cm diameter) [50,162]. Prior to assembly, the carbon felt anodes were treated by partial oxidation in a UV/O_3 cleaner 144AX (Jelight Company, Irvine, CA) for 45 min to maximize bacterial adhesion and EET as reported previously [162]. All electrochemical cells were purged with nitrogen and sealed with Parafilm (Sigma) in order to maintain micro-aerobic conditions, which is essential for optimal EET. All electrochemical tests were done using a Gamry Reference 600 potentiostat (Gamry Instruments, Warminster, PA). Chronoamperometric measurements were performed for 24 hours in all bacterial strains at a constant potential of −0.30 V vs. Ag/AgCl followed by acquisition of potentiostatic polarization curves. These studies consisted on chronoamperometry steps starting from open circuit potential set at roughly –0.45 V and ending at 0.3 V vs. Ag/AgCl using 0.05 V increments.

8.2.3 Biofilm imaging and quantification

Upon the completion of electrochemical characterization, biofilm-containing carbon felt electrodes were imaged using a Hitachi S-5200 Nano Scanning Electron Microscope (Hitachi High Technologies America, Inc.) and a Zeiss LSM-510 Meta Confocal Fluorescence Microscope (Carl Zeiss Microscopy, Jena).

SEM sample preparation consisted in bacterial cell fixation to the electrode material following the methodology described previously [61,162]. Briefly, 2.5% glutaraldehyde solution was applied to the samples for a period of 24 hours followed by dehydration in ethanol from 50% to 100% at 10% increments ending with 3 washes of 100% ethanol. This was followed by additional solvent replacement by 50% (v/v) hexamethyl-disilazane (HMDS, Sigma) in ethanol and 100 % HMDS at 15 min of treatment time per immersion before air drying the samples. In order to increase sample conductivity in this microscopy studies. The samples were then coated with a layer of 15 nm of gold-palladium by sputter coating (Emitech K950X). SEM image acquisition was done at an accelerating voltage of 10 kV. The images where then analyzed by greyscale image thresholding using ImageJ (U. S. National Institutes of Health, Bethesda, MD). Gray level pixel intensities from each image where then correlated to the amount of bacterial coverage on a single carbon felt fiber.

Samples for confocal laser scanning microscopic images were fixed in glutaraldehyde as described above and followed by fluorescence nucleic acid staining by submerging each carbon felt electrode in 5 μM Syto 21green stain (Life Technologies, Grand Island, NY, USA) in DI water for 15 min. The stained samples were imaged using an LSM510 Meta confocal microscope using a 63X/0.95W Achroplan water immersion objective, and LSM software. Z stacks were acquired with a slice separation of 0.50 μm. Image processing

was done using a MatLab GUI described previously [64]. This method enables quantitative analysis of such biofilm parameters as biofilm porosity, volume, roughness, cluster size, average diffusion distance (ADD) and Euler dimension (ED).

8.2.4 Principal component analysis

Principal Component Analysis (PCA) is a multivariate method of converting large number of variables into new mathematical variables called principal components. The first principal component (PC 1) captures the largest possible variance in the data and the second, orthogonal to the first, captures the second large variance. Loadings are the coefficients of the linear combinations of the original variables that generate principal component, while scores contain coordinates of the original samples in the new coordinate system. Biplots display both scores for each sample and loadings for each variable visualizing clustering of samples for identification of variables that the most or least important for separating the samples between each other. The 3D biofilm metrics extracted from confocal images along with area coverage calculated from SEM was combined into one dataset with maximum current and startup time extracted from chronoamperommetric measurements. PCA (in PLS_Toolbox 7.9 in Matlab) auto scaling was used to visualize correlations between variables and samples.

8.3 – Results and discussion

8.3.1 Electrochemical characterization and biofilm development

Chronoamperometric and polarization analyses (Figures 8.2a and 8.2b respectively) demonstrate the importance of both structural and motility components of type IV pili in producing an EET-competent biofilm. The ΔPilD mutant, lacking the peptidase required to cleave pre-pilins into structural subunits necessary for assembly of mature pili, presented the lowest current generation and anode performance. Chronoamperometry measurements for this specific mutant exhibited a maximum current density of 1.41 $\mu A/cm^2$, which is 11% of the current values obtained from WT. This result suggests that mature pili are required to form a biofilm capable of EET. Similar results were obtained from mutants lacking the PilT motor protein, required for retraction. This suggests that not only must mature pili be present, but also that they must be capable of surface motility (i.e. twitching). Potentiostatic polarization curves for these mutants also presented poor anodic performance (Figure 8.2b).

In contrast, mutants unable to produce specific individual types of pili (PilA and Msh) recovered an intermediate ability to produce electricity after 10 hours, suggesting that, while both types of pili are required for optimal performance, either on its own will eventually form an electrically active biofilm. In contrast, mutants lacking flagella formed biofilms that were nearly equivalent in their ability to mediate electron transfer. Taken together, these results suggest that twitching motility using both types of pili is required to form an electrically active biofilm in response to electrical poising on ozone-treated carbon felt. These results are in agreement with previous data suggesting that that pili are required in *S. oneidensis* for electrical activity and that twitching motility, specifically, may be required. Given that it has been shown that, unlike in *Geobacter spp,*

the pili do not directly mediate electron transfer [163] imply that perhaps they play a role in biofilms development itself.

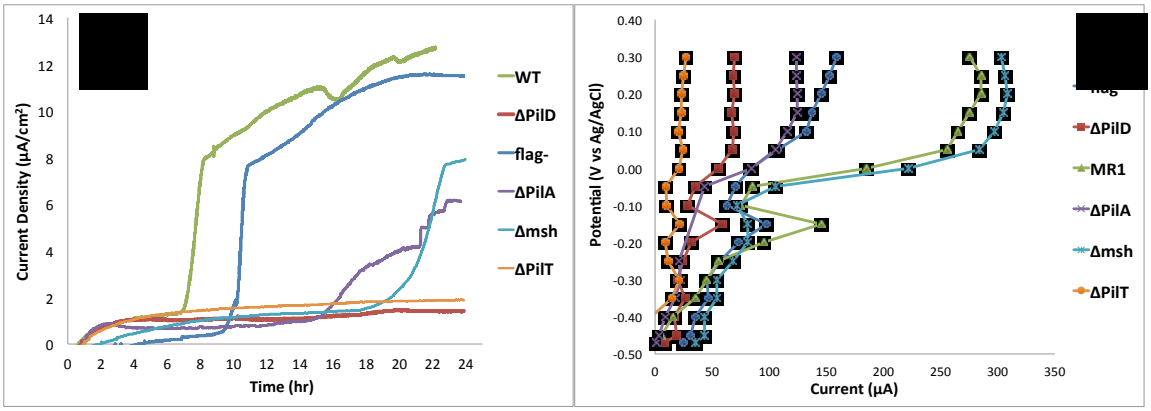

Figure 8.2: Electrochemical characterization of various *S. oneidensis* strains including wild type and motility mutants. a) Chronoamperometric measurements with an applied potential of -0.3 V vs. Ag/AgCl for 24 hours. b) Polarization curves immediately elaborated after chronoamperometric measurements.

Our previous studies [64] demonstrated a direct correlation between biofilm structure and electron transfer performance. SEM imaging of the attached biofilms (figure 8.4) formed by WT and the mutants show that the amount of biofilm formed reflects the amount of current produced: While the biofilm formed by Δflg is more clustered, it seems to be of similar coverage to WT, which had similar electronic performance. The case with the pili mutants is less clear from initial examination of the pictures is less clear. When the amount area % of biofilm was calculated (Figure 8.4), the amount of biofilm present was statistically similar.

In addition, SEM and confocal images from carbon felt fibers containing the ΔPilD *S. oneidensis* mutant strain show the highest deficiency in biofilm coverage (Figures 8.4 and 8.5). These results indicate that ΔPilD pre-pilin peptide processing enzyme while it is

responsible for type IV pili formation, it is also essential for biofilm attachment and thus, EET efficiency. The ΔPilT presents a similar case as the previous mutant in terms of current production and anode performance but it also shows a slight improvement in biofilm development and surface coverage than the ΔPilD mutant. The ΔPilA and ΔMsh mutants show limited electrochemical competency as well as poor electrode biofilm coverage compared to WT while they show significant improvement in all parameters compared to ΔPilD and ΔPilT. This validates the information gathered regarding these two separate protein complexes. In the case of the PilA-lacking strain, Msh pili remain present in the cell and the opposite is occurs in the case of ΔMsh. This suggests that both type IV pili structures are important in surface attachment, biofilm formation, and current production.

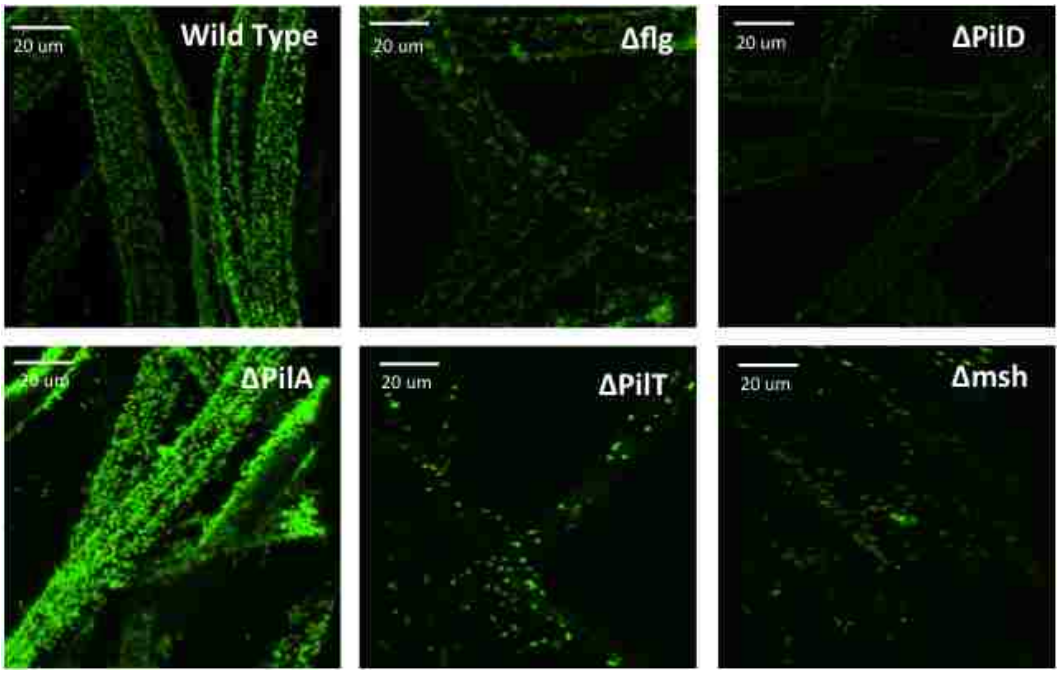

Figure 8.3: Confocal images of wild type *S. oneidensis* and motility mutants attached to carbon felt anodes after anodic polarization.

The Δflg mutant did not present significant variations from the WT results. Although its startup current presented a delayed response compared to that of WT, their final current showed no significant difference. (Figure 8.2a). Similarly, image analysis on this particular strain showed the second most abundant bacterial surface area coverage and biofilm development. This leads us to determine that the absence of this specific appendage is non crucial in the electrochemical process capabilities of *S. oneidensis*. It has been showed elsewhere that its major role of the flagellum pertains to cell motility such swarming in solid substrata and swimming in planktonic environments [163].

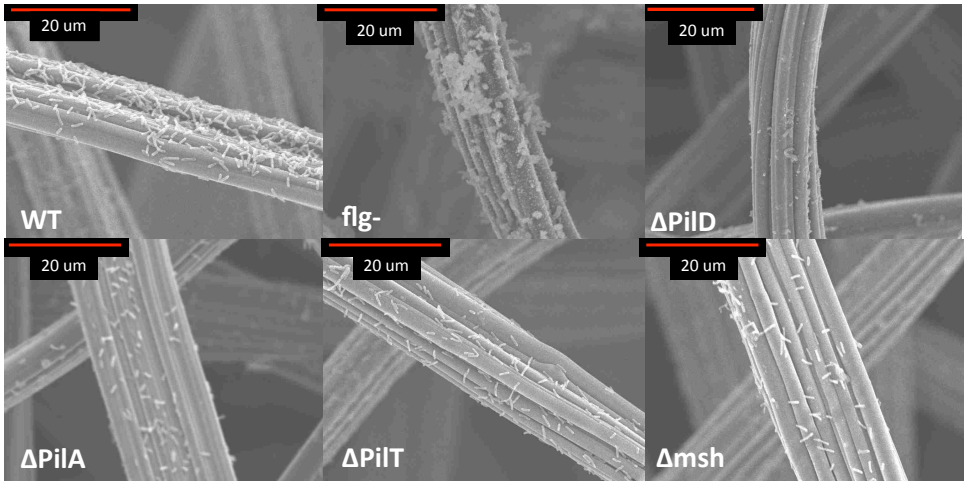

Figure 8.4: SEM images of wild type, pili-lacking and flagella-lacking mutants of *S. oneidensis* attached to carbon felt fibers.

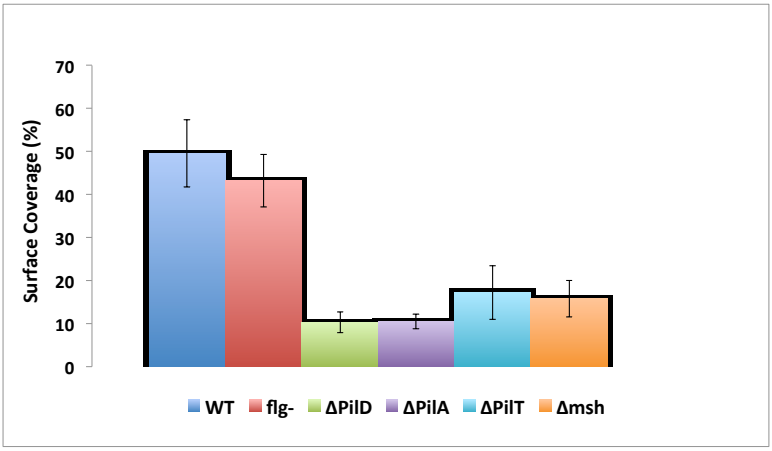

Figure 8.5: Bacterial surface area coverage per carbon felt fiber based on SEM images and processing by ImageJ showing wild type and motility-impaired mutants of *S. oneidensis*.

8.3.2 Image processing and quantitative analysis

Both confocal laser scanning microscopy and SEM images present bacterial surface area coverage on carbon felt electrodes after polarization. Further image analysis tools were utilized in order to characterize the biofilm development from each individual *S. oneidensis* strain, and to determine strong correlations among the given groups of parameters presented in this study. From the electrochemical measurements we utilized final current production from 24 hours of polarization, delay in startup current during chronoamperometry and electrochemical performance from polarization curves. Biofilm-related parameters included biofilm volume, biomass roughness, cluster size, average diffusion distance (ADD), porosity, and surface area coverage per electrode fiber. *Biofilm volume* is a total volume of biomass in the biofilm, while biomass *roughness* describes thickness variation in biomass. *Cluster size* is an average size of consecutive biomass pixels representing cell clusters in X direction. Average diffusion distance (*ADD*) is the average distance from a cell cluster pixel to the nearest pore pixel in the image. This is a

measure of closeness of individual cell clusters to each other. In previous study we have shown that the ratio of between-cluster distance (ADD) and cluster size is an important metrics that serves as a measure of connectivity between cells facilitating electron transfer [64].

All these parameters were combined into one dataset and principal component analysis was applied. Figure 8.6 shows PCA biplot visualizing the correlation between morphological properties of biofilms resulting in efficient electron transfer. The parameters that describe the biofilm that has the most efficient electron transfer are high area coverage and large cell cluster size. Growth in roughness, porosity and connectivity as measured by the average diffusion distance relative to size of cell cluster worsen the performance as seen for the biofilm pertaining to the ΔPilA sample, which lacks a major segment of the pilus filament. The ΔPilD biofilm has the highest biofilm volume from confocal microscopy measurements, but at the same time has worst performance indicating that total biofilm volume is not as important as a cell structure morphological parameter in *S. oneidensis*. The PilD peptidase plays a crucial role in pili synthesis by triggering the activity of the subsequent pili peptides, and as stated previously, it is implicated in cell motility. Size in ADD also worsened the performance as shown for ΔMsh samples. This particular strain presents deficiencies in surface attachment due to the lack of the Msh pili structure, as stated earlier in this report.

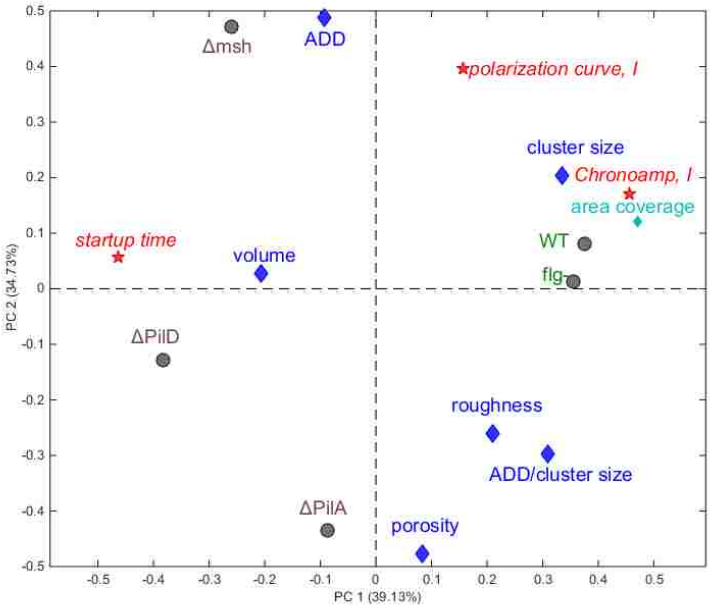

Figure 8.6: Principal component analysis biplot for data set combining 3D metrics from confocal microscopy and electrochemical performance for all tested mutants and wild type *S. oneidensis*.

8.4 – Conclusions

We have presented another important aspect in biofilm formation in electrochemically active microorganisms for the process of extracellular electron transfer (EET). This involves microbial appendages, which have been suggested to be involved in motility and attachment. There are ongoing studies regarding the identification and characterization of the roles of such appendages. In this study, we utilized motility mutants of *S. oneidensis* that lack key proteins involved in the secretion of type IV pili and flagella in order to take a further look at the importance of each of these individual proteins.

We utilized electrochemical characterization techniques to compare performance and current generation in each tested mutant as well as in wild type *S. oneidensis.*

Furthermore, we studied and quantified the anodic biofilm 3D morphological characteristics based on microscopic techniques. PilD (pre-pilin processing protein) lacking mutant exhibited the highest deficiencies in terms of electrochemical performance and biofilm coverage while wild type bacteria presented the most optimal conditions. The PilD peptide was therefore identified as a major component in *S. oneidensis* that strongly influences bacterial attachment to the electrode and therefore EET.

Chapter 9 – Summary of Accomplishments and Future Work Outlook

Electrochemical tools were utilized to measure electrical current (chronoamperometry) and anode performance (polarization curves) using cultures of *S. oneidensis* MR-1. Recognition of electrochemically active metabolites was done by cyclic voltammetry. This allowed us to identify molecular interactions in the *S. oneidensis* outer membrane that leads to electron transfer and current production, particularly, those between cytochromes and flavins, which lead to electron flow from the cellular outer membrane to the anode material. Molecular docking simulations of these components were also done in order to calculate the degree of affinity of a particular cytochrome (e.g. MtrC, MtrF) with flavin molecules, which in turn allowed us to better understand the role of individual types of outer membrane cytochromes in EET for *S. oneidensis.*

Surface-treated anodes were evaluated for optimal *Shewanella oneidensis* biofilm development and electrochemical performance by utilizing UV/O_3 treatment of carbon felt anodes. This simple and inexpensive treatment method allowed us to achieve maximum currents generated by *S. oneidensis* by increasing surface wettability which was dependent on the time of treatment.

In addition, biofilm morphology studies were done in order to further analyze bacterial-anode interactions at the completion of all electrochemical measurements. We investigated the influence of electrode surface charge and degree of hydrophobicity on biofilm formation and current generation. The anode platform models that were utilized for these studies consisted of SAMs formed on gold substrates. Positively charged SAMs provided the most developed biofilm and the highest electrochemical performance in an electrochemical cell. We employed information to mixed cultures found in activated

sludge from municipal wastewater reclamation in order to identify potential electrogenic cultures on the most biofilm compatible electrode surfaces. A significant amount of δ-proteobacteria was found on the hydrophilic SAM electrodes. Specifically the positively charged SAM anode created the most abundant population of δ-proteobacteria and the highest MFC performance and power generation.

We also took a further look at the protein complexes that make up type IV pili found in *S. oneidensis* in order to identify the proteins that influence biofilm formation and current production the most. For this, we utilized motility mutants that either partially or totally lacked pili and results where compared to wild type cultures. The ΔPilD strain, which totally lacks type IV pili, presented the lowest current and poorest biofilm coverage and development. The PilD pre-pilin processing peptide was therefore identified as a major component in *S. oneidensis* that strongly influences bacterial attachment to the electrode and therefore EET. Our studies conclude that flavin molecules are indeed bound to outer membrane cytochromes, therefore presenting surface confinement at the anode material during the EET process. This is crucial for further studies in metabolomics of *S. oneidensis* and its impact on current output.

References

1. Bretschger, O.; Obraztsova, A.; Sturm, C. A.; Chang, I. S.; Gorby, Y. A.; Reed, S. B.; Culley, D. E.; Reardon, C. L.; Barua, S.; Romine, M. F.; Zhou, J.; Beliaev, A. S.; Bouhenni, R.; Saffarini, D.; Mansfeld, F.; Kim, B.-H.; Fredrickson, J. K.; Nealson, K. H., Current production and metal oxide reduction by Shewanella oneidensis MR-1 wild type and mutants. *Applied and Environmental Microbiology* **2007,** *73* (21), 7003-7012.

2. Myers, C. R.; Nealson, K. H., BACTERIAL MANGANESE REDUCTION AND GROWTH WITH MANGANESE OXIDE AS THE SOLE ELECTRON-ACCEPTOR. *Science* **1988,** *240* (4857), 1319-1321.

3. Nealson, K. H.; Scott, J., Ecophysiology of the Genus Shewanella. In *Prokaryotes: a Handbook on the Biology of Bacteria, Vol 6, Third Edition: Proteobacteria: Gamma Subclass*, Dworkin, M.; Falkow, S.; Rosenberg, E.; Schleifer, K. H.; Stackebrandt, E., Eds. Springer: New York, 2006; pp 1133-1151.

4. Rabaey, K.; Rodriguez, J.; Blackall, L. L.; Keller, J.; Gross, P.; Batstone, D.; Verstraete, W.; Nealson, K. H., Microbial ecology meets electrochemistry: electricity-driven and driving communities. *Isme Journal* **2007,** *1* (1), 9-18.

5. Myers, C. R.; Myers, J. M., LOCALIZATION OF CYTOCHROMES TO THE OUTER-MEMBRANE OF ANAEROBICALLY GROWN SHEWANELLA-PUTREFACIENS MR-1.*Journal of Bacteriology* **1992,** *174* (11), 3429-3438.

6. Rabaey, K.; Boon, N.; Hofte, M.; Verstraete, W., Microbial phenazine production enhances electron transfer in biofuel cells. *Environmental Science & Technology* **2005,** *39* (9), 3401-3408.

7. Rabaey, K.; Boon, N.; Siciliano, S. D.; Verhaege, M.; Verstraete, W., Biofuel cells select for microbial consortia that self-mediate electron transfer. *Applied and Environmental Microbiology* **2004,** *70* (9), 5373-5382.

8. Marsili, E.; Baron, D. B.; Shikhare, I. D.; Coursolle, D.; Gralnick, J. A.; Bond, D. R., Shewanella Secretes flavins that mediate extracellular electron transfer. *Proceedings of the National Academy of Sciences of the United States of America* **2008,** *105* (10), 3968-3973.

9. Fredrickson, J. K.; Romine, M. F.; Beliaev, A. S.; Auchtung, J. M.; Driscoll, M. E.; Gardner, T. S.; Nealson, K. H.; Osterman, A. L.; Pinchuk, G.; Reed, J. L.; Rodionov, D. A.; Rodrigues, J. L. M.; Saffarini, D. A.; Serres, M. H.; Spormann, A. M.; Zhulin, I. B.; Tiedje, J. M., Towards environmental systems biology of Shewanella. *Nature Reviews Microbiology* **2008,** *6* (8), 592-603.

10. Gorby, Y. A.; Yanina, S.; McLean, J. S.; Rosso, K. M.; Moyles, D.; Dohnalkova, A.; Beveridge, T. J.; Chang, I. S.; Kim, B. H.; Kim, K. S.; Culley, D. E.; Reed, S. B.; Romine, M. F.; Saffarini, D. A.; Hill, E. A.; Shi, L.; Elias, D. A.; Kennedy, D. W.; Pinchuk, G.; Watanabe, K.; Ishii, S. i.; Logan, B.; Nealson, K. H.; Fredrickson, J. K., Electrically conductive bacterial nanowires produced by Shewanella oneidensis strain MR-1 and other microorganisms. *Proceedings of the National Academy of Sciences of the United States of America* **2006,** *103* (30), 11358-11363.

11. El-Naggar, M. Y.; Wanger, G.; Leung, K. M.; Yuzvinsky, T. D.; Southam, G.; Yang, J.; Lau, W. M.; Nealson, K. H.; Gorby, Y. A., Electrical transport along bacterial nanowires from Shewanella oneidensis MR-1. *Proceedings of the National Academy of Sciences of the United States of America* **2010,** *107* (42), 18127-18131.

12. Myers, C. R.; Myers, J. M., Cell surface exposure of the outer membrane cytochromes of Shewanella oneidensis MR-1. *Letters in Applied Microbiology* **2003,** *37* (3), 254-258.

13. Covington, E. D.; Gelbmann, C. B.; Kotloski, N. J.; Gralnick, J. A., An essential role for UshA in processing of extracellular flavin electron shuttles by Shewanella oneidensis. *Molecular Microbiology* **2010,** *78* (2), 519-532.

14. Pitts, K. E.; Dobbin, P. S.; Reyes-Ramirez, F.; Thomson, A. J.; Richardson, D. J.; Seward, H. E., Characterization of the Shewanella oneidensis MR-1 decaheme cytochrome MtrA. *Journal of Biological Chemistry* **2003,** *278* (30), 27758-27765.

15. Beliaev, A. S.; Saffarini, D. A.; McLaughlin, J. L.; Hunnicutt, D., MtrC, an outer membrane decahaem c cytochrome required for metal reduction in Shewanella putrefaciens MR-1. *Molecular Microbiology* **2001,** *39* (3), 722-730.

16. Beliaev, A. S.; Saffarini, D. A., Shewanella putrefaciens mtrB encodes an outer membrane protein required for Fe(III) and Mn(IV) reduction. *Journal of Bacteriology* **1998,** *180* (23), 6292-6297.

17. Myers, C. R.; Myers, J. M., MtrB is required for proper incorporation of the cytochromes OmcA and OmcB into the outer membrane of Shewanella putrefaciens MR-1. *Applied and Environmental Microbiology* **2002,** *68* (11), 5585-5594.

18. Myers, C. R.; Myers, J. M., The outer membrane cytochromes of Shewanella oneidensis MR-1 are lipoproteins. *Letters in Applied Microbiology* **2004,** *39* (5), 466-470.

19. Breuer, M.; Rosso, K. M.; Blumberger, J., Electron flow in multiheme bacterial cytochromes is a balancing act between heme electronic interaction and redox potentials. *Proceedings of the National Academy of Sciences of the United States of America* **2014,** *111* (2), 611-616.

20. von Canstein, H.; Ogawa, J.; Shimizu, S.; Lloyd, J. R., Secretion of flavins by Shewanella species and their role in extracellular electron transfer. *Applied and Environmental Microbiology* **2008,** *74* (3), 615-623.

21. Foster, C.; Jones, J. H.; Henle, W.; Dorfman, F., THE EFFECT OF VITAMIN B(1) DEFICIENCY AND OF RESTRICTED FOOD INTAKE ON THE RESPONSE OF MICE TO THE LANSING STRAIN OF POLIOMYELITIS VIRUS. *Journal of Experimental Medicine* **1944,** *79* (2), 221-234.

22. Tsuneda, S.; Aikawa, H.; Hayashi, H.; Yuasa, A.; Hirata, A., Extracellular polymeric substances responsible for bacterial adhesion onto solid surface. *Fems Microbiology Letters* **2003,***223* (2), 287-292.

23. Merz, A. J.; Forest, K. T., Bacterial surface motility: Slime trails, grappling hooks and nozzles. *Current Biology* **2002,** *12* (8), R297-R303.

24. Saville, R. M.; Dieckmann, N.; Spormann, A. M., Spatiotemporal activity of the mshA gene system in Shewanella oneidensis MR-1 biofilms. *Fems Microbiology Letters* **2010,** *308* (1), 76-83.

25. Rinaldi, A.; Mecheri, B.; Garavaglia, V.; Licoccia, S.; Di Nardo, P.; Traversa, E., Engineering materials and biology to boost performance of microbial fuel cells: a critical review. *Energy & Environmental Science* **2008,** *1* (4), 417-429.

26. Xie, X.; Hu, L.; Pasta, M.; Wells, G. F.; Kong, D.; Criddle, C. S.; Cui, Y., Three-Dimensional Carbon Nanotube-Textile Anode for High-Performance Microbial Fuel Cells. *Nano Letters* **2011,** *11* (1), 291-296.

27. Luckarift, H. R.; Sizemore, S. R.; Roy, J.; Lau, C.; Gupta, G.; Atanassov, P.; Johnson, G. R., Standardized microbial fuel cell anodes of silica-immobilized Shewanella oneidensis. *Chemical Communications* **2010,** *46* (33), 6048-6050.

28. Mink, J. E.; Hussain, M. M., Sustainable Design of High-Performance Microsized Microbial Fuel Cell with Carbon Nanotube Anode and Air Cathode. *Acs Nano* **2013,** *7* (8), 6921-6927.

29. Santoro, C.; Guilizzoni, M.; Baena, J. P. C.; Pasaogullari, U.; Casalegno, A.; Li, B.; Babanova, S.; Artyushkova, K.; Atanassov, P., The effects of carbon electrode surface properties on bacteria attachment and start up time of microbial fuel cells. *Carbon* **2014,** *67*, 128-139.

30. L. Xian-Wei, et al., Integration of a microbial fuel cell with activated sludge process for energy-saving wastewater treatment: Taking a sequencing batch reactor as an example. *Biotechnology and Bioengineering* **2011**, 108 (6), 1260-1267.

31. Bond, D. R.; Lovley, D. R., Electricity production by Geobacter sulfurreducens attached to electrodes. *Applied and Environmental Microbiology* **2003,** *69* (3), 1548-1555.

32. Kotloski, N. J.; Gralnick, J. A., Flavin electron shuttles dominate extracellular electron transfer by Shewanella oneidensis. *mBio* **2013,** *4* (1).

33. Coursolle, D.; Baron, D. B.; Bond, D. R.; Gralnick, J. A., The Mtr Respiratory Pathway Is Essential for Reducing Flavins and Electrodes in Shewanella oneidensis. *Journal of Bacteriology* **2010,** *192* (2), 467-474.

34. Wang, V. B.; Kirchhofer, N. D.; Chen, X.; Tan, M. Y. L.; Sivakumar, K.; Cao, B.; Zhang, Q.; Kjelleberg, S.; Bazan, G. C.; Loo, S. C. J.; Marsili, E., Comparison of flavins and a conjugated oligoelectrolyte in stimulating extracellular electron transport from Shewanella oneidensis MR-1. *Electrochemistry Communications* **2014,** *41*, 55-58.

35. Okamoto, A.; Hashimoto, K.; Nealson, K. H., Flavin Redox Bifurcation as a Mechanism for Controlling the Direction of Electron Flow during Extracellular Electron Transfer. *Angewandte Chemie-International Edition* **2014,** *53* (41), 10988-10991.

36. Okamoto, A.; Hashimoto, K.; Nealson, K. H.; Nakamura, R., Rate enhancement of bacterial extracellular electron transport involves bound flavin semiquinones. *Proceedings of the National Academy of Sciences of the United States of America* **2013,** *110* (19), 7856-7861.

37. Okamoto, A.; Kalathil, S.; Deng, X.; Hashimoto, K.; Nakamura, R.; Nealson, K. H., Cell-secreted Flavins Bound to Membrane Cytochromes Dictate Electron Transfer Reactions to Surfaces with Diverse Charge and pH. *Scientific Reports* **2014,** *4*.

38. Okamoto, A.; Saito, K.; Inoue, K.; Nealson, K. H.; Hashimoto, K.; Nakamura, R., Uptake of self-secreted flavins as bound cofactors for extracellular electron transfer in Geobacter species.*Energy & Environmental Science* **2014,** *7* (4), 1357-1361.

39. Trott, O.; Olson, A. J., Software News and Update AutoDock Vina: Improving the Speed and Accuracy of Docking with a New Scoring Function, Efficient Optimization, and Multithreading.*Journal of Computational Chemistry* **2010,** *31* (2), 455-461.

40. Morris, G. M.; Huey, R.; Lindstrom, W.; Sanner, M. F.; Belew, R. K.; Goodsell, D. S.; Olson, A. J., AutoDock4 and AutoDockTools4: Automated Docking with Selective Receptor Flexibility.*Journal of Computational Chemistry* **2009,** *30* (16), 2785-2791.

41. Huey, R.; Morris, G. M.; Olson, A. J.; Goodsell, D. S., A semiempirical free energy force field with charge-based desolvation. *Journal of Computational Chemistry* **2007,** *28* (6), 1145-1152.

42. Li, R.; Tiedje, J. M.; Chiu, C.; Worden, R. M., Soluble Electron Shuttles Can Mediate Energy Taxis toward Insoluble Electron Acceptors. *Environmental Science & Technology* **2012,** *46* (5), 2813-2820.

43. Edwards, M. J.; Baiden, N. A.; Johs, A.; Tomanicek, S. J.; Liang, L.; Shi, L.; Fredrickson, J. K.; Zachara, J. M.; Gates, A. J.; Butt, J. N.; Richardson, D. J.; Clarke, T. A., The X-ray crystal structure of Shewanella oneidensis OmcA reveals new insight at the microbe-mineral interface. *Febs Letters* **2014,** *588* (10), 1886-1890.

44. Gaussian 09, Revision B.01 (Gaussian, Inc., Wallingford CT, 2009).

45. J Roy, J. N.; Luckarift, H. R.; Lau, C.; Falase, A.; Garcia, K. E.; Ista, L. K.; Chellamuthu, P.; Ramasamy, R. P.; Gadhamshetty, V.; Wanger, G.; Gorby, Y. A.; Nealson, K. H.; Bretschger, O.; Johnson, G. R.; Atanassov, P., A study of the flavin response by Shewanella cultures in carbon-limited environments. *Rsc Advances* **2012,** *2* (26), 10020-10027.

46. Reardon, C. L.; Dohnalkova, A. C.; Nachimuthu, P.; Kennedy, D. W.; Saffarini, D. A.; Arey, B. W.; Shi, L.; Wang, Z.; Moore, D.; McLean, J. S.; Moyles, D.; Marshall, M. J.; Zachara, J. M.; Fredrickson, J. K.; Beliaev, A. S., Role of outer-membrane cytochromes MtrC and OmcA in the biomineralization of ferrihydrite by Shewanella oneidensis MR-1. *Geobiology* **2010,** *8* (1), 56-68.

47. Shi, L.; Richardson, D. J.; Wang, Z.; Kerisit, S. N.; Rosso, K. M.; Zachara, J. M.; Fredrickson, J. K., The roles of outer membrane cytochromes of Shewanella and Geobacter in extracellular electron transfer. *Environmental Microbiology Reports* **2009,** *1* (4), 220-227.

48. Shi, L.; Squier, T. C.; Zachara, J. M.; Fredrickson, J. K., Respiration of metal (hydr)oxides by Shewanella and Geobacter: a key role for multihaem c-type cytochromes. *Molecular Microbiology* **2007,** *65* (1), 12-20.

49 Roy, J. N.; Garcia, K. E.; Luckarift, H. R.; Falase, A.; Cornejo, J.; Babanova, S.; Schuler, A. J.; Johnson, G. R.; Atanassov, P. B., Applied Electrode Potential Leads to Shewanella oneidensis MR-1 Biofilms Engaged in Direct Electron Transfer. *Journal of the Electrochemical Society* **2013,** *160* (11), 866-871.

50. Roy, J. N.; Babanova, S.; Garcia, K. E.; Cornejo, J.; Ista, L. K.; Atanassov, P., Catalytic biofilm formation by Shewanella oneidensis MR-1 and anode characterization by expanded uncertainty. *Electrochimica Acta* **2014,** *126*, 3-10.

51. H. Luckarift, P. Atanassov, and G. Johnson, Enzymatic fuel cells: From fundamentals to applications. Hoboken, New Jersey: John Wiley and Sons, Inc.; **2014**.

52. Wei, J.; Liang, P.; Huang, X., Recent progress in electrodes for microbial fuel cells. *Bioresource Technology* **2011,** *102* (20), 9335-9344.

53. Cheng, S.; Logan, B. E., Ammonia treatment of carbon cloth anodes to enhance power generation of microbial fuel cells. *Electrochemistry Communications* **2007,** *9* (3), 492-496.

54. Crittenden, S. R.; Sund, C. J.; Sumner, J. J., Mediating electron transfer from bacteria to a gold electrode via a self-assembled monolayer. *Langmuir* **2006,** *22* (23), 9473-9476.

55. Guo, K.; Freguia, S.; Dennis, P. G.; Chen, X.; Donose, B. C.; Keller, J.; Gooding, J. J.; Rabaey, K., Effects of Surface Charge and Hydrophobicity on Anodic Biofilm Formation, Community Composition, and Current Generation in Bioelectrochemical Systems. *Environmental Science & Technology* **2013,** *47* (13), 7563-7570.

56. Higgins, S. R.; Foerster, D.; Cheung, A.; Lau, C.; Bretschger, O.; Minteer, S. D.; Nealson, K.; Atanassov, P.; Cooney, M. J., Fabrication of macroporous chitosan scaffolds doped with carbon nanotubes and their characterization in microbial fuel cell operation. *Enzyme and Microbial Technology* **2011,** *48* (6-7), 458-465.

57. Hubenova, Y. V.; Rashkov, R. S.; Buchvarov, V. D.; Arnaudova, M. H.; Babanova, S. M.; Mitov, M. Y., Improvement of Yeast-Biofuel Cell Output by Electrode Modifications. *Industrial & Engineering Chemistry Research* **2011,** *50* (2), 557-564.

58. Santoro, C.; Artyushkova, K.; Babanova, S.; Atanassov, P.; Ieropoulos, I.; Grattieri, M.; Cristiani, P.; Trasatti, S.; Li, B.; Schuler, A. J., Parameters characterization and optimization of activated carbon (AC) cathodes for microbial fuel cell application. *Bioresource Technology* **2014,** *163*, 54-63.

59. Li, B.; Zhou, J.; Zhou, X.; Wang, X.; Li, B.; Santoro, C.; Grattieri, M.; Babanova, S.; Artyushkova, K.; Atanassov, P.; Schuler, A. J., Surface Modification of Microbial Fuel Cells Anodes: Approaches to Practical Design. *Electrochimica Acta* **2014,** *134*, 116-126

60. Biffinger, J. C.; Pietron, J.; Ray, R.; Little, B.; Ringeisen, B. R., A biofilm enhanced miniature microbial fuel cell using Shewanella oneidensis DSP10 and oxygen reduction cathodes. *Biosensors & Bioelectronics* **2007,** *22* (8), 1672-1679.

61. Santoro, C.; Babanova, S.; Artyushkova, K.; Cornejo, J.A.; Ista, L.; Bretschger, O.; Marsili, E.; Atanassov, P.; Schuler, A.J.; Influence of anode surface chemistry on microbial fuel cell operation. *Bioelectrochemistry* **2015,** DOI:10.1016/j.bioelechem.2015.05.002.

62. Torres, C. I.; Marcus, A. K.; Lee, H.-S.; Parameswaran, P.; Krajmalnik-Brown, R.; Rittmann, B. E., A kinetic perspective on extracellular electron transfer by anode-respiring bacteria. *Fems Microbiology Reviews* **2010,** *34* (1), 3-17.

63. Liang, P.; Wang, H.; Xia, X.; Huang, X.; Mo, Y.; Cao, X.; Fan, M., Carbon nanotube powders as electrode modifier to enhance the activity of anodic biofilm in microbial fuel cells. *Biosensors & Bioelectronics* **2011,** *26* (6), 3000-3004.

64. Artyushkova, K.; Cornejo, J. A.; Ista, L. K.; Babanova, S.; Santoro, C.; Atanassov, P.; Schuler, A. J., Relationship between surface chemistry, biofilm structure, and electron transfer in Shewanella anodes. *Biointerphases* **2015,** *10* (1).

65. Saito, T.; Mehanna, M.; Wang, X.; Cusick, R. D.; Feng, Y.; Hickner, M. A.; Logan, B. E., Effect of nitrogen addition on the performance of microbial fuel cell anodes. *Bioresource Technology* **2011,** *102* (1), 395-398.

66. Lowy, D. A.; Tender, L. M., Harvesting energy from the marine sediment-water interface III. Kinetic activity of quinone- and antimony-based anode materials. *Journal of Power Sources* **2008,** *185* (1), 70-75.

67. Wang, H. Z.; Huang, Z. P.; Cai, Q. J.; Kulkarni, K.; Chen, C. L.; Carnahan, D.; Ren, Z. F., Reversible transformation of hydrophobicity and hydrophilicity of aligned carbon nanotube arrays and buckypapers by dry processes. *Carbon* **2010,** *48* (3), 868-875.

68. Grujicic, M.; Cao, G.; Rao, A. M.; Tritt, T. M.; Nayak, S., UV-light enhanced oxidation of carbon nanotubes. *Applied Surface Science* **2003,** *214* (1-4), 289-303.

69. Najafi, E.; Kim, J.-Y.; Han, S.-H.; Shin, K., UV-ozone treatment of multi-walled carbon nanotubes for enhanced organic solvent dispersion. *Colloids and Surfaces a-Physicochemical and Engineering Aspects* **2006,** *284*, 373-378.

70. Sham, M. L.; Kim, J. K., Surface functionalities of multi-wall carbon nanotubes after UV/Ozone and TETA treatments. *Carbon* **2006,** *44* (4), 768-777.

71. Bard, A.J.; Faulkner, L.R.; Fundamentals and applications. *Electrochemical Methods* **2001**, 2nd ed.; Wiley: New York.

72. Brocato, S.; Lau, C.; Atanassov, P., Mechanistic study of direct electron transfer in bilirubin oxidase. *Electrochimica Acta* **2012,** *61*, 44-49.

73. Bretschger, O.; Cheung, A. C. M.; Mansfeld, F.; Nealson, K. H., Comparative Microbial Fuel Cell Evaluations of Shewanella spp. *Electroanalysis* **2010,** *22* (7-8), 883-894.

74. Hsu, L.; Masuda, S. A.; Nealson, K. H.; Pirbazari, M., Evaluation of microbial fuel cell Shewanella biocathodes for treatment of chromate contamination. *Rsc Advances* **2012,** *2* (13), 5844-5855.

75. Higgins, S. R.; Lau, C.; Atanassov, P.; Minteer, S. D.; Cooney, M. J., Hybrid Biofuel Cell: Microbial Fuel Cell with an Enzymatic Air-Breathing Cathode. *Acs Catalysis* **2011,** *1* (9), 994-997.

76. Nevin, K. P.; Kim, B.-C.; Glaven, R. H.; Johnson, J. P.; Woodard, T. L.; Methe, B. A.; DiDonato, R. J., Jr.; Covalla, S. F.; Franks, A. E.; Liu, A.; Lovley, D. R., Anode Biofilm Transcriptomics Reveals Outer Surface Components Essential for High Density Current Production in Geobacter sulfurreducens Fuel Cells. *Plos One* **2009,** *4* (5).

77. Wang, X.; Cheng, S.; Feng, Y.; Merrill, M. D.; Saito, T.; Logan, B. E., Use of Carbon Mesh Anodes and the Effect of Different Pretreatment Methods on Power Production in Microbial Fuel Cells. *Environmental Science & Technology* **2009,** *43* (17), 6870-6874.

78. Manickam, S. S.; Karra, U.; Huang, L.; Nhu-Ngoc, B.; Li, B.; McCutcheon, J. R., Activated carbon nanofiber anodes for microbial fuel cells. *Carbon* **2013,** *53*, 19-28.

79. Zhou, M.; Chi, M.; Wang, H.; Jin, T., Anode modification by electrochemical oxidation: A new practical method to improve the performance of microbial fuel cells. *Biochemical Engineering Journal* **2012,** *60*, 151-155.

80. Santoro, C.; Ieropoulos, I.; Greenman, J.; Cristiani, P.; Vadas, T.; Mackay, A.; Li, B., Power generation and contaminant removal in single chamber microbial fuel cells (SCMFCs) treating human urine. *International Journal of Hydrogen Energy* **2013,** *38* (26), 11543-11551.

81. Logan, B. E., Exoelectrogenic bacteria that power microbial fuel cells. *Nature Reviews Microbiology* **2009,** *7* (5), 375-381.

82. Cumpson, P. J., Angle-resolved XPS depth-profiling strategies. *Applied Surface Science* **1999,** *144-45*, 16-20.

83. Artyushkova, K.; Fulghum, J. E.; Reznikov, Y., Orientation of 5CB molecules on aligning substrates studied by angle resolved X-ray photoelectron spectroscopy. *Molecular Crystals and Liquid Crystals* **2005,** *438*, 1769-1777.

84. Baer, D. R.; Engelhard, M. H., XPS analysis of nanostructured materials and biological surfaces. *Journal of Electron Spectroscopy and Related Phenomena* **2010,** *178*, 415-432.

85. Eby, D. M.; Artyushkova, K.; Paravastu, A. K.; Johnson, G. R., Probing the molecular structure of antimicrobial peptide-mediated silica condensation using X-ray photoelectron spectroscopy.*Journal of Materials Chemistry* **2012,** *22* (19), 9875-9883.

86. Ivnitski, D.; Artyushkova, K.; Atanassov, P., Surface characterization and direct electrochemistry of redox copper centers of bilirubin oxidase from fungi Myrothecium verrucaria.*Bioelectrochemistry* **2008,** *74* (1), 101-110.

87. Nelson, K. E.; Gamble, L.; Jung, L. S.; Boeckl, M. S.; Naeemi, E.; Golledge, S. L.; Sasaki, T.; Castner, D. G.; Campbell, C. T.; Stayton, P. S., Surface characterization of mixed self-assembled monolayers designed for streptavidin immobilization. *Langmuir* **2001,** *17* (9), 2807-2816.

88. Vericat, C.; Vela, M. E.; Benitez, G. A.; Gago, J. A. M.; Torrelles, X.; Salvarezza, R. C., Surface characterization of sulfur and alkanethiol self-assembled monolayers on Au(111). *Journal of Physics-Condensed Matter* **2006,** *18* (48), R867-R900.

89. Beyenal, H.; Donovan, C.; Lewandowski, Z.; Harkin, G., Three-dimensional biofilm structure quantification. *Journal of Microbiological Methods* **2004,** *59* (3), 395-413.

90. Beyenal, H.; Lewandowski, Z.; Harkin, G., Quantifying biofilm structure: Facts and fiction. *Biofouling* **2004,** *20* (1), 1-23.

91. Yang, X. M.; Beyenal, H.; Harkin, G.; Lewandowski, Z., Quantifying biofilm structure using image analysis. *Journal of Microbiological Methods* **2000,** *39* (2), 109-119.

92. Artyushkova, K.; Atanassov, P., X-Ray Photoelectron Spectroscopy for Characterization of Bionanocomposite Functional Materials for Energy-Harvesting Technologies. *Chemphyschem* **2013,** *14* (10), 2071-2080.

93. Artyushkova, K; "GUI," http://goo.gl/IHavd6.

94. Artyushkova, K.; Pylypenko, S.; Dowlapalli, M.; Atanassov, P., Structure-to-property relationships in fuel cell catalyst supports: Correlation of surface chemistry and morphology with oxidation resistance of carbon blacks. *Journal of Power Sources* **2012,** *214*, 303-313.

95. Artyushkova, K.; Pylypenko, S.; Dowlapalli, M.; Atanassov, P., Use of digital image processing of microscopic images and multivariate analysis for quantitative correlation of morphology, activity and durability of electrocatalysts. *Rsc Advances* **2012,** *2* (10), 4304-4310.

96. Cheng-Ting, S.; Yuan-Jen, C.; Bor-Tsung, H.; Wu, J.; IEEE Trans. Nucl. Sci **2013**, 60, 2155.

97. N. C. Popa, "Microstructural properties: Texture and macrostress effects," in Powder Diffraction, Theory and Practice, edited by R. E. Dinnebier and S. J. L. Billinge (RSC Publishing, Cambridge, **2008**).

98. Sastry, S.S.; Rao, B.G.S.; Mahalakshmi, K.B.; Mallika, K.; Rao, C.N.; Tiong, H.S.; Image Analysis Studies for Phase Transitions of Ferroelectric Liquid Crystals ISRN Condens. Matter Phys. **2012**, 2012, 423650.

99. Khan, M. M. T.; Ista, L. K.; Lopez, G. P.; Schuler, A. J., Experimental and Theoretical Examination of Surface Energy and Adhesion of Nitrifying and Heterotrophic Bacteria Using Self-Assembled Monolayers. *Environmental Science & Technology* **2011,** *45* (3), 1055-1060.

100. Cumpson, P. J., Angle-resolved XPS depth-profiling strategies. *Applied Surface Science* **1999,** *144-45*, 16-20.

101. Cumpson, P. J.; Seah, M. P., Elastic scattering corrections in AES and XPS .2. Estimating attenuation lengths and conditions required for their valid use in overlayer/substrate experiments.*Surface and Interface Analysis* **1997,** *25* (6), 430-446.

102. Penn, D. R., QUANTITATIVE CHEMICAL-ANALYSIS BY ESCA. *Journal of Electron Spectroscopy and Related Phenomena* **1976,** *9* (1), 29-40.

103. Biebuyck, H. A.; Bian, C. D.; Whitesides, G. M., COMPARISON OF ORGANIC MONOLAYERS ON POLYCRYSTALLINE GOLD SPONTANEOUSLY ASSEMBLED FROM SOLUTIONS CONTAINING DIALKYL DISULFIDES OR ALKENETHIOLS. *Langmuir* **1994,** *10* (6), 1825-1831.

104. Holmlin, R. E.; Chen, X. X.; Chapman, R. G.; Takayama, S.; Whitesides, G. M., Zwitterionic SAMs that resist nonspecific adsorption of protein from aqueous buffer. *Langmuir* **2001,** *17* (9), 2841-2850.

105. Bain, C. D.; Troughton, E. B.; Tao, Y. T.; Evall, J.; Whitesides, G. M.; Nuzzo, R. G., FORMATION OF MONOLAYER FILMS BY THE SPONTANEOUS ASSEMBLY OF ORGANIC THIOLS FROM SOLUTION ONTO GOLD. *Journal of the American Chemical Society* **1989,** *111* (1), 321-335.

106. Gunter, P. L. J.; Niemantsverdriet, J. W., THICKNESS DETERMINATION OF UNIFORM OVERLAYERS ON ROUGH SUBSTRATES BY ANGLE-DEPENDENT XPS. *Applied Surface Science* **1995,** *89* (1), 69-76.

107. S Pirbadian, S.; Barchinger, S. E.; Leung, K. M.; Byun, H. S.; Jangir, Y.; Bouhenni, R. A.; Reed, S. B.; Romine, M. F.; Saffarini, D. A.; Shi, L.; Gorby, Y. A.; Golbeck, J. H.; El-Naggar, M. Y., Shewanella oneidensis MR-1 nanowires are outer membrane and periplasmic extensions of the extracellular electron transport components. *Proceedings of the National Academy of Sciences of the United States of America* **2014,** *111* (35), 12883-12888.

108. Aureau, D.; Ozanam, F.; Allongue, P.; Chazalviel, J. N., The titration of carboxyl-terminated monolayers revisited: In situ calibrated Fourier transform infrared study of well-defined monolayers on silicon. *Langmuir* **2008,** *24* (17), 9440-9448.

109. Bain, C. D.; Whitesides, G. M., A STUDY BY CONTACT-ANGLE OF THE ACID-BASE BEHAVIOR OF MONOLAYERS CONTAINING OMEGA-MERCAPTOCARBOXYLIC ACIDS ADSORBED ON GOLD - AN EXAMPLE OF REACTIVE SPREADING. *Langmuir* **1989,** *5* (6), 1370-1378.

110. Carnazza, S.; Marletta, G.; Frasca, M.; Fortuna, L.; Guglielmino, S., Spatial Patterns of Microbial Retention on Polymer Surfaces. *Journal of Adhesion Science and Technology* **2011,** *25* (17), 2255-2280.

111. Dalton, H. M.; Stein, J.; March, P. E., A biological assay for detection of heterogeneities in the surface hydrophobicity of polymer coatings exposed to the marine environment. *Biofouling* **2000,** *15* (1-3), 83.

112. Carnazza, S.; Satriano, C.; Guglielmino, S.; Marletta, G., Fast exopolysaccharide secretion of Pseudomonas aeruginosa on polar polymer surfaces. *Journal of Colloid and Interface Science* **2005,** *289* (2), 386-393.

113. Miller, D. J.; Araujo, P. A.; Correia, P. B.; Ramsey, M. M.; Kruithof, J. C.; van Loosdrecht, M. C. M.; Freeman, B. D.; Paul, D. R.; Whiteley, M.; Vrouwenvelder, J. S., Short-term adhesion and long-term biofouling testing of polydopamine and poly(ethylene glycol) surface modifications of membranes and feed spacers for biofouling control. *Water Research* **2012,** *46* (12), 3737-3753.

114. Busscher, H. J.; Bos, R.; Vandermei, H. C., INITIAL MICROBIAL ADHESION IS A DETERMINANT FOR THE STRENGTH OF BIOFILM ADHESION. *Fems Microbiology Letters* **1995,** *128* (3), 229-234.

115. O'Toole, G.; Kaplan, H. B.; Kolter, R., Biofilm formation as microbial development. *Annual Review of Microbiology* **2000,** *54*, 49-79.

116. Callow, J. A.; Callow, M. E.; Ista, L. K.; Lopez, G.; Chaudhury, M. K., The influence of surface energy on the wetting behaviour of the spore adhesive of the marine alga Ulva linza (synonym Enteromorpha linza). *Journal of the Royal Society Interface* **2005,** *2* (4), 319-325.

117. Barken, K. B.; Pamp, S. J.; Yang, L.; Gjermansen, M.; Bertrand, J. J.; Klausen, M.; Givskov, M.; Whitchurch, C. B.; Engel, J. N.; Tolker-Nielsen, T., Roles of type IV pili, flagellum-mediated motility and extracellular DNA in the formation of mature multicellular structures in Pseudomonas aeruginosa biofilms. *Environmental Microbiology* **2008,** *10* (9), 2331-2343.

118. Bos, R.; van der Mei, H. C.; Gold, J.; Busscher, H. J., Retention of bacteria on a substratum surface with micro-patterned hydrophobicity. *Fems Microbiology Letters* **2000,** *189* (2), 311-315.

119. Hall-Stoodley, L.; Costerton, J. W.; Stoodley, P., Bacterial biofilms: From the natural environment to infectious diseases. *Nature Reviews Microbiology* **2004,** *2* (2), 95-108.

120. Mukherjee, J.; Karunakaran, E.; Biggs, C. A., Using a multi-faceted approach to determine the changes in bacterial cell surface properties influenced by a biofilm lifestyle. *Biofouling* **2012,** *28*(1), 1-14.

121. Mohan, S.V.; Velvizhi, G.; Modestra,J.A; Srikanth, S., Microbial fuel cell: critical factors regulating bio-catalyzed electrochemical process and recent advancements, Renew. *Sust. Energ. Rev*. **2014,** 40, 779–797.

122. He, Y.R.; Xiao, X.; Li, W.W.; Sheng, G.P.; Yan, F.F.; Yu, H.Q.; Yuan, H.; Wu, L.J., Enhanced electricity production from microbial fuel cells with plasma-modified carbon paper anode, Phys. *Chem. Chem. Phys*. **2012**, 14,9966–9971.

123. Zhou, M.; Chi, M.; Luo, J.; He, H.; Jin, T., An overview of electrode materials in microbial fuel cells, *J. Power Sources* **2011,** 196, 4427–4435.

124. Wang, X.; Cheng, S.; Feng, Y.; Merrill, M.D.; Saito, T.; Logan, B.E., Use of carbon mesh anodes and the effect of different pretreatment methods on power production in microbial fuel cells, *Environ. Sci. Technol*. **2009**, 43, 6870–6874.

125. Ketep, S.F.; Bergel, A.; Calmet, A.; Erable, B., Stainless steel foam increases the current produced by microbial bioanodes in bioelectrochemical systems, *Energy Environ. Sci.* **2014,** 7(5), 1633–1637.

126. Karra, U.; Manickam, S.S.; McCutcheon, J.R.; Patel, N.; Li, B., Power generation and organics removal fromwastewater using activated carbon nanofiber (ACNF) microbial fuel cells (MFCs), *Int. J. Hydrog. Energy* **2013,** 38, 1588–1597.

127. Zhu, N.; Chen, X.; Zhang, T.; Wu, P.; Li, P.; Wu, J., Improved performance of membrane free single-chamber air-cathode microbial fuel cells with nitric acid and ethylenediamine surface modified activated carbon fiber felt anodes, *Bioresour. Technol.* **2011**,102,422–426.

128. Zhou, M.; Chi, M.; Wang, H.; Jin, T., Anode modification by electrochemical oxidation: a new practical method to improve the performance of microbial fuel cells, *Biochem. Eng. J.* **2012,** 60, 151–155.

129. Lai, B.; Tang, X.; Li, H.; Du, Z.; Liu, X.; Zhang, Q., Power production enhancement with a polyaniline modified anode in microbial fuel cells, *Biosens. Bioelectron*. **2011,** 28,

373–377.

130. Babanova, S.; Bretschger, O.; Roy, J.; Cheung, A.; Artyushkova, K.; Atanassov, P., Innovative statistical interpretation of Shewanella oneidensis microbial fuel cells data. *Physical Chemistry Chemical Physics* **2014,** *16* (19), 8956-8969.

131. Babanova, S.; Artyushkova, K.; Ulyanova, Y.; Singhal, S.; Atanassov, P., Design of experiments and principal component analysis as approaches for enhancing performance of gas-diffusional air-breathing bilirubin oxidase cathode. *Journal of Power Sources* **2014,** *245*, 389-397.

132. Picot, M.; Lapinsonniere, L.; Rothballer, M.; Barriere, F., Graphite anode surface modification with controlled reduction of specific aryl diazonium salts for improved microbial fuel cells power output. *Biosensors & Bioelectronics* **2011,** *28* (1), 181-188.

133. Nagaoka, T.; Yoshino, T., SURFACE-PROPERTIES OF ELECTROCHEMICALLY PRETREATED GLASSY-CARBON. *Analytical Chemistry* **1986,** *58* (6), 1037-1042.

134. Ista, L. K.; Lopez, G. P., Thermodynamic analysis of marine bacterial attachment to oligo(ethylene glycol)-terminated self-assembled monolayers. *Biointerphases* **2013,** *8*.

135. Ista, L. K.; Callow, M. E.; Finlay, J. A.; Coleman, S. E.; Nolasco, A. C.; Simons, R. H.; Callow, J. A.; Lopez, G. P., Effect of substratum surface chemistry and surface energy on attachment of marine bacteria and algal spores. *Applied and Environmental Microbiology* **2004,** *70* (7), 4151-4157.

136. Khan, M. M. T.; Ista, L. K.; Lopez, G. P.; Schuler, A. J., Experimental and Theoretical Examination of Surface Energy and Adhesion of Nitrifying and Heterotrophic Bacteria Using Self-Assembled Monolayers. *Environmental Science & Technology* **2011,** *45* (3), 1055-1060.

137. Santoro, C.; Ieropoulos, I.; Greenman, J.; Cristiani, P.; Vadas, T.; Mackay, A.; Li, B., Power generation and contaminant removal in single chamber microbial fuel cells (SCMFCs) treating human urine. *International Journal of Hydrogen Energy* **2013,** *38* (26), 11543-11551.

138. Santoro, C.; Guilizzoni, M.; Baena, J. P. C.; Pasaogullari, U.; Casalegno, A.; Li, B.; Babanova, S.; Artyushkova, K.; Atanassov, P., The effects of carbon electrode surface properties on bacteria attachment and start up time of microbial fuel cells. *Carbon* **2014,** *67*, 128-139.

139. Santoro, C.; Ieropoulos, I.; Greenman, J.; Cristiani, P.; Vadas, T.; Mackay, A.; Li, B., Current generation in membraneless single chamber microbial fuel cells (MFCs) treating urine. *Journal of Power Sources* **2013,** *238*, 190-196.

140. Mitchell, K. R.; Takacs-Vesbach, C. D., A comparison of methods for total community DNA preservation and extraction from various thermal environments. *Journal of Industrial Microbiology & Biotechnology* **2008,** *35* (10), 1139-1147.

141. Quince, C.; Lanzen, A.; Curtis, T. P.; Davenport, R. J.; Hall, N.; Head, I. M.; Read, L. F.; Sloan, W. T., Accurate determination of microbial diversity from 454 pyrosequencing data. *Nature Methods* **2009,** *6* (9), 639-U27.

142. Dowd, S. E.; Callaway, T. R.; Wolcott, R. D.; Sun, Y.; McKeehan, T.; Hagevoort, R. G.; Edrington, T. S., Evaluation of the bacterial diversity in the feces of cattle using 16S rDNA bacterial tag-encoded FLX amplicon pyrosequencing (bTEFAP). *Bmc Microbiology* **2008,** *8*.

143. McDonald, D.; Price, M. N.; Goodrich, J.; Nawrocki, E. P.; DeSantis, T. Z.; Probst, A.; Andersen, G. L.; Knight, R.; Hugenholtz, P., An improved Greengenes taxonomy with explicit ranks for ecological and evolutionary analyses of bacteria and archaea. *Isme Journal* **2012,** *6* (3), 610-618.

144. Jung, S.; Regan, J. M., Comparison of anode bacterial communities and performance in microbial fuel cells with different electron donors. *Applied Microbiology and Biotechnology* **2007,** *77*(2), 393-402.

145. Cristiani, P.; Carvalho, M. L.; Guerrini, E.; Daghio, M.; Santoro, C.; Li, B., Cathodic and anodic biofilms in Single Chamber Microbial Fuel Cells. *Bioelectrochemistry* **2013,** *92*, 6-13.

146. Winfield, J.; Ieropoulos, I.; Greenman, J.; Dennis, J., The overshoot phenomenon as a function of internal resistance in microbial fuel cells. *Bioelectrochemistry* **2011,** *81* (1), 22-27.

147. Wrighton, K. C.; Agbo, P.; Warnecke, F.; Weber, K. A.; Brodie, E. L.; DeSantis, T. Z.; Hugenholtz, P.; Andersen, G. L.; Coates, J. D., A novel ecological role of the Firmicutes identified in thermophilic microbial fuel cells. *Isme Journal* **2008,** *2* (11), 1146-1156.

148. Ishii, S. i.; Suzuki, S.; Norden-Krichmar, T. M.; Tenney, A.; Chain, P. S. G.; Scholz, M. B.; Nealson, K. H.; Bretschger, O., A novel metatranscriptomic approach to identify gene expression dynamics during extracellular electron transfer. *Nature Communications* **2013,** *4*.

149. Ishii, S. i.; Suzuki, S.; Norden-Krichmar, T. M.; Nealson, K. H.; Sekiguchi, Y.; Gorby, Y. A.; Bretschger, O., Functionally Stable and Phylogenetically Diverse Microbial Enrichments from Microbial Fuel Cells during Wastewater Treatment. *Plos One* **2012,** *7* (2).

150. Ishii, S. i.; Suzuki, S.; Norden-Krichmar, T. M.; Phan, T.; Wanger, G.; Nealson, K. H.; Sekiguchi, Y.; Gorby, Y. A.; Bretschger, O., Microbial population and functional dynamics associated with surface potential and carbon metabolism. *Isme Journal* **2014,** *8* (5), 963-978.

151. shii, S. i.; Suzuki, S.; Norden-Krichmar, T. M.; Wu, A.; Yamanaka, Y.; Nealson, K. H.; Bretschger, O., Identifying the microbial communities and operational conditions for optimized wastewater treatment in microbial fuel cells. *Water Research* **2013,** *47* (19), 7120-7130.

152. Daghio, M.; Gandolfi, I.; Bestetti, G.; Franzetti, A.; Guerrini, E.; Cristiani, P., Anodic and cathodic microbial communities in single chamber microbial fuel cells. *New Biotechnology* **2015,** *32*(1), 79-84.

153. Crittenden, S. R.; Sund, C. J.; Sumner, J. J., Mediating electron transfer from bacteria to a gold electrode via a self-assembled monolayer. *Langmuir* **2006,** *22* (23), 9473-9476.

154. Klausen, M.; Heydorn, A.; Ragas, P.; Lambertsen, L.; Aaes-Jørgensen, A.; Molin, S.; Tolker-Nielsen, T., Biofilm formation by Pseudomonas aeruginosa wild type, flagella and type IV pili mutants. *Mol. Microbiol*. **2003**, 48, 1511–1524.

155. O'Toole, G.A.; Kolter, R., Flagellar and twitching motility are necessary for Pseudomonas aeruginosa biofilm development. *Mol. Microbiol*. **1998,** 30, 295–304.

156. Thormann, K.M.; Saville, R.M.; Shukla, S.; Pelletier, D.A.; Spormann, A.M., Initial phases of biofilm formation in Shewanella oneidensis MR-1. *Journal of Bacteriology* **2004.** 186, 8096–8104.

157. Chao, L.; Rakshe, S.; Leff, M.; Spormann, A. M., PdeB, a Cyclic Di-GMP-Specific Phosphodiesterase That Regulates Shewanella oneidensis MR-1 Motility and Biofilm Formation. *Journal of Bacteriology* **2013,** *195* (17), 3827-3833.

158. Jarrell, K.F.; McBride, M.J., The surprisingly diverse ways that prokaryotes move Nature Rev. Microbiol. **2008**, 6, 466–76.

159. Giltner, C. L.; Nguyen, Y.; Burrows, L. L., Type IV Pilin Proteins: Versatile Molecular Modules. *Microbiology and Molecular Biology Reviews* **2012,** *76* (4), 740-772.

160. Merz, A. J.; So, M.; Sheetz, M. P., Pilus retraction powers bacterial twitching motility. *Nature* **2000,** *407* (6800), 98-102.

161. Fitzgerald, L. A.; Petersen, E. R.; Ray, R. I.; Little, B. J.; Cooper, C. J.; Howard, E. C.; Ringeisen, B. R.; Biffinger, J. C., Shewanella oneidensis MR-1 Msh pilin proteins are

involved in extracellular electron transfer in microbial fuel cells. *Process Biochemistry* **2012,** *47* (1), 170-174.

162. Cornejo, J. A.; Lopez, C.; Babanova, S.; Santoro, C.; Artyushkoya, K.; Ista, L.; Schuler, A. J.; Atanassov, P., Surface Modification for Enhanced Biofilm Formation and Electron Transport in Shewanella Anodes. *Journal of the Electrochemical Society* **2015,** *162* (9), H597-H603.

163. Harris, H. W.; El-Naggar, M. Y.; Bretschger, O.; Ward, M. J.; Romine, M. F.; Obraztsova, A. Y.; Nealson, K. H., Electrokinesis is a microbial behavior that requires extracellular electron transport. *Proceedings of the National Academy of Sciences of the United States of America* **2010,** *107* (1), 326-331.3.